NASA CR-159458
R78AEG319

(NASA-CR-159458) EXPERIMENTAL CLEAN COMBUSTOR PROGRAM, PHASE 3: NOISE MEASUREMENT ADDENDUM Final Report (General Electric Co.) 139 p HC A07/MF A01 CSCL 20A G3/71

N79-17656

Unclas 13969

EXPERIMENTAL CLEAN COMBUSTOR PROGRAM - PHASE III
NOISE MEASUREMENT ADDENDUM
FINAL REPORT

by

V.L. DOYLE

GENERAL ELECTRIC COMPANY

Prepared For

National Aeronautics and Space Administration

NASA Lewis Research Center
CONTRACT NAS3-19736

1. Report No.	2. Government Accession No.	3. Recipient's Catalog No.
NASA CR-159458		

4. Title and Subtitle	5. Report Date
Experimental Clean Combustor Program - Phase III Noise Measurement Addendum Final Report	December 1978
	6. Performing Organization Code
7. Author(s)	8. Performing Organization Report No.
V.L. Doyle	R78AEG319
	10. Work Unit No.
9. Performing Organization Name and Address	11. Contract or Grant No.
General Electric Company Aircraft Engine Group Cincinnati, Ohio 45215	NAS3-19736
	13. Type of Report and Period Covered
12. Sponsoring Agency Name and Address	Final Report
NASA Lewis Research Center 21000 Brookpark Road Cleveland, Ohio 44135	14. Sponsoring Agency Code

15. Supplementary Notes

NASA Project Manager: Ronald G. Huff
Lewis Research Center

16. Abstract

The experimental work sponsored under the Noise Measurement Addendum to the Experimental Clean Combustor Program was conducted to investigate the acoustic characteristics of the Double Annular combustor in a CF6-50 high bypass turbofan engine. Internal fluctuating pressure measurements were made in the combustor region and in the core exhaust. The transmission loss across the turbine and nozzle was determined from the measurements and compared to previous component results and present theory. The primary noise source location in the combustor was investigated. Spectral comparisons of test rig results from ECCP Phases I and II were made with the engine results. Comparisons of measured overall power level were made with component and engine correlating parameters.

17. Key Words (Suggested by Author(s))	18. Distribution Statement
Internal combustor noise measurements CF6-50 engine core noise Double Annular combustor noise	Unclassified - Unlimited

19. Security Classif. (of this report)	20. Security Classif. (of this page)	21. No. of Pages	22. Price*
Unclassified	Unclassified	135	

* For sale by the National Technical Information Service, Springfield, Virginia 22151

TABLE OF CONTENTS

Section		Page
1.0	SUMMARY	1
2.0	INTRODUCTION	2
3.0	DESCRIPTION OF TEST	3
	3.1 CF6-50 Engine Test Vehicle	3
	3.2 Double Annular Combustor, Duct Rig and Engine	3
	3.3 Test Objectives	6
	3.4 Engine Setup for Acoustic Measurements	6
	3.5 Test Matrix	8
	3.6 Data Acquisition Systems	8
	3.7 Data Reduction and Processing	23
4.0	ANALYSIS AND DISCUSSION OF RESULTS	39
	4.1 Spectra Comparisons	39
	4.2 Turbine Transfer Function Comparison	58
	4.3 Primary Noise Source Location	64
	4.4 Overall Power Level Comparison	73
5.0	CONCLUSIONS	87
	5.1 Double Annular Combustor Spectra Comparisons	87
	5.2 Noise Source Locations	87
	5.3 Engine to Duct Rig Comparisons	88
APPENDIX A - 2 Hz NARROWBAND SPECTRA RESULTS		89
APPENDIX B - 1/3 OCTAVE BAND SPECTRA RESULTS		101
APPENDIX C - TURBINE TRANSFER FUNCTION RESULTS		114
APPENDIX D - EVALUATION OF PROBE RESPONSE AT ELEVATED TEMPERATURES		119
APPENDIX E - CROSS-CORRELATION RESULTS		123
APPENDIX F - NOMENCLATURE		126
REFERENCES		130

LIST OF ILLUSTRATIONS

Figure No.		Page
3-1	CF6-50 Engine Demonstrator Double Annular, Low Emission Combustor.	7
3-2	Internal Sensor Locations for Engine Combustor Noise Measurements.	9
3-3	Sound Separation Probe Location for Combustor Noise Measurements on a CF6-50 Engine.	10
3-4	Kulite Sensor Installations for ECCP Phase III Acoustic Test (7708283).	11
3-5	Combustor Borescope Kulite (282°) Sensor Installation for ECCP Phase III Acoustic Test (7708284).	12
3-6	Setup of Core Exhaust and External Probes for ECCP Phase III Acoustic Test (7708286).	13
3-7	Schematic of Acoustic Data Acquisition System Setup.	16
3-8	Calibration Setup for Waveguide Probes.	18
3-9	Frequency Response of Waveguide Probe Systems.	20
3-10	Ambient Phase Calibrations of Waveguide Probe Systems.	21
3-11	Noise floor of Coherent Spectrum.	25
3-12	Typical Cross-Correlation Function for Flow with Sound Dominant.	27
3-13	Comparison of Core Probe Power Levels with Farfield Measurements.	31
3-14	Core Exhaust Power Level Spectra Comparison.	32
3-15	Comparison of Common Measurements for Repeat Readings at 45.6 Percent Thrust.	36
3-16	Comparison of Common Measurements for Repeat Readings at 64.6 Percent Thrust.	37
3-17	Comparison of Common Measurements for Repeat Readings at 82.0 Percent Thrust.	38

LIST OF ILLUSTRATIONS (Continued)

Figure No.		Page
4-1	Plane 3.0 (MADAR Probe) 1/3 Octave Band Spectra Variation with Engine Speed.	41
4-2	Plane 3.0 (MADAR Probe) Spectra Variation with Engine Speed.	42
4-3	Plane 3.5 (282° Borescope Probe) 1/3 Octave Band Spectra Variation with Engine Speed.	43
4-4	Plane 3.5 (282° Borescope Probe) Spectra Variation with Engine Speed.	44
4-5	Plane 4.0 (HPTN Probe) 1/3 Octave Band Spectra Variation with Engine Speed.	46
4-6	Plane 4.0 (HPTN Probe) Spectra Variation with Engine Speed.	47
4-7	Plane 8.0 (Exhaust Probe B) 1/3 Octave Band Spectra Variation with Engine Speed.	48
4-8	Plane 8.0 (Exhaust Probe B) Spectra Variation with Engine Speed.	49
4-9	Acoustic Probe Locations for Duct Rig Test.	52
4-10	Engine-to-Duct Rig Pressure Spectra Comparison for Double Annular Combustor at Idle.	54
4-11	Engine-to-Duct Rig Pressure Spectra Comparison for Double Annular Combustor at Approach.	55
4-12	Engine-to-Duct Rig Pressure Spectra Comparison for Double Annular Combustor at Takeoff.	56
4-13	Engine-to-Duct Rig Power Spectra Comparison for Double Annular Combustor at Idle.	57
4-14	Engine-to-Duct Rig Power Spectra Comparison for Double Annular Combustor at Approach.	59
4-15	Engine-to-Duct Rig Power Spectra Comparison for Double Annular Combustor at Takeoff.	60
4-16	Measured Attenuation Spectrum and Predicted Results for CF6-50 Six-Stage Turbine.	63

LIST OF ILLUSTRATIONS (Continued)

Figure No.		Page
4-17	Attenuation Spectrum from 3-Stage Low Pressure Turbine.	63
4-18	Cross-Correlation of Plane 3.0 to Plane 3.5 (102° Probe).	66
4-19	Cross-Correlation of Plane 3.0 to Plane 3.5 (282° Probe).	66
4-20	Cross-Correlation of Plane 3.0 to Plane 4.0.	67
4-21	Cross-Correlation of Plane 3.5 (102° Probe) to Plane 4.0.	67
4-22	Cross-Correlation of Plane 3.5 (282° Probe) to Plane 4.0.	67
4-23	Cross-Correlation at Plane 3.5 Between 102° to 282° Sensors.	68
4-24	Cross-Correlation of Plane 3.0 Probe to Plane 8.0 Probe, Element A.	69
4-25	Cross-Correlation of Plane 3.0 Probe to Plane 8.0 Probe, Element B.	69
4-26	Cross-Correlation of Core Probe Element B with Element A.	71
4-27	Coherent Spectrum at Core Nozzle Discharge, Plane 8.0.	72
4-28	Comparison of Core Probe Spectra at Each Immersion.	74
4-29	Core Probe Immersion 4 at 30 Percent Thrust.	75
4-30	Core Probe Immersion 4 at 19.7 Percent Thrust.	77
4-31	Core Probe Immersion 4 at 29.7 Percent Thrust.	78
4-32	Core Probe Immersion 4 at 64.6 Percent Thrust.	79
4-33	Comparison of Raw and Coherent OASPL with Core Speed.	80

LIST OF ILLUSTRATIONS (Continued)

Figure No.		Page
4-34	Comparison of $FPWL_{meas}$ to PWL_{GE} for Internal Sensors.	82
4-35	Comparison of PWL_{meas} to PWL_{GEEFAA}.	84
4-36	Comparison of PWL_{meas} to PWL_{GEFAA} using Adjusted Fuel-Air Ratio for 100% Pilot Points.	86
A-1	As Measured Narrowband Spectra for CF6-50 Engine Condition at 3.8 Percent Thrust, Reading 6 (Idle).	90
A-2	As Measured Narrowband Spectra for CF6-50 Engine Condition at 19.7 Percent Thrust, Reading 16.	91
A-3	As Measured Narrowband Spectra for CF6-50 Engine Condition at 30 Percent Thrust, Reading 23. (Approach Power with 100 Percent Pilot Fuel).	92
A-4	As Measured Narrowband Spectra for CF6-50 Engine Condition at 29.7 Percent Thrust, Reading 39 (Approach Power with 50/50 Fuel Split).	93
A-5	As Measured Narrowband Spectra for CF6-50 Engine Condition at 45.4 Percent Thrust, Reading 34.	94
A-6	As Measured Narrowband Spectra for CF6-50 Engine Condition at 45.4 Percent Thrust, Reading 28.	95
A-7	As Measured Narrowband Spectra for CF6-50 Engine Condition at 64.6 Percent Thrust, Reading 40.	96
A-8	As Measured Narrowband Spectra for CF6-50 Engine Condition at 64.6 Percent Thrust, Reading 13.	97
A-9	As Measured Narrowband Spectra for CF6-50 Engine Condition at 82 Percent Thrust, Reading 18.	98
A-10	As Measured Narrowband Spectra for CF6-50 Engine Condition at 82 Percent Thrust, Reading 43.	99
A-11	As Measured Narrowband Spectra for CF6-50 Engine Condition at 94.6 Percent Thrust, Reading 33.	100

LIST OF ILLUSTRATIONS (Concluded)

Figure No.		Page
B-1	One-Third Octave Band Spectra for CF6-50 Engine Condition at 3.8 Percent Thrust.	106
B-2	One-Third Octave Band Spectra for CF6-50 Engine Condition at 19.7 Percent Thrust.	107
B-3	One-Third Octave Band Spectra for CF6-50 Engine Condition at 30 Percent Thrust.	108
B-4	One-Third Octave Band Spectra for CF6-50 Engine Condition at 29.7 Percent Thrust.	109
B-5	One-Third Octave Band Spectra for CF6-50 Engine Condition at 45.4 Percent Thrust.	110
B-6	One-Third Octave Band Spectra for CF6-50 Engine Condition at 64.6 Percent Thrust.	111
B-7	One-Third Octave Band Spectra for CF6-50 Engine Condition at 82.0 Percent Thrust.	112
B-8	One-Third Octave Band Spectra for CF6-50 Engine Condition at 94.6 Percent Thrust.	113
C-1	Coherent Spectra Comparisons for Turbine Attenuation from ECCP Phase III Engine Test.	115-118

LIST OF TABLES

Number		Page
1.	CF6-50C Engine Specifications.	4
2.	Double Annular Combustor Design Parameters.	5
3.	Summary of ECCP Phase III Acoustic Test Conditions.	14
4.	Ambient Frequency Response Corrections for ECCP Phase III Waveguide Sensors.	22
5.	ECCP Phase III Program Aerodynamic Performance Summary.	33
6.	Summary of Local Static Conditions for Combustor Test.	34
7.	Test Condtions for Comparison of ECCP Phase I, II and III Results.	51
8.	CF6-50 Turbine Attenuation Summary from ECCP Phase III Test Results.	53
B-1	One-Third Octave Band Spectra from ECCP Phase III CF6-50 Engine Test.	102-105
E-1	Time Delays and Amplitudes of Cross-Correlation Peaks for ECCP Phase III Test Data.	124,125

1.0 SUMMARY

The purpose of the Noise Measurement Addendum to the Experimental Clean Combustor Program sponsored by the NASA Lewis Research Center under Contract NAS3-19736 was to investigate by experiment the noise characteristics of the Double Annular combustor in the CF6-50 high bypass turbofan engine. The program objectives were to measure and compare the engine combustor internal pressure spectra with test rig results from ECCP Phases I and II, to determine the acoustic transfer function, comparing the results with component tests and theoretical predictions, and to investigate the primary noise source location in the combustor.

The salient results and conclusions from this investigation are as follows:

- Engine test results show spectra from internal measurments to exhibit the typical core noise spectra shape at approach power settings and below with peaks in the 400 to 600 Hz frequency bands.

- Engine to duct rig results show large differences (10 to 25 dB) on a pressure basis but exhibit much closer agreement (3 to 8 dB) on a power level basis. The spectral shapes for both the inlet and discharge planes of the engine and duct rig were similar. Differences in test conditions, fuel splits, measurement locations and the presence of the choked HPT nozzle diaphragm in the engine were cited as possible causes for the level differences.

- The turbine transfer function in terms of attenuation agreed well with component results and theoretical predictions.

- The exact location of the primary noise source within the combustor was undefined from present measurements. The best indication for the primary source location is in the region between the combustor exit and the region forward of the core nozzle exit.

- Operation of the Double Annular combustor with pilot fuel only results in higher OAPWL than when fuel splits between inner and outer burner stages are used. This is particularly critical at approach power since the difference can be as much as 9 dB.

A better understanding of combustor noise during engine operation was gained from this program. These results will be useful in evaluating the core noise transmitted from the engine to the farfield in tests to be conducted under another NASA Lewis program.

2.0 INTRODUCTION

The NASA/General Electric Experimental Clean Combustor Program has been specifically directed toward developing an advanced low emission, low noise combustor for use in the General Electric CF6-50 engine family. The CF6-50 engine family is the higher power series of the two CF6 high bypass turbofan engine families developed by General Electric.

Noise evaluation as well as emissions testing have played important roles in the development work conducted during this program. Acoustic measurements have been made on several full size, annular combustor configurations tested in Phases I and II of the Experimental Clean Combustor Program (ECCP) during duct rig testing. These measurements indicated that the peak sound pressure level (SPL) occurred near a frequency of 1000 Hz. Generally, far-field data on engines have been found to peak at 400-500 Hz. This difference between an isolated combustor running in a component test stand and a combustor on an engine is the basis for the study reported here. In order to investigate the effect of the engine installation on the combustor acoustics it is necessary to take acoustic measurements on a given combustor both in the combustor development rig and in the engine. During Phase I and II of the ECCP, acoustic measurements were made in a combustor development rig on a combustor similar to the one used in the engine demonstration tests under ECCP Phase III.

The work sponsored under this acoustic addendum to NASA Lewis Contract NAS3-19736 provided the measurements in the engine necessary to evaluate the combustor engine acoustic signature and the acoustic transmission loss of the low frequency combustor noise through turbine.

3.0 DESCRIPTION OF TEST

3.1 CF6-50 ENGINE TEST VEHICLE

The tests conducted under Phase III were performed on a CF6-50 high bypass turbofan engine. The basic engine description and details of the specific configurations tested for the emissions investigation are found in Reference 1. The CF6-50 engine model operating parameters were selected for use as the combustor design and test conditions of this program. Key overall specifications of this engine are presented in Table 1.

3.2 DOUBLE ANNULAR COMBUSTOR, DUCT RIG AND ENGINE

3.2.1 Design Concept

In the Phase I and II Programs, four advanced combustor design concepts were evaluated in CF6-50 engine-size full annular combustor duct rig tests (References 2-5). The best overall results for engine application were obtained with the Double Annular combustor configuration D-12, which was the prototype for the flightworthy demonstrator Double Annular combustor designed in the Phase II Program for use in these Phase III Program combustor rig and CF6-50 engine tests. Acoustic component tests were conducted in Phase II (Reference 5, on a Double Annular combustor configuration D-13 which was very similar to th D-12 design. The D-13 differed from the D-12 by the percentages of airflow distribution through ilot and main stages as noted in Table 2.

The Double Annular combustor comprises two annular primary burning zones, in parallel, separated by a short centerbody. Thirty fuel nozzles are used in each annulus. The outer annulus is the pilot stage and is always fueled. The inner annulus is the main stage and is fueled only at higher engine-power operating conditions. The airflow distribution is highly biased to the main stage in order to reduce both idle and high-power emissions. The pilot stage airflow is specifically sized to provide nearly stoichiometric fuel-air ratios and long residence times at idle power settings, thereby minimizing CO and HC emissions levels. At high-power operating conditions, most of the fuel is supplied to the main stage. In this stage, the residence times are very short. Also, at high-power operating conditions, lean fuel-air ratios are maintained in both stages to minimize NO_x and smoke emissions levels.

3.2.2 Engine Demonstrator Combustor Design

With this Double Annular combustor concept, program goals for CO and HC emissions at idle operating conditions were achieved early in the Phase II Program, and maintained throughout the final combustor refinement test series. The emphasis in this final series of refinement tests was therefore to more nearly approach the NO_x emission goal, and to meet the engine installation

Table 1. CF6-50C Engine Specifications.

Takeoff Rating (SLS)	
Thrust	224.2 kN (50,400 lb_f)
Specific Fuel Consumption	10.7 mg/Ns (0.377 lbm/lb_f-hr)
Maximum Cruise (Mach 0.85/10.7 km)	
Thrust	48 kN (10,800 lb_f)
Specific Fuel Consumption	18.6 mg/Ns (0.656 lbm/lb_f-hr)
Weight	3780 kg (8330 lb)
Length	482 cm (190 in)
Maximum Diameter	272 cm (107 in)
Pressure Ratio	
Takeoff	29.4
Maximum Cruise	31.4
Bypass Ratio (Takeoff)	4.4
Total Airflow (Takeoff)	659 kg/s (1452 lbm/s)

Table 2. Double Annular Combustor Design Parameters.

	Prototype Combustor (D-12)	Prototype Combustor For Acoustic Tests (D-13)	Engine Demonstrator Combustor
Airflow Distribution, % W36			
Pilot Stage			
Swirlers	13.4	12.5	12.6
Dilution, 2nd Outer Panel	4.7	4.6	4.5
Dome Cooling	4.5	4.4	7.2
Main Stage			
Swirlers	33.1	32.9	33.0
Dilution, 1st Inner Liner Panel	10.8	17.0	10.6
Dome Cooling	4.1	4.1	5.4
Centerbody and Liner Cooling	23.1	23.0	23.3
Profile Trim	4.8	0	2.0
Aft Seal Leakage	1.5	1.5	1.4
	100.0	100.0	100.0
Key Velocities, m/s			
Pilot Stage Dome	11	11	10
Main Stage Dome	29	29	29
Outer Passage	24	24	37
Inner Passage	59	59	46
Reference	26	26	23
Key Dimensions, cm			
Pilot Stage Dome Height	5.7	5.7	7.1
Main Stage Dome Height	5.3	5.3	6.1
Combustion Length	32.5	32.5	32.5

and performance requirements. In this series, very little change in NO_x emission levels was obtained and engine installation and performance requirements were most nearly met with configuration D-12 which was therefore selected as the prototype for a more sophisticated second generation version of this advanced low emission combustor design for use in the Phase III demonstration engine tests. This second generation combustor configuration was needed because the prototype configuration used in Phases I and II was designed to accommodate differential thermal growths, pressure loads, vibration loads, and mechanical assembly were not adequate to permit the use of this combustor in engine tests.

The resulting demonstrator engine combustor design is shown in Figure 3-1. The aerothermal design features of this demonstrator engine combustor was patterned after those of the prototype combustor. In addition, advanced aeromechanical design features derived from other General Electric programs were incorporated into its design.

Key aerothermal design parameters of the Double Annular combustors are compared in Table 2. Airflow distributions are very similar except that the demonstrator combustor dome cooling airflows are slightly higher which is accomplished primarily by reducing profile trim airflow. Key velocities are also very similar except that inner and outer passage velocities of the demonstrator combustor are more nearly equalized to reduce parasitic pressure losses. Dome heights of the demonstrator combustor were increased about 20 percent to provide the additional room within the cowl to accommodate the needed radial movements of the swirl cup slip joints.

3.3 TEST OBJECTIVES

The acoustic test of the Double Annular combustor in the CF6-50 engine provided the first indication of internal fluctuating pressure measurements for this type of combustor in an engine environment. Previous duct rig measurements gave levels of noise based on tests conducted at scaled engine conditions at local static pressures of up to 10 atm. compared to engine pressure levels of 26 atm at takeoff. The engine test provided a base for comparison with the duct rig results from Phase I and II.

Other test objectives included determining the acoustic transfer function across the turbine by evaluating the attenuation of the acoustic signal upstream and downstream of the turbine, and identifying the location of the primary noise source within the combustor from cross-correlation analysis results.

3.4 ENGINE SETUP FOR ACOUSTIC MEASUREMENTS

The acoustic tests of the ECCP Phase III Double Annular combustor installed in CF6-50 engine number 445-105/7 were conducted after completion of the combustor performance and emissions tests. The engine test cell installation and setup for these tests is described in the ECCP Phase III final

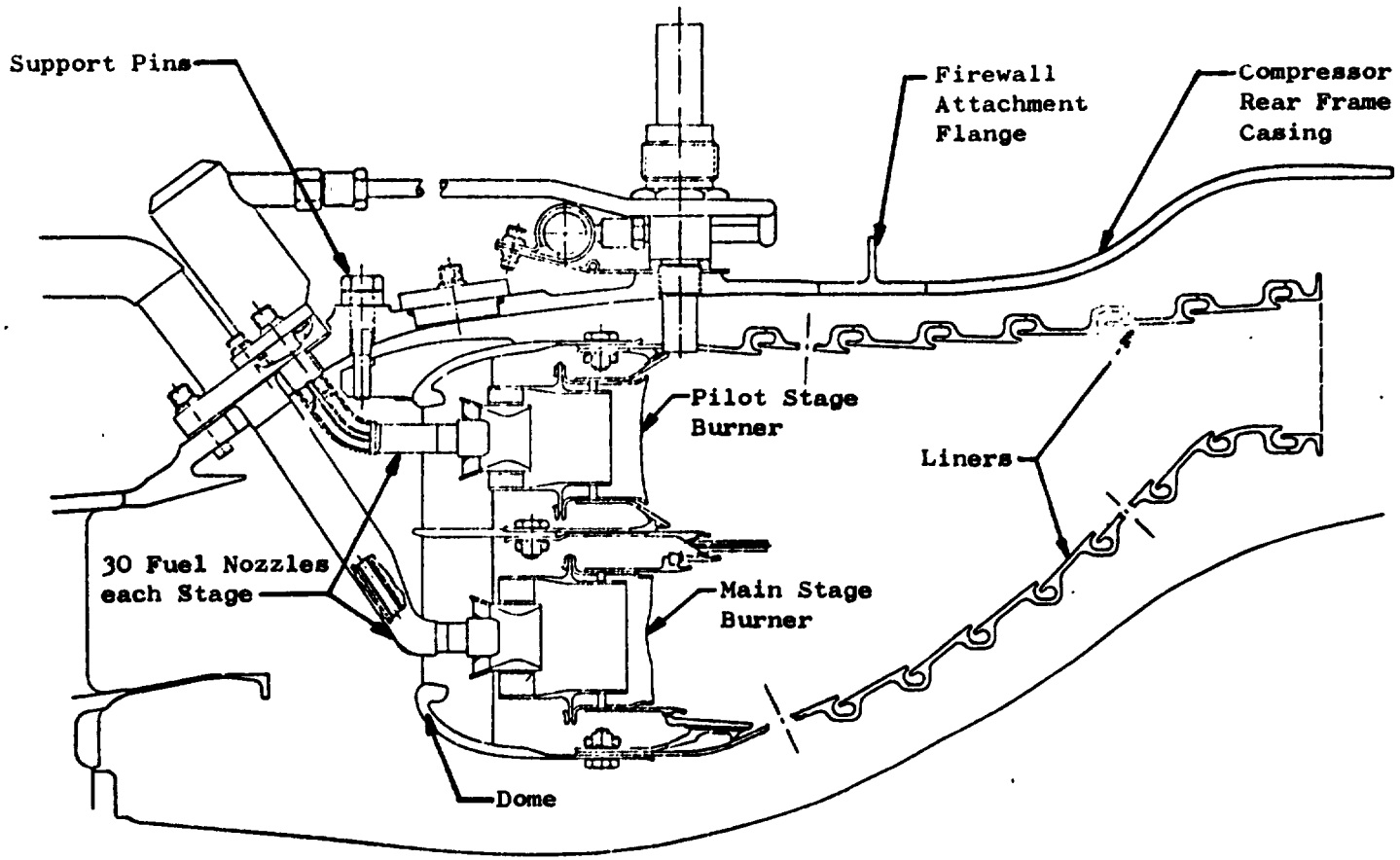

Figure 3-1. CF6-50 Engine Demonstrator Double Annular, Low Emission Combustor

report on the emissions test, Reference 1. The acoustic test setup utilized the same engine configuration except that the gas sampling rakes in the core exhaust and those in the turbine rear frame were removed. The basic aerodynamic performance and engine safety instrumentation remained essentially the same as described in Reference 1.

Dynamic pressure instrumentation was installed in available access ports at three axial planes in the combustor region and at the core nozzle. An external probe mounted in the test cell was used to indicate cell noise levels and to attempt to determine the amount of combustor noise transferred outside the engine. Acoustic probes were positioned in the MADAR port at the compressor discharge, Plane 3.0; in the borescope ports at combustor entrance, Plane 3.5; in the borescope port of the first stage turbine nozzle at the combustor exit, Plane 4.0; and at the core nozzle discharge, Plane 8.0, as illustrated in Figures 3-2 and 3-3 respectively, and shown in the photographs of Figures 3-4, 3-5 and 3-6.

3.5 TEST MATRIX

The test matrix for acoustic data paralleled the conditions set for the combustor performance and emissions tests. This was done to match the noise signature of the combustor with comparable emissions results in order to assess the overall effectiveness of the Double Annular combustor. The test points, based on percent net thrust, covered the sea level static operating line of the CF6-50 engine and included idle, approach and takeoff power settings. A total of eight (8) test conditions were set. Repeat readings were taken to check data repeatability and to supplement sensor measurements of several that were lost during the run due to equipment malfunctions. Table 3 summarizes the test matrix for acoustic data and shows that all required conditions were obtained. Matching repeat points and redundant probes at two of the four axial planes provided complete sets of measurements at every plane for each test point. The eight test conditions included two approach points at 30% net thrust. The first approach setting consisted of the 100% pilot fuel only, while the second condition approximated the 50% fuel split between inner and outer sets of fuel nozzles.

Aerodynamic performance data was provided at each test condition through a combination of the on-line DMS (Data Management System) readings supplied for each engine point setting and some performance data supplied by readings taken at similar set points during the running of the emissions tests. This was necessary as a result of digital system problems encountered during the acoustic run. The paired aero and acoustic data are compatible for all test conditions and represent typical settings with this engine.

3.6 DATA ACQUISITION SYSTEMS

The data acquisition systems for this test included both analog and digital systems. The acoustic data was acquired from combustor internal fluctuating pressure measurements made with four single-element waveguide

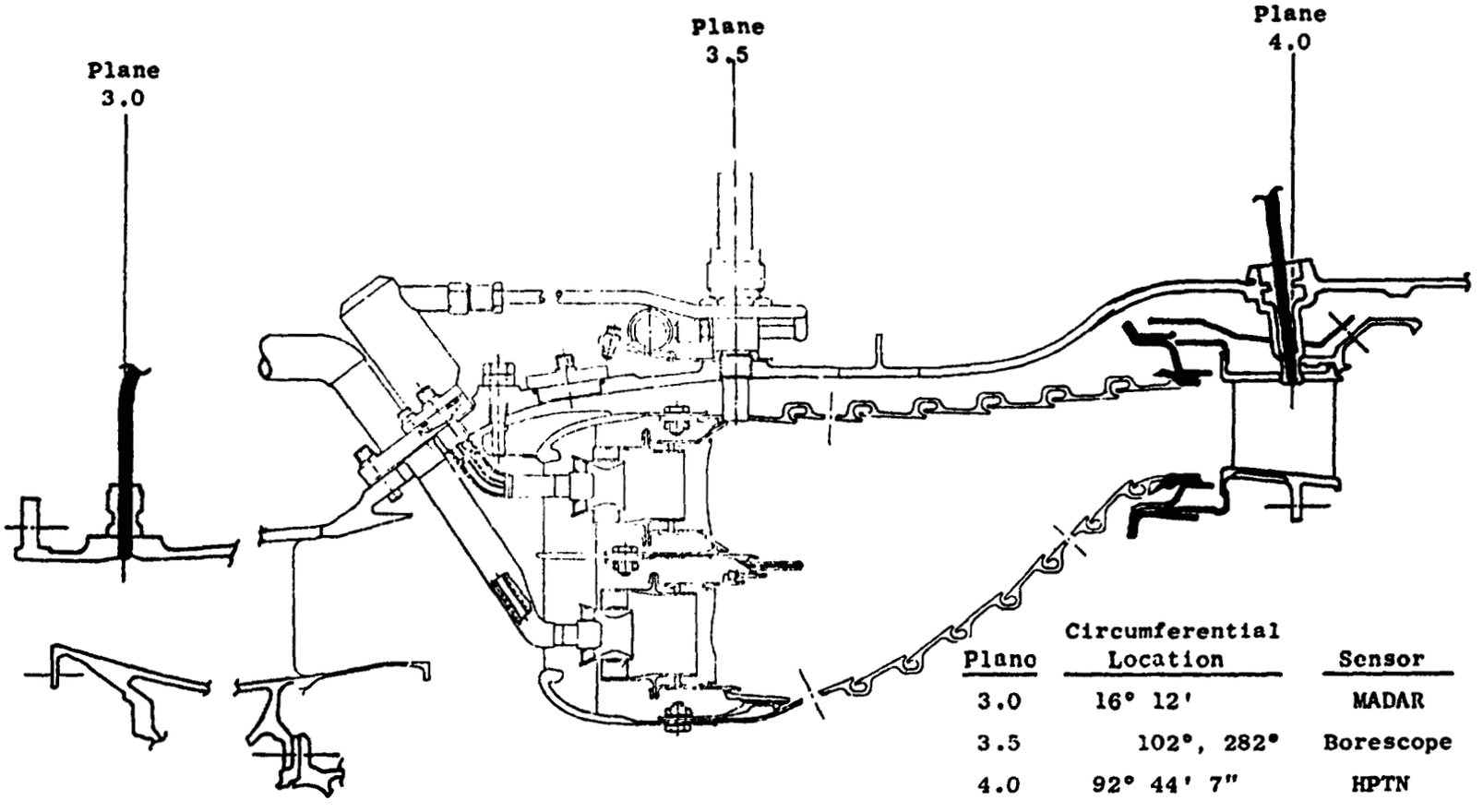

Plane	Circumferential Location	Sensor
3.0	16° 12'	MADAR
3.5	102°, 282°	Borescope
4.0	92° 44' 7"	HPTN

Figure 3-2. Internal Sensor Locations for Engine Combustor Noise Measurements.

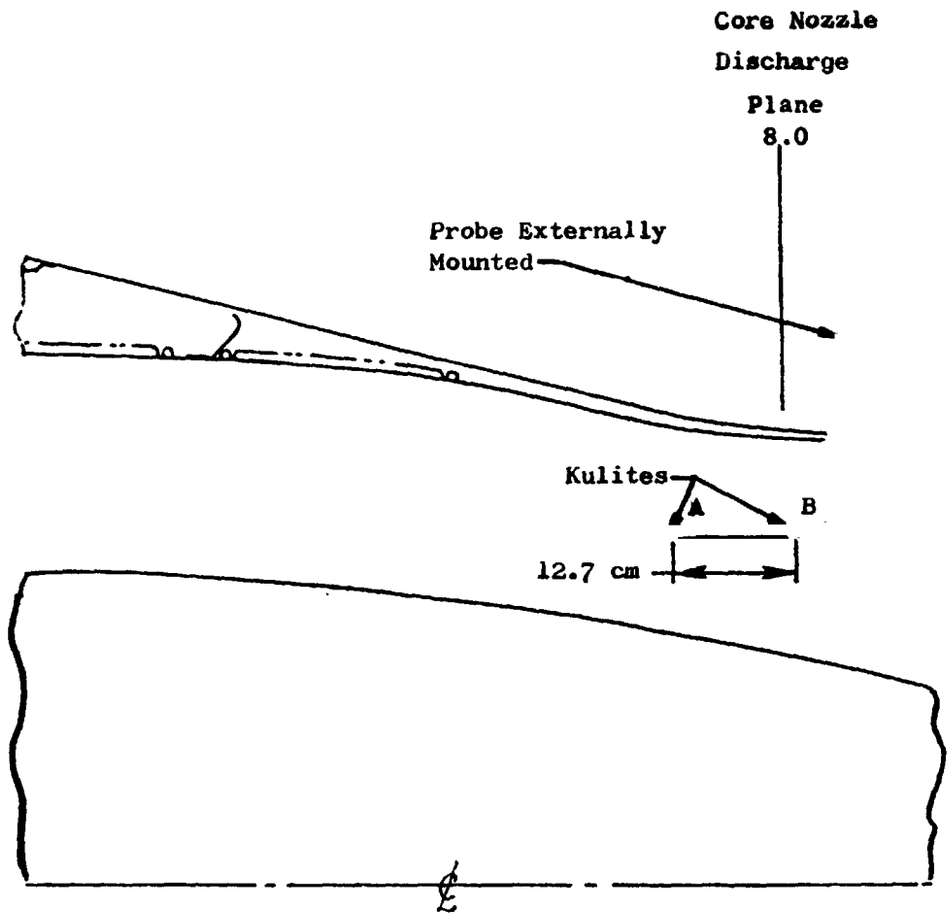

Figure 3-3. Sound Separation Probe Location for Combustor Noise Measurements on CF6-50 Engine

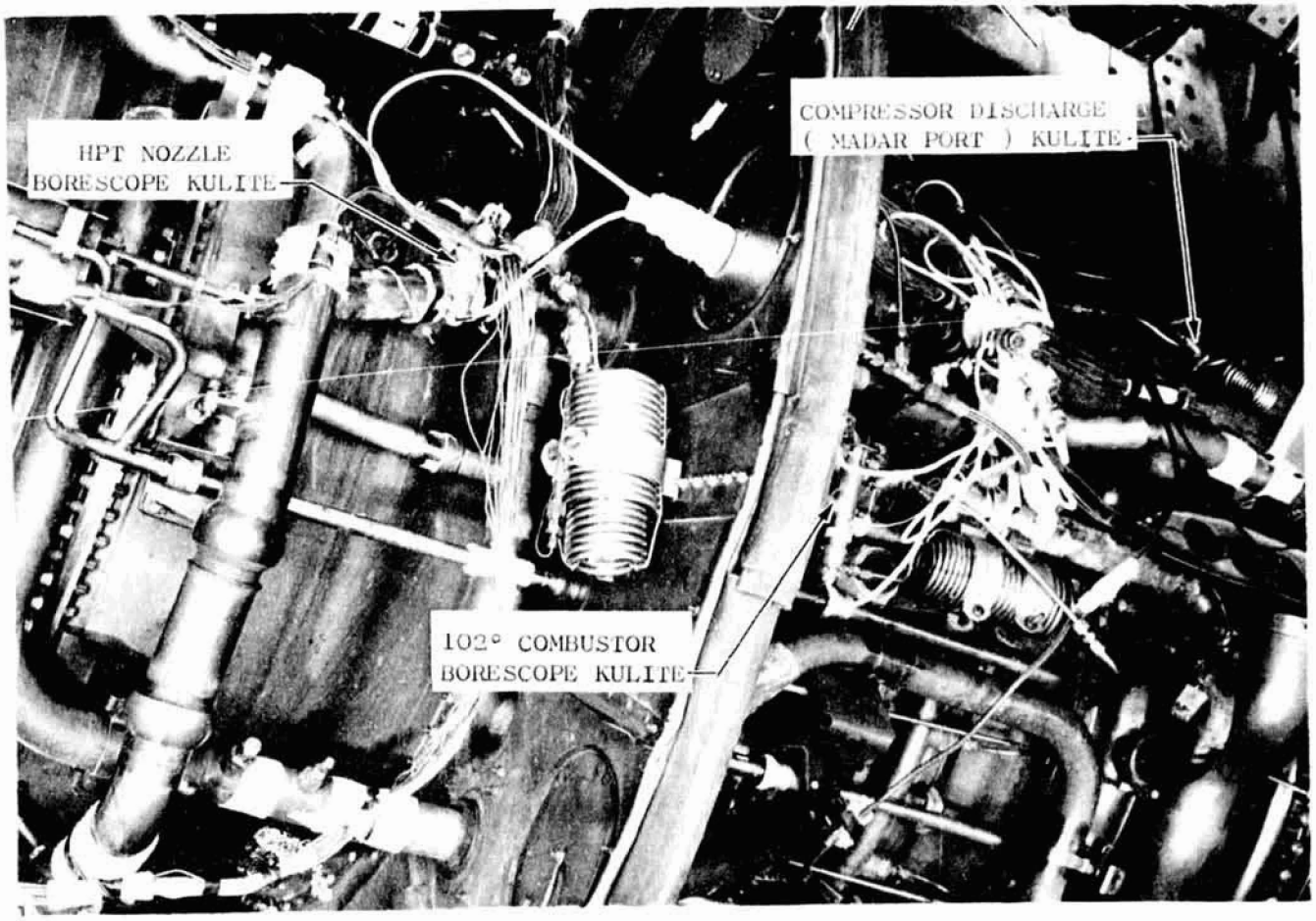

Figure 3-4. Kulite Sensor Installations For ECCP Phase III Acoustic Test (7708283)

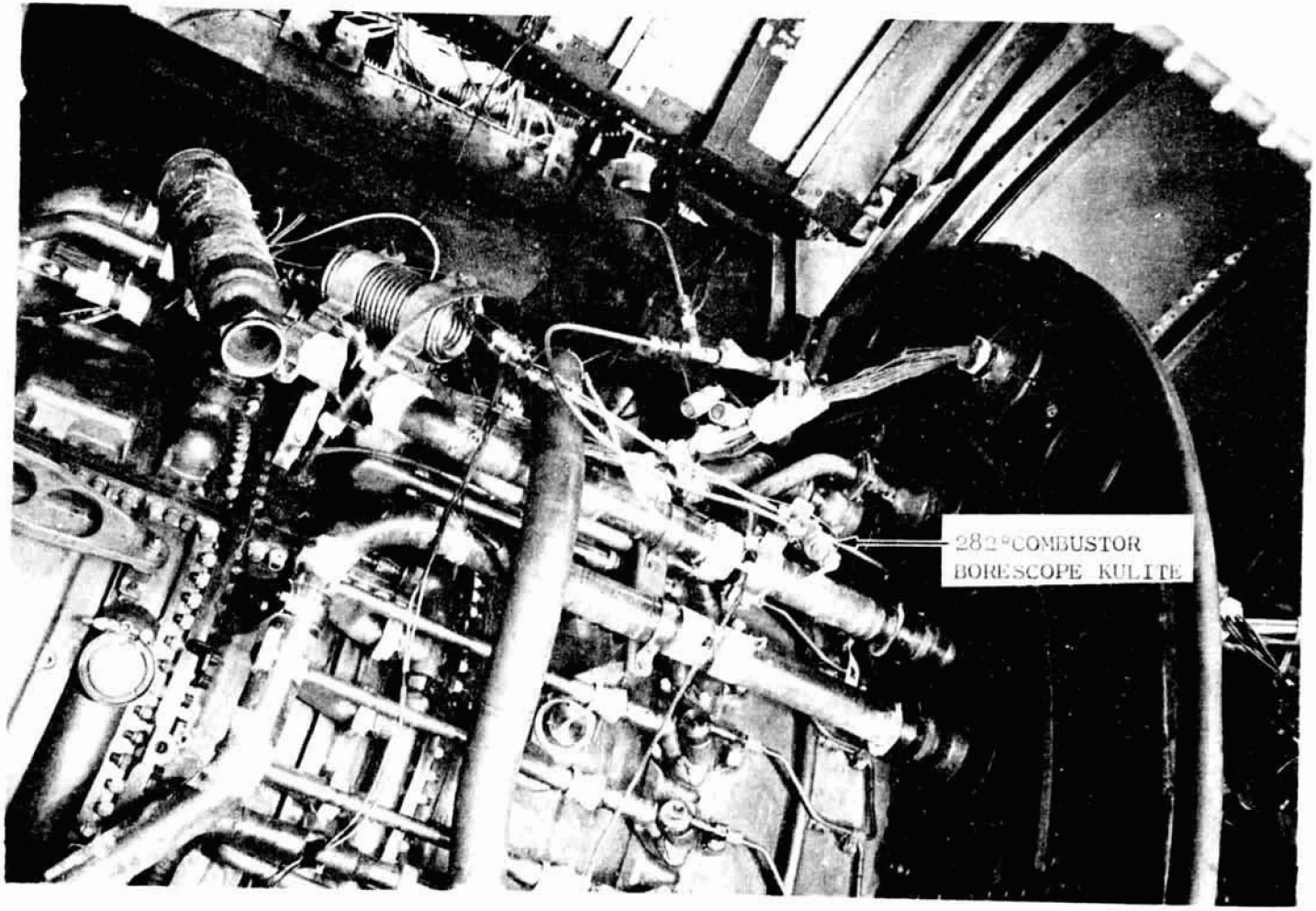

Figure 3-5. Combustor Borescope Kulite (282°) Sensor Installation For ECCP Phase III Acoustic Test (7708284)

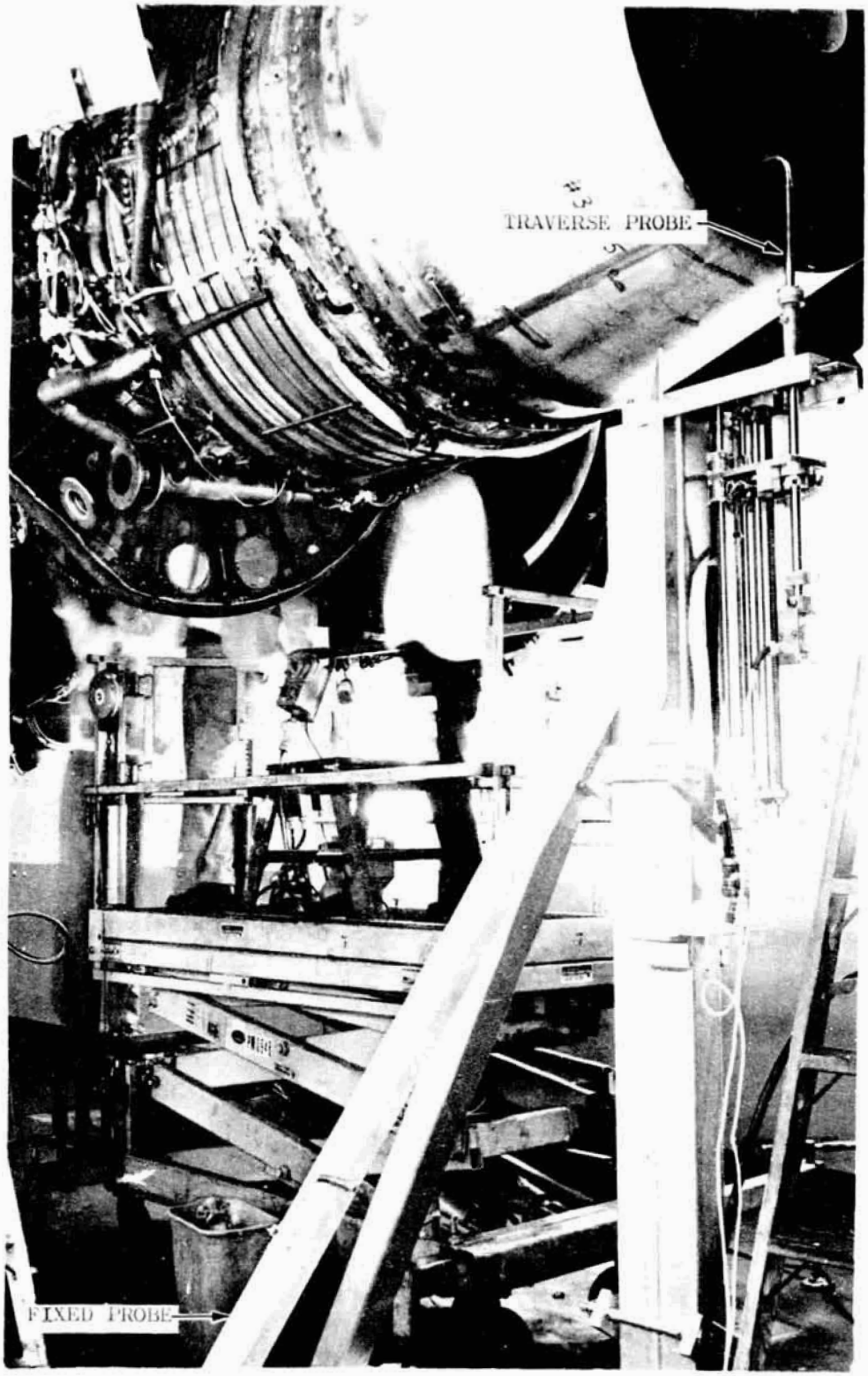

Figure 3-6. Setup of Core Exhaust and External Probes For ECCP Phase III Acoustic Test (7708286)

Table 3. Summary of ECCP Phase III Acoustic Test Conditions.

Fuel Splits	Nominal % F_n	Actual % F_n	N_c rpm	Plane 3.0 MADAR	Plane 3.5 102°	Plane 3.5 282°	Plane 4.0 HPTN	Plane 8.0 Core Probe A	Plane 8.0 Core Probe B	Cell Probe
100% Pilot	3.4	3.8	6376	X	X	X	X	X	X	
	19.8	19.7	8144	X	X	X	X	X	X	
	30.0	30.0	8645	X	X	X	X	X	X	
Fuel Split Between Pilot/Main Stages	30.0	29.7	8661	X	---	X	X	X	X	
	45.0	45.4	9125	(X)	X	(X)	○	○	(X)	
	65.0	64.6	9522	X	X	X	○	○	(X)	○
	85.0	82.0	9878	(X)	X	(X)	○	○	○	○
	100.0	94.6	10191	X	---	X	X	X	X	X

○ - Repeat Reading

probe systems located as illustrated in Figure 3-2. The internal measurements at the core nozzle exit were acquired with a dual-element sound separation probe with 12.7 cm axial spacing between sensors. Figure 3-3 shows this probe.

The waveguide sensors consisted of Kulite pressure transducers (XGE-1S-375-200D) AC-coupled and mounted in air-cooled tee-blocks. A capped 12.192 meter long semi-infinite coil was fitted to one end of the tee, while the other end of the tee was connected to a standoff tube approximately 30.48 cm long which was mounted to the engine to complete the system. The Kulite system excitation voltage was provided by a constant 10 VDC source. The output signal was amplified prior to recording on magnetic tape. Initial amplification was provided by the tape recorder preamplifiers which were set on constant gain settings. A second set of amplifiers in series with the preamplifiers had adjustable gain settings which provided the final signal boost ensuring the signal transmitted from the Kulite was well above the system noise floor.

The signals were recorded on a 28 channel Sabre IV magnetic tape recorder at 76.2 cm/s up to 10000 Hz. Approximately 1.5 to 2 min. of data were recorded at each test condition. Signal polarity was checked for all sensors prior to recording data. A spectrum analyzer connected in parallel with the tape recorder and coupled to an X-Y plotter enabled on-line 10 Hz narrowband spectra to be acquired during the test run. This provided a check of the measurements and an indicator of sensor signal validity. The spectrum analyzer did not, however, give a check on polarity. Figure 3-7 is a schematic illustration of the data acquisition system setup.

3.6.1 Kulite Waveguide Probe Pretest Calibration

Prior to recording data, the Kulite sensor calibrations were established for each recorder channel. Bench sensitivities determined for each Kulite sensor in the laboratory were used to setup the tape recorder calibration. The bench sensitivities and excitation voltage combinations were set with a dial-a-source voltage for a high pressure (0.68 atm) system used with the waveguide probes, and a low pressure (0.068 atm) system for the exhaust and cell probes. Gain setting adjustments were made on both sets of amplifiers to match a 4 volt peak-to-peak tape recorder input signal requirement. Once this was established an AC calibration from an electrical source was recorded on all channels which referenced each Kulite sensor level.

3.6.2 Frequency Response and Phase Calibration

Frequency response and phase calibrations at ambient conditions (room temperature) were performed on the Kulite sensors located in the combustor region (MADAR, 102°, 282° and HPTN borescope ports). This was done to account for probe losses resulting from the standoff tube length required on each sensor. The acoustic probe located in the core exhaust did not require calibration since the Kulites were flush mounted on the probe and previous calibrations showed a flat frequency response over the range of interest and up to 10 KHz.

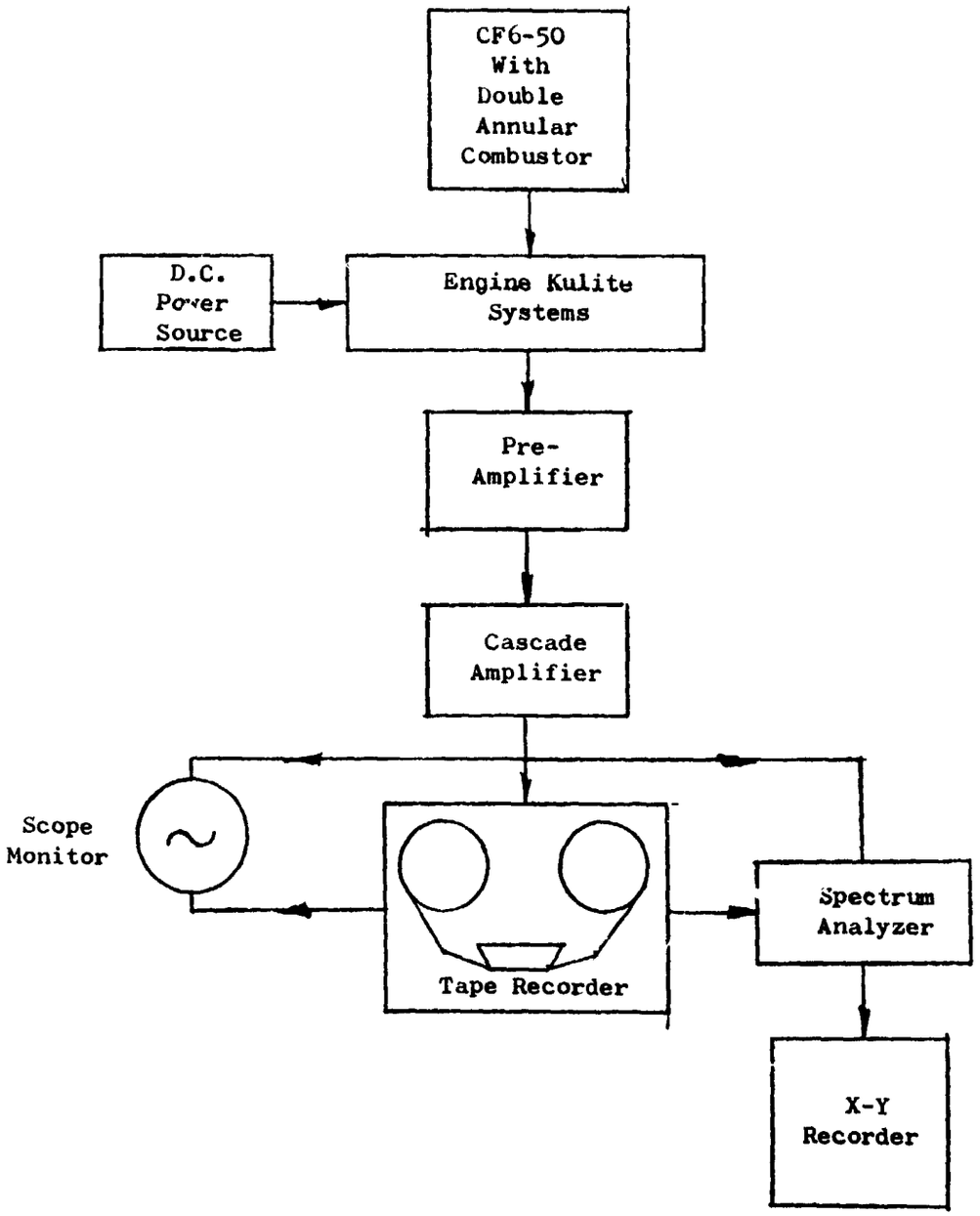

Figure 3-7. Schematic of Acoustic Data Acquisition System Setup

Calibration System

The apparatus setup for the frequency response and phase calibrations is as shown in the schematic of Figure 3-8. The calibration system consisted of a plane wave tube with sufficient tube length to dampen reflections in the frequency range of 100 to 5000 Hz.

At the test section, a flush mounted Kulite pressure transducer, type CQL-125-25D, was used as the reference. The test probe in each case was positioned at the same axial plane and displaced 90° from the reference. The Kulite excitation voltage was supplied by 6 volt batteries. The output of each system went through a low noise amplifier and then into the signal generating unit.

The monitor signal was a pure tone swept through the frequency range. The signal was supplied by a sweep oscillator which was controlled by a automatic level regulator and amplified by pre and power amplifiers before being fed into the speaker mounted at one end of the plane wave tube. The output of the sweep oscillator was connected to the X-axis (frequency scale) of an X-Y recorder.

The frequency response of the test probe and reference Kulite were measured consecutively with a dynamic analyzer. The output of each Kulite system was plotted on the Y-axis (dB scale) of the X-Y recorder. The sensitivity of each Kulite system was adjusted to measure the same level of sound pressure in the tube at the test section. This assured that both Kulites sensed the same signal in plane wave form.

Phase calibrations were performed with the use of a phase meter. The output signals of the reference and test probe Kulite were lead into the phase meter input channels, A & B, respectively. Adjustments to account for any electronic differences between the Kulite systems (sensitivities, etc.) were performed to ensure that the output signal plotted on the Y-axis (phase angle, deg.) represented the complete phase difference between the flush mounted reference and the test Kulite.

Limitations to the calibration system were as follows:

- Frequencies below 100 Hz were not attainable because of the danger of exceeding the speaker maximum voltage limitation.
- Ambient calibrations (frequency response and phase) do not represent actual test conditions unless the state properties are measured at the Kulite location. Care must therefore be used when applying ambient corrections (especially phase) to the hot test data.

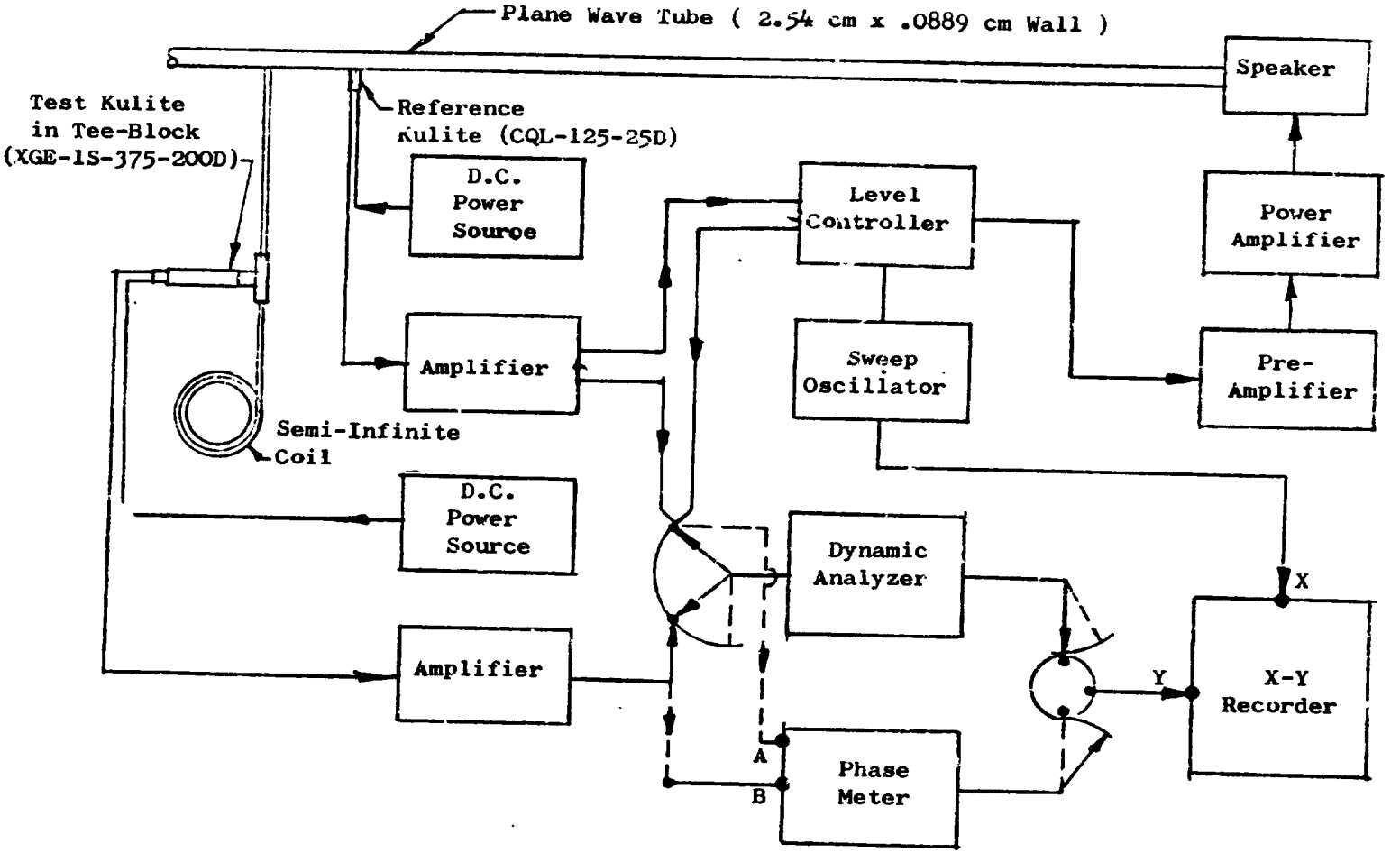

Figure 3-8. Calibration Setup For Waveguide Probes

Waveguide Probe Calibration Results

Two types of probe systems were calibrated. One system (System A) consisted of 0.635 cm OD, 0.00711 cm wall tubing and had a 33.02 cm long standoff tube. This system was used in the MADAR port and combustor borescope ports at 102° and 282°. The other system (System B) used in the HPT nozzle borescope port consisted of 0.635 cm OD, 0.01245 cm wall tubing with a 19.05 cm long standoff tube. Both types of systems used a standard tee Kulite mount fitted with an air-cooled jacket. All systems used a type XGE-1S-375-200D Kulite pressure transducer with the reference pressure tube pneumatically coupled to the semi-infinite coil mounted at the end of the probe.

The frequency response of the systems are shown in Figures 3-9a-c. The response of System A is shown in Figure 3-9a with a straight standoff tube and in Figure 3-9b with the curved tube as run on the engine. Both response curves are smooth to 1000 Hz with a loss of about 1.5 dB. At 2000 Hz they are down 2 dB while at 5000 Hz the loss is 3.5 and 4.5 dB, respectively. Agreement was excellent, showing no significant loss due to the curved tube, and the response was well within the specified requirements. The system response curves apply to the borescope Kulites at 102° and 282° also, since they were of the same configuration.

The HPT nozzle Kulite, System B, had a response as shown in Figure 3-9c. It is smooth to 1000 Hz with a drop of 2.5 dB at 2000 Hz. However, above 2000 Hz the dropoff rate increased to 7 dB at 5000 Hz which was attributed to the smaller diameter tubing required to fit into the physical constraint of the HPT nozzle borescope plug. Since the major portion of the frequency range below 3500 Hz had significantly less than a 5 dB loss there was no serious technical limitation on the data acquired with this sensor.

The response in the low frequencies (30-100 Hz) is flat from previous experience. Therefore, a smooth extrapolation of the response curve from 100 Hz to 30 Hz was performed to complete the curve.

The phase calibration of System A is shown in Figure 3-10a for the curved standoff tube configuration on the MADAR sensor. This is representative of the other System A Kulites (102° and 282° combustor borescope).

System B phase calibration in Figure 3-10b shows the phase to be smooth up to approximately 2500 Hz. Above that frequency, the results reflect those of the frequency response. However, the System B phase angle has a different linear relationship than that of System A causing the phase information from System B to be questionable.

The Kulite probe calibrations for both types of systems give a good representation of the frequency response and phase relationships for the ambient state. A tabulation of the frequency response corrections for each type of waveguide sensor are presented in Table 4.

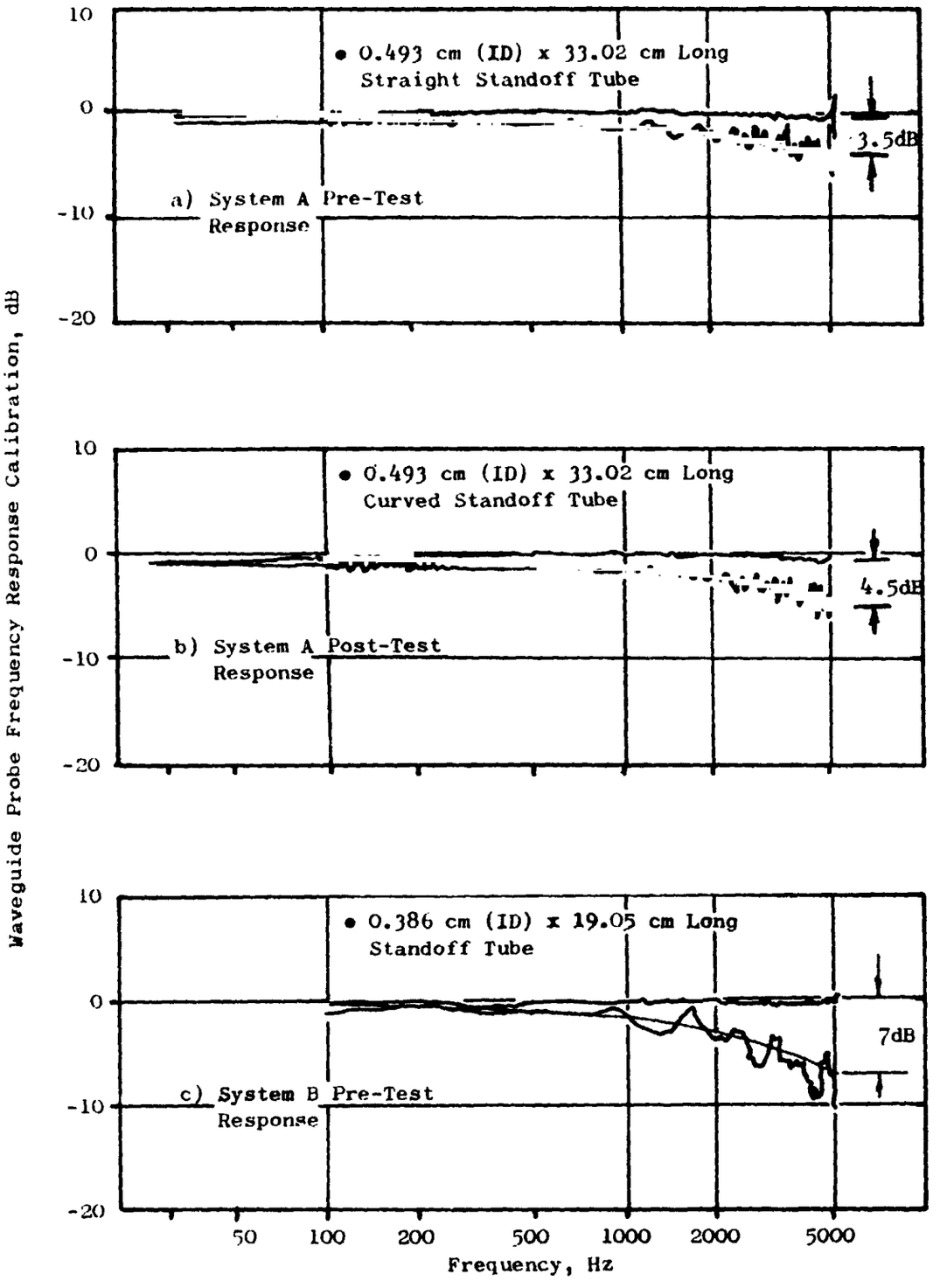

Figure 3-9. Frequency Response of Waveguide Probe Systems

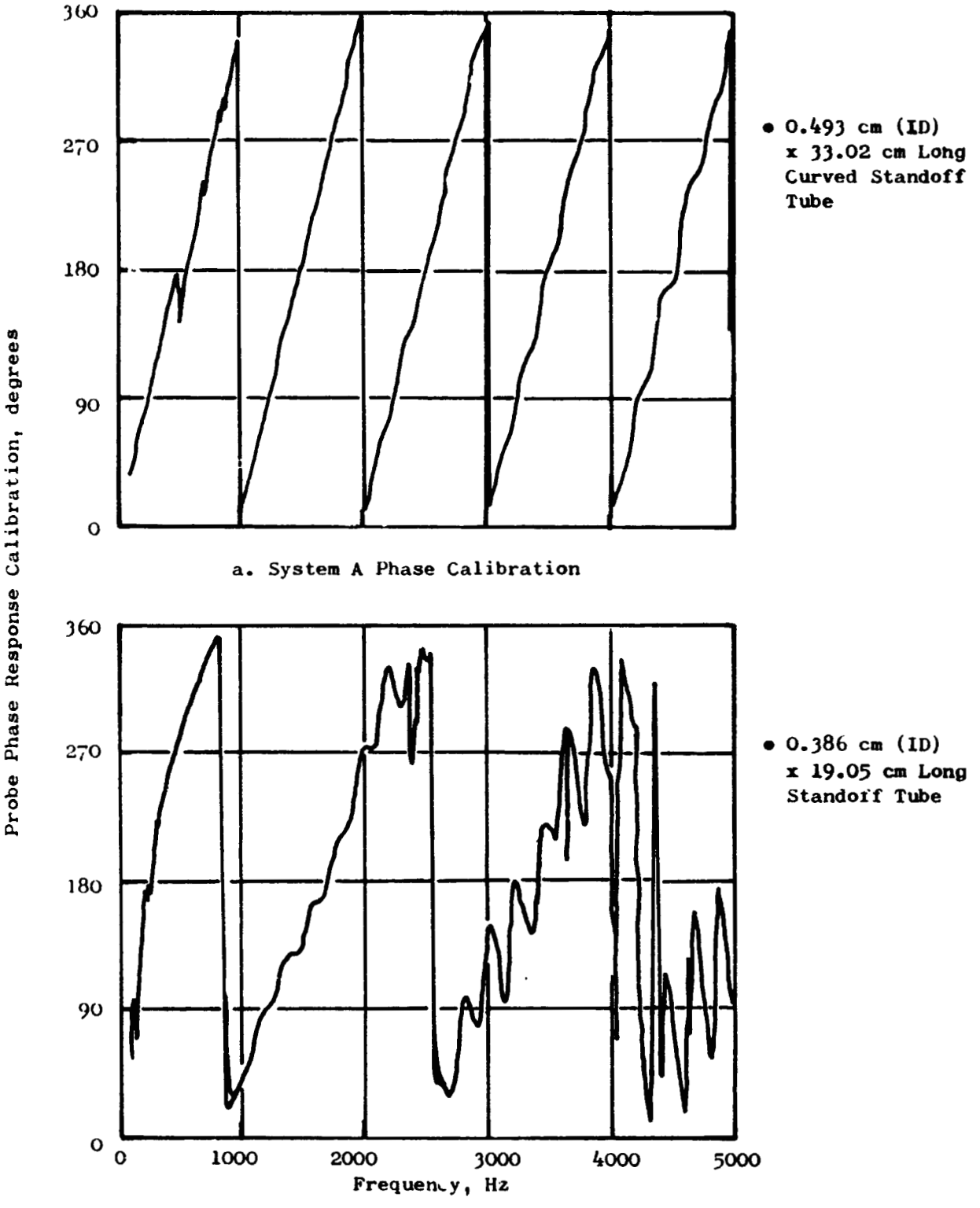

Figure 3-10. Ambient Phase Calibrations of Waveguide Probe Systems

Table 4. Ambient Frequency Response Corrections for ECCP Phase III Waveguide Sensors.

Frequency Hz	Planes 3.0 and 3.5 (0.492 cm ID System)	Plane 4.0 (0.386 cm ID System)
31.5	0	0
40	0	0
50	0	0
63	0	0
80	0.2	0
100	0.5	0
125	0.6	0
160	0.75	0
200	1.0	0.2
250	1.0	0.2
315	1.0	0.2
400	1.0	0.5
500	1.0	1.0
630	1.0	1.0
800	1.2	1.0
1000	1.5	1.0
1250	1.6	1.2
1600	1.8	1.5
2000	2.0	2.5
2500	2.0	3.5
3150	2.5	4.0
4000	3.5	5.8
5000	4.5	7.0

- Applied to Measured 1/3 Octave Band Values

3.7 DATA REDUCTION AND PROCESSING

3.7.1 Description and Implementation of Techniques

Several different techniques were employed in the reduction of the acoustic data from the engine test. Among these were narrowband and 1/3 octave band spectral analysis, and digital fast Fourier transform techniques of coherence analysis and cross-correlation analysis.

Narrowband Spectral Analysis

Narrowband spectral analysis consists of investigating a small segment of the acoustic energy using a constant bandwidth filter. On-line 10 Hz bandwidth spectra was obtained from a conventional spectrum analyzer for frequencies from 0 to 2500 Hz with sample times of 0.1 sec and 32 averages to yield a total analysis record length of 3.2 seconds. Considerably finer resolution was obtained using a digital fourier transform analyzer. The spectra obtained from this system at frequencies from 0 to 2000 Hz was of 2 Hz bandwidth at sample times of 0.1 sec and employed 100 to 150 averages to yield a total analysis record length of 10 to 15 seconds. The high resolution narrowband spectra obtained for each Kulite sensor were used to assist in evaluating trends from the internal pressure measurements. Fluctuating pressure level (FPL) was used instead of sound pressure level (SPL) since the pressure signal contains turbulence in addition to sound. Plots of the narrowband spectra for the working sensors from all eight test conditions are found in Appendix A.

One-Third Octave Band Spectral Analysis

The 1/3 octave band spectra were processed from the recorded data by standard techniques for frequencies of 50 through 2000 Hz. Overall pressure levels were computed from the resulting spectra which were corrected for probe response losses. The 1/3 octave band FPL spectra (1/3 OBFPL) determined for the eight test conditions were used for evaluating the combustor internal measurement trends and for comparisons with the ECCP Phase I and II component spectra results. Tabulations and plots of the 1/3 OBFPL results are presented in Appendix B. The overall fluctuating pressure level (OAFPL) obtained from these 1/3 OBFPL spectra were used to determine the measured power level ($FPWL_{meas}$) assuming the total pressure signal was acoustic.

Coherence Analysis

Coherence analysis is a measure of the amount of similarity or coherence between two signals in the frequency domain. Pressure signals generated upstream in the combustor and received downstream of the turbine contain frequencies which have the same or similar characteristics as the upstream signal. The coherent portion of the downstream spectrum is considered to be mostly sound if the signal falls above the noise floor established for an uncorrelated random signal input. Coherent 1/3 OASPL spectra were used to

determine the turbine transfer function between upstream and downstream Kulites in the CF6-50 engine. The coherent spectra at Plane 4 (turbine inlet) were obtained relative to Plane 3.5 (combustor inlet). Similarly, the coherent spectra at Plane 8.0 (core nozzle exit) were obtained relative to Plane 3.5. The turbine attenuation was computed from the difference between the Plane 4.0 and Plane 8.0 coherent spectra. Processing of the coherent spectra was done with a constant number of averages (50) for all sensor pairs. The noise floor between the raw and coherent spectra was an average of 18 dB below the raw signal for the 50 to 2000 Hz frequency range.

The noise floor of the coherent spectral analysis procedure was determined using an independent random noise source directly into the analyzer from a white noise signal generator as the input sensor signal. The coherent spectral analysis was performed using the fluctuating pressure signal as the output sensor.

The coherent spectra displayed represents that portion of the input signal that is apparently coherent with the output signal. For a completely independent input the signals are completely incoherent which would result in a zero dB coherent spectrum using an unlimited number of averages. However, the data analysis procedure used for this program was limited to the number of averages dictated by the length of the sample. The sample length was designated by the 1.5 to 2 min recording time at each data point. The number of averages were set at 25 for the cross-correlation analysis and 50 for the coherence analysis. The coherent noise floor due to the limited number of averages for each sensor was approximately 18 dB below the raw signal. This can be seen in Figure 3-11 which shows the typical results of the coherence analysis at the output sensor location using the 50 averages and an uncorrelated input signal.

The electronic noise floor of the data acquisition system (Kulite sensors, amplifiers and tape recorder) was checked prior to each test by recording an "ambient" reading with the engine off. Comparisons of these ambient readings with the data runs indicated the spectra of the noise floor to be 25 to 30 dB below the level of the data at the idle power setting and 40 to 50 dB below the data at the higher power settings. The electronic noise floor did not present a problem in the analysis of the data.

The majority of the coherent spectra frequencies below 1000 Hz were above the noise floor for the low power settings below 45% F_n. The coherent spectra above 800 Hz were affected by the noise floor at almost all test conditions. A 3 dB reduction in the noise floor level requires doubling the number of averages from 50 to 100. The coherent spectra at the high frequencies could be 6 dB or more below the noise floor which would require a greater number of averages than the 90 sec to 130 sec sample time available. The attenuation results from this present study are concentrated primarily between frequencies of 100 to 800 Hz. Previous attenuation data were obtained (Reference 6) between 100 to 1200 Hz.

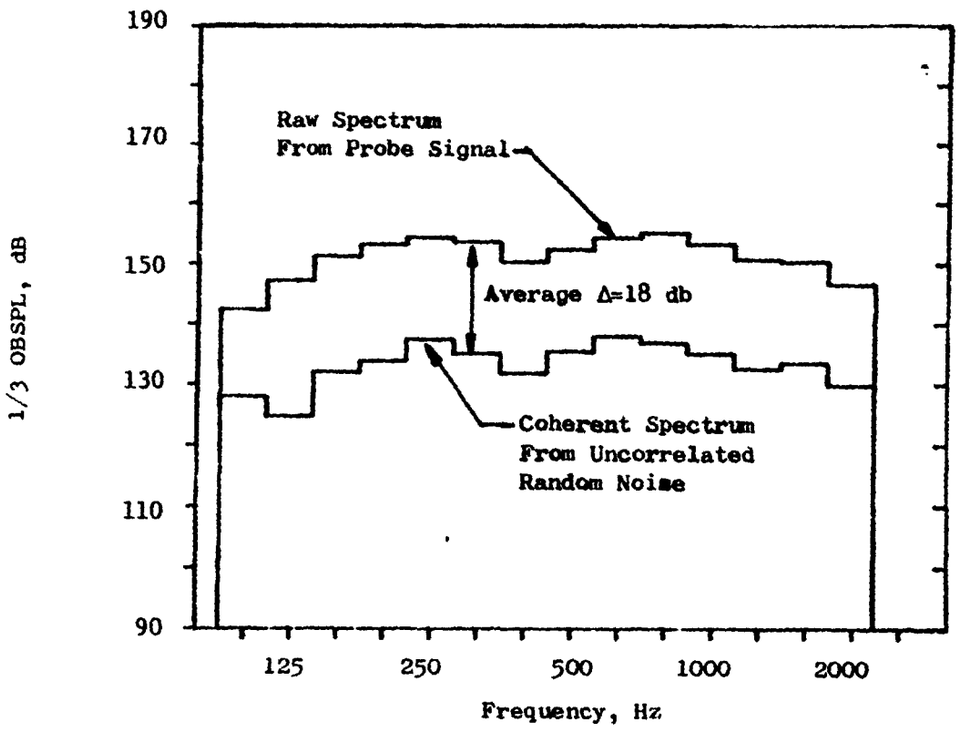

Figure 3-11. Noise Floor of Coherent Spectrum

Negative time delays in the cross-correlation of Kulite pairs were not directly incorporated into the coherent spectra results, since the analysis only handles positive time delays. The bias errors due to these negative time delays were computer from the method detailed in Reference 7. The bias error calculating procedure pertinent to the analysis method used during this program is found in the appendix of that paper. Typical negative delay times ranged from -0.0015 to -0.007 seconds which corresponded to errors in coherent spectra level of 0.1 to 0.6 dB greater level. These differences were subtracted from the overall coherent spectra levels. Appendix C presents the coherent spectra plots used to determine the turbine transfer function on the CF6-50 engine.

Cross-Correlation Analysis

While spectral analysis consists of examination of a signal content in the frequency domain, correlation analysis may be thought of as an analogous inspection in the time domain. Cross-correlation analysis is a measure of the propagation-time-delay characteristics of signal transmission. In cross-correlation, one signal is compared with a time-delayed second signal to determine the amount of similarity between the two signals. By this technique, time delays associated with acoustic and turbulent signals over short distances can be identified and their relative strengths determined from the amplitudes of the normalized correlation coefficient, R_{xy}. For example, Figure 3-12 displays the cross-correlation between two axially spaced sensors located in a flow. The cross-correlation function displays several peaks. The largest peak (R_{xy} = 0.75) is representative of a signal propagating at this speed of sound relative tc the flow and corresponds to the acoustic perturbations. Two similar peaks, smaller in magnitude (R_{xy} = 0.18), but with opposite time delays are noted on the figures. The positive time delay is a signal convected by the flow and corresponds to the turbulence. The negative time delay represents a signal travelling upstream at a velocity corresponding to the difference between the flow and acoustic velocities.

With large spacings between sensors, (distances much greater than the quarter wavelengths of the frequencies of interest) only the acoustic signal is well correlated. The turbulence is less correlated. In this case, the peaks observed will be primarily acoustic. This is typical of cross-correlations between combustor sensors and the downstream probes.

3.7.2 Data Processing

Frequency Response Corrections

The acoustic data acquired during the combustor test was corrected on a 1/3 OBFPL basis by the ambient frequency response determined from room temperature calibrations. The ambient response corrections applied to the measured data (between 50 to 2000 Hz) acquired from the waveguide sensors are presented in Table 4.

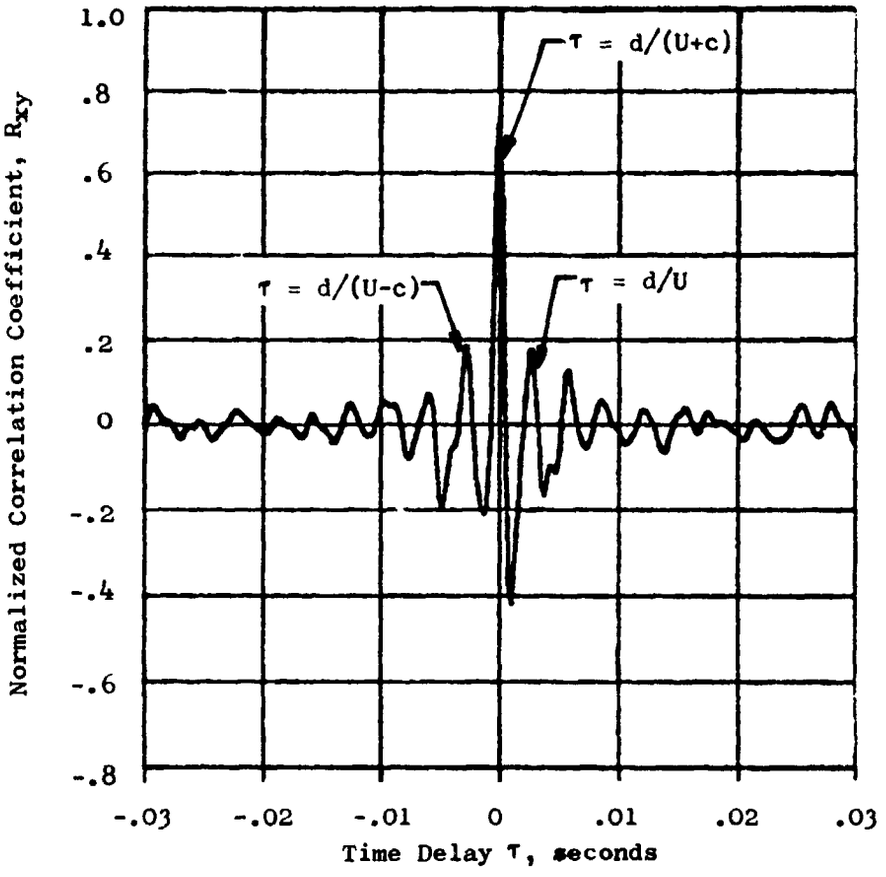

Figure 3-12. Typical Cross-Correlation Function for Flow with Sound Dominant

The effect of elevated temperature and pressure on the response correction was evaluated. Appendix D gives the details of the evaluation which is based on the transmission loss due to viscous damping within a tube of circular cross-section assuming no internal reflections and no non-linear effects associated with sound pressure levels above 120 dB. The waveguide sensors in the combustor region were located under the engine cowling where the volume of air may be considered to reach a sink temperature of about 477.8K forward of the firewall and 533.3K in the aft regions. Using this temperature (477.8K) and the static pressure at Plane 3.0 and 3.5 of 26 atm for the takeoff condition the transmission loss of the 2000 Hz frequency was determined and compared to the transmission loss calculated from the ambient calibration conditions. The result showed the loss at elevated conditions to actually be smaller than the ambient calibration loss by approximately a ratio of 4 to 1. Comparing these calculated results to the actual ambient response loss of 2 dB at 2000 Hz suggests that the actual loss was approximately 0.5 dB. Since 2000 Hz was the upper limit of our spectral comparisons and the lower frequencies had much lower losses (1 to 1.5 dB) any correction for elevated conditions would be in fractions of a dB and in the order of measurement accuracy. Therefore, the ambient response corrections were applied to the data.

The phase calibrations determined for the waveguide sensors for the ambient calibrations were not applied to the data at elevated conditions since there was no way of determining the temperature gradient in the sensor tube without extensive measurement. Instead, the time delay between the pairs of sensors used in cross-correlation analysis was removed which effectively accounted for the phase differences between the pairs of sensors. Similarly, the same consideration was applied during the coherence analysis between pairs of sensors in determining the transfer function across the turbine.

Exhaust Probe Level Corrections

The exhaust probe Kulite A and B spectra were checked for SPL level and spectral shape. Both Probe A and B had similar spectral shapes as would be expected since the Kulites were on the same probe separated by a 12.7 cm axial spacing. The Probe B level was consistent for the majority of the points on both test runs which included repeat readings that gave the same result. The signal levels of Probe A matched those of Probe B for one run but were higher for the second run, making the Probe A data suspect. An adjustment of -6 dB corresponding to an amplifier attenuation change was applied to Probe A to realign the data with Probe B. The Probe A narrowband spectra reflect this corrected level.

Power Level Calculation

The measured power level, $FPWL_{meas}$ was calculated at each measurement plane assuming the entire fluctuating pressure measurement was acoustic signal propagating in a plane wave axially through the engine. The power

level was calculated using Blokhintsev's results (as noted in Reference 6), for the acoustic intensity flux vector which can be written:

$$\vec{I} = \frac{p^2}{\rho c^3} (c + \vec{V}\,\hat{e}_p)\ (c\,\hat{e}_p + \vec{V}) \qquad (1)$$

P, ρ and c are used in the conventional sense, where $\vec{V}$ is the absolute flow velocity and $\hat{e}_p$ the unit vector normal to the acoustic wave front.

We are interested primarily in the axial component, hence

$$I_x = \vec{I} \cdot \hat{e}_x$$

$$= \frac{p^2}{\rho c^3} (c + \vec{V} \cdot \hat{e}_p)\ (c\,\hat{e}_p + \vec{V}) \cdot \hat{e}_x$$

$$= \frac{p^2}{\rho c}\ (1 + M \cos\theta)\ (\cos\theta + M \cos\phi) \qquad (2)$$

where θ and ϕ are the angles made by the acoustic wave front and the flow with the axial direction. M is the flow Mach number. The flow at the measuring planes is near axial and if a plane wave assumption is used here,

$$I_x = \frac{p^2}{\rho c}\ (1 + M)^2 \qquad (3)$$

The plane wave assumption also permits the acoustic power to be computed from a measurement at any point of the cross-section. Using a consistent set of reference pressure (P_o) and specific impedance ($\rho \cdot c_o$), the acoustic power level (PWL referenced to 10^{-13} Watts) is given by:

$$PWL = SPL + 20 \log (1 + M) + 10 \log \left(\frac{\rho_o c_o}{\rho c} \right) + 10 \log A + 9.9 \qquad (4)$$

or

$$PWL = SPL + 20 \log (1 + M) + 10 \log \left(\frac{P_o}{P_S} \sqrt{\frac{T_S}{T_o}} \right) + 10 \log A + 9.9 \qquad (5)$$

were SPL = sound pressure level re 2×10^{-5} N/m^2

P_S, T_S = static pressure and temperature at the measuring station

P_o, T_o = ambient (standard day) pressure and temperature

A = cross-sectional area in m^2.

3.7.3 Engine Test Internal Measurements Verification

Checks on Measurement Level

Several cross checks of the data obtained during the CF6-50 engine test were performed to ensure the validity of the fluctuating pressure levels determined. These included on-line 10 Hz narrowband spectra compared with the same data processed posttest through the narrowband spectral analyzer; comparison of P_{S3} levels obtained during emissions testing with acoustic test results; and checks of peak-to-peak pressure levels obtained on similar engine tests. The levels agreed in each case within ±1.5 dB.

The probe overall FPWL (re 10^{-13} watts) for the engine test was compared to farfield power levels determined from unpublished data from previous tests on CF6-50 engines to evaluate the region of core noise dominance. The PWL was calculated for the low frequencies (50 to 2000 Hz) at which core noise would be manifested at each test condition encompassing the operating range of the engine. The PWL were plotted against an effective jet velocity of the fan and core exhaust streams. This velocity, V_e was determined from the fan bypass ratio BPR and jet velocities of the fan and core streams using:

$$V_e = \frac{(BPR)\ V_f + V_c}{BPR + 1} \qquad (6)$$

The results of the comparison are shown in Figure 3-13 and indicate the region of core noise dominance at V_e below 230 m/s. Above this velocity the jet noise overtakes and dominates the overall power level. This trend is as expected and parallels closely the results of Reshotko (Reference 8).

Internal pressure measurements taken in the core exhaust during the present tests with the sound separation probe were obtained at five immersions located on centers of equal areas across the annulus of the core exhaust nozzle. Comparisons of PWL calculated from the average SPL spectra from the five immersions agreed very well with the PWL calculated using the pitchline or center immersion and the total annulus area illustrated by the power level spectra comparison in Figure 3-14. The comparison is for the approach (30% F_n) condition, but is also typical of the other test conditions. The data presented for the exhaust probe in the analysis section of this report are based on pitchline immersion measurements.

Aerodynamic Acoustic Readings

The aero performance parameters required by the ECCP Phase III contract are listed in Table 5 for the eight test conditions. These parameters were obtained from the engine performance program readings obtained from this ECCP Phase III tests. The detailed calculation procedure for the majority of these parameters are found in Reference 1. Other aerodynamic parameters associated with the overall power level calculations are presented in Table 6. Included in the table are the static pressures and temperatures determined

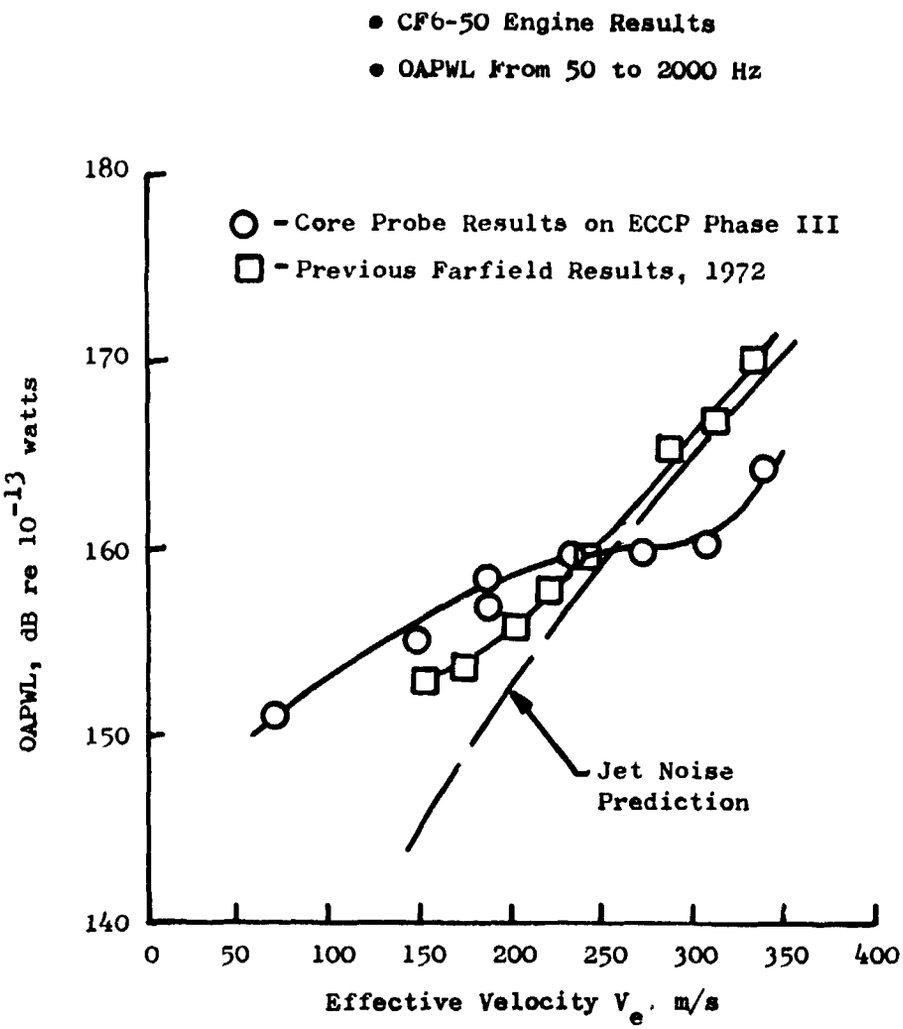

Figure 3-13. Comparison of Core Probe Power Levels with Farfield Measurements

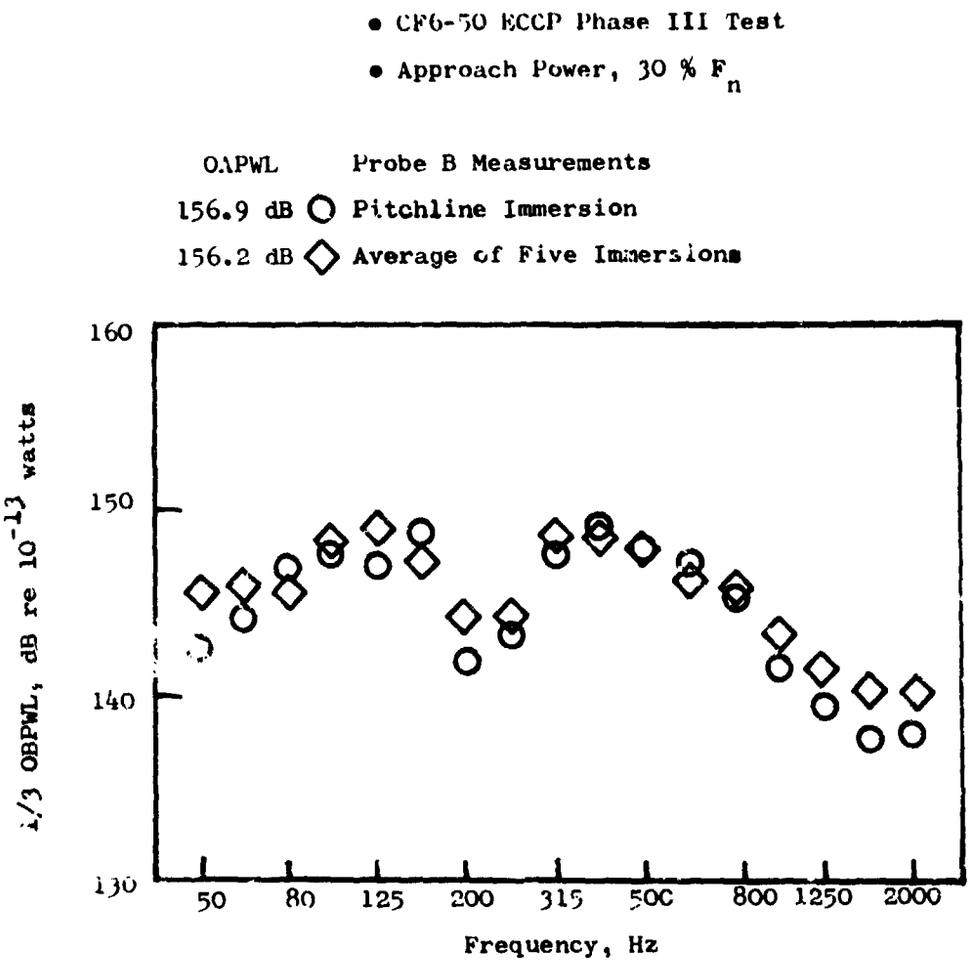

Figure 3-14. Core Exhaust Power Level Spectra Comparison

Table 5. ECCP Phase III Program Aerodynamic Performance Summary.

- Acoustic Test, 1977

Test Pt.	PCT Net Thrust	Aero Rdg	Acoustic Tape Rdg	N_c rpm	N_f rpm	P_o atm	T_o K	P_{T3} atm	P_{S3} atm	T_{T3} K	W_3 kg/sec	W_{36} kg/sec	$\left(\frac{W_{36}\sqrt{T_{T3}}}{P_{T3}\ A_3}\right)$ $\frac{kg\ \sqrt{K}}{sec\text{-}atm\text{-}m^2}$	V_r m/s	WFT kg/hr
1	3.8	147	6	6376	877	0.981	296.7	2.95	2.86	442.8	14.9	12.5	892.7	16.9	699.9
2	19.7	149	16	8144	1952	0.978	297.2	8.23	7.96	586.7	39.2	32.9	969.4	21.2	1843.4
3	30.0	151	23	8645	2384	0.976	298.3	10.94	10.61	641.1	43.8	36.8	852.7	19.4	2728.4
4	29.7	119	39	8661	2393	0.976	298.3	11.48	11.19	642.8	53.6	45.0	995.0	22.2	2698.9
5	45.4	154	28/34	9125	2847	0.974	300.6	15.15	14.69	709.4	67.0	56.2	989.2	23.8	3938.6
6	64.6	163	13/40	9522	3223	0.976	293.9	19.66	19.07	749.4	83.9	70.5	982.8	24.2	5617.4
7	82.0	156	18/43	9878	3506	0.970	301.1	23.38	22.67	808.3	95.5	80.3	977.6	25.0	7315.2
8	94.6	107	33	10191	3726	0.971	298.3	26.95	26.27	830.6	105.8	88.5	951.8	25.3	8814.4

Test Pt.	PCT Net Thrust	Aero Rdg	Acoustic Tape Rdg	PCT Out	PCT In	FAR_{36} k_{gf}/k_{ga}	P_{T4} atm	T_{T4} K	ΔP_{T34} atm	$\frac{\Delta PT}{PT3}$ PCT	ΔT_{43} K	HRR kw	P_{T8} atm	T_{T8} K	η_b
1	3.8	147	6	100	0	0.01555	2.85	1042.8	0.102	3.5	600	27.15	0.987	672.2	98.55
2	19.7	149	16	100	0	0.01555	7.89	1170.0	0.340	4.13	583.3	71.52	1.048	693.3	99.57
3	30.0	151	23	100	0	0.02060	10.51	1374.4	0.429	3.91	733.3	105.85	1.096	711.7	99.60
4	29.7	119	39	46.9	53.1	0.01664	10.98	1256.7	0.504	4.39	613.9	104.71	1.102	712.8	97.24
5	45.4	154	28/34	17.0	83.0	0.01944	14.46	1403.9	0.687	4.55	694.4	152.80	1.191	763.9	99.65
6	64.6	163	13/40	17.8	82.2	0.02213	18.76	1521.7	0.885	4.48	772.2	217.93	1.313	802.2	99.92
7	82.0	156	18/43	17.5	82.5	0.02530	22.35	1647.2	1.034	4.43	838.9	283.80	1.429	873.9	99.96
8	94.6	107	33	12.6	87.4	0.02754	25.76	1733.3	1.184	4.39	902.8	341.96	1.565	908.9	99.96

Table 6. Summary of Local Static Conditions for Combustor Test.

				Plane 3.0			Plane 3.5			Plane 4.0			Plane 8.0		
Aero Rdg	Tape Rdg	PCT Net Thrust	N_c (rpm)	P_{S3} (atm)	T_{S3} (K)	$\bar{M}_3$	$P_{S3.5}$ (atm)	$T_{S3.5}$ (K)	$\bar{M}_{3.5}$	P_{S4} (atm)	T_{S4} (K)	M_4	P_{S8} (atm)	T_{S8} (K)	M_8
147	6	3.8	6376	2.86	439.4	0.16	2.86	449.4	0.04	2.40	976.7	0.52	0.98	671.1	0.086
149	16	19.7	8144	7.97	597.8	0.16	7.97	597.8	0.04	6.36	1103.9	0.53	0.98	679.4	0.316
151	23	30.0	8645	10.61	641.7	0.16	10.61	641.7	0.04	8.82	1234.4	0.54	0.98	688.3	0.413
119	39	29.7	8661	11.19	647.2	0.16	11.19	647.2	0.04	8.82	1234.4	0.54	0.98	688.3	0.418
154	28/34	45.4	9125	14.69	715.6	0.16	14.69	715.6	0.04	11.83	1303.9	0.55	0.97	720.6	0.548
163	13/40	64.6	9522	19.07	741.1	0.16	19.07	741.1	0.04	15.42	1448.3	0.55	0.96	734.4	0.675
156	18/43	82.0	9878	22.67	825.0	0.16	22.67	825.0	0.04	18.20	1553.3	0.55	0.96	778.9	0.778
107	33	94.6	10191	26.27	830.6	0.16	26.27	830.6	0.04	20.97	1634.4	0.55	0.95	789.4	0.867
Plane Areas (m^2)				9.988×10^{-2}			26.829×10^{-2}			8.002×10^{-2}			63.478×10^{-2}		
Reference Area (m^2)				37.287×10^{-2}											

from isentropic relationships along with an estimate of the local Mach number at each measurement plane.

The eight conditions listed in the tables were obtained from two engine runs on consecutive days. Repeat readings taken during the engine test served a dual purpose of establishing a check for data repeatability and providing a replacement source for sensor measurements lost due to equipment problems at the same test condition.

The low nominal power settings (3.4, 19.8, and 30% F_n) have a full compliment of measurements at all planes. Repeat readings were used in combination with the initial readings taken at 45, 65, and 85% F_n to obtain a full set of measurements at each plane for these conditions. At takeoff (100% F_n) and approach power with the 50/50 split fuel flow (29.7 % F_n), measurements were obtained at each plane; except for the redundant sensor 102° at Plane 3.5.

Cell probe measurements were acquired at all test conditions. However, only the data at 65% F_n and above are presented since the levels below this condition were in the system noise floor. Cell probe narrowband spectra are included in the spectra plots of the 65, 85 and 100% F_n points found in Appendix A.

Comparison of the measurements acquired during the initial and repeat readings was excellent as can be attested by the following 2 Hz narrowband FPL spectra comparisons for the nominal power settings of 45, 65 and 85 percent thrust.

Figure 3-15a-c shows the MADAR, 282° borescope and exhaust Probe B spectra comparisons for separate readings at 45.6% F_n taken on the different days. Agreement is good at all planes compared.

Figure 3-16a and b illustrates the excellent agreement obtained from separate readings at 64.6% F_n for the MADAR Probe and core exhaust Probe B.

At 82% F_n, the MADAR comparison in Figure 3-17a and the 282° borescope probe comparison in Figure 3-17b also show exceptually good agreement at the different readings. These examples serve to substantiate the rationale for combining the initial and repeat readings in order to form the 1/3 OBSPL spectra tabulations at the eight test conditions.

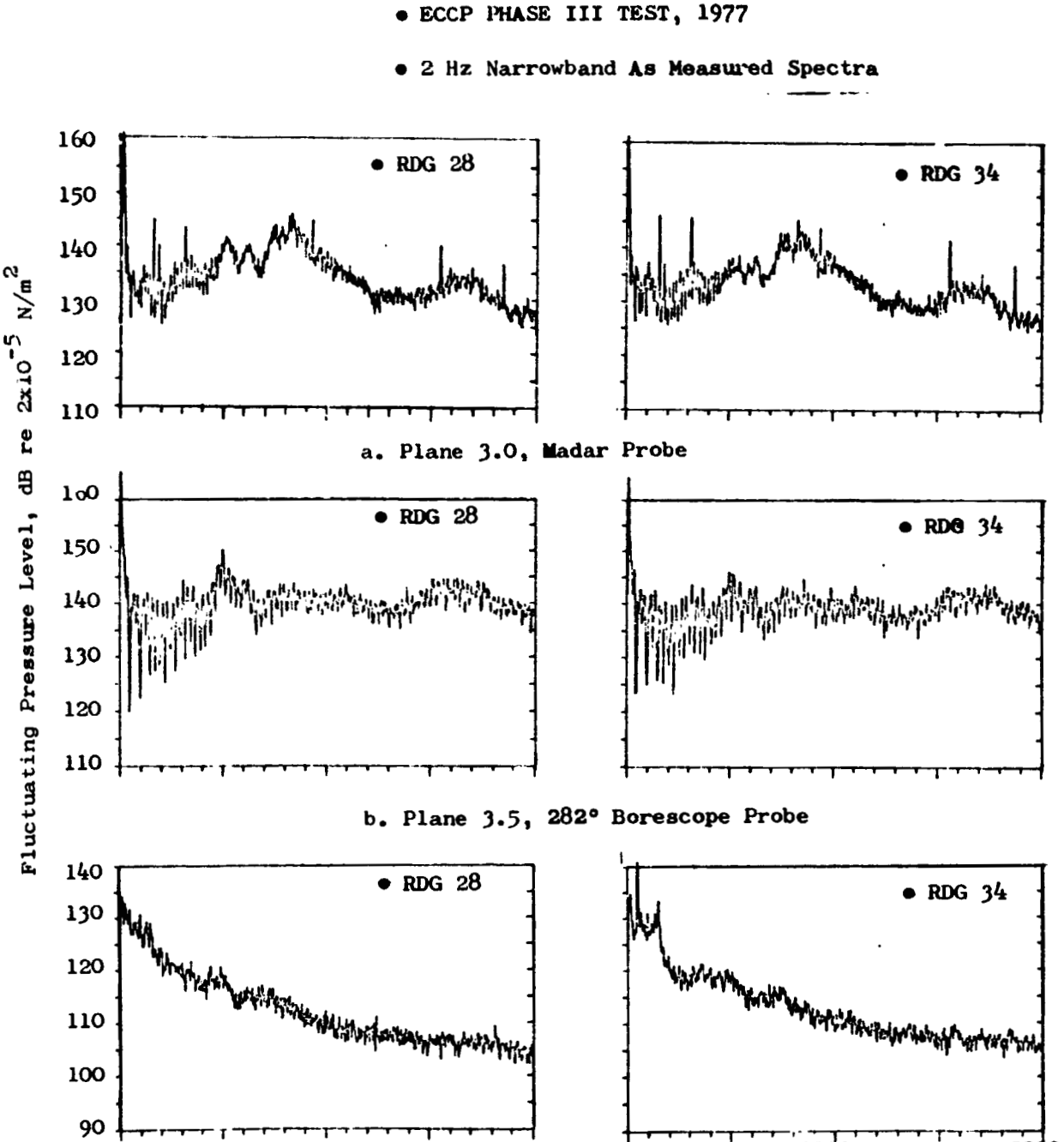

Figure 3-15. Comparison of Common Measurements For Repeat Readings at 45.4 Percent Thrust

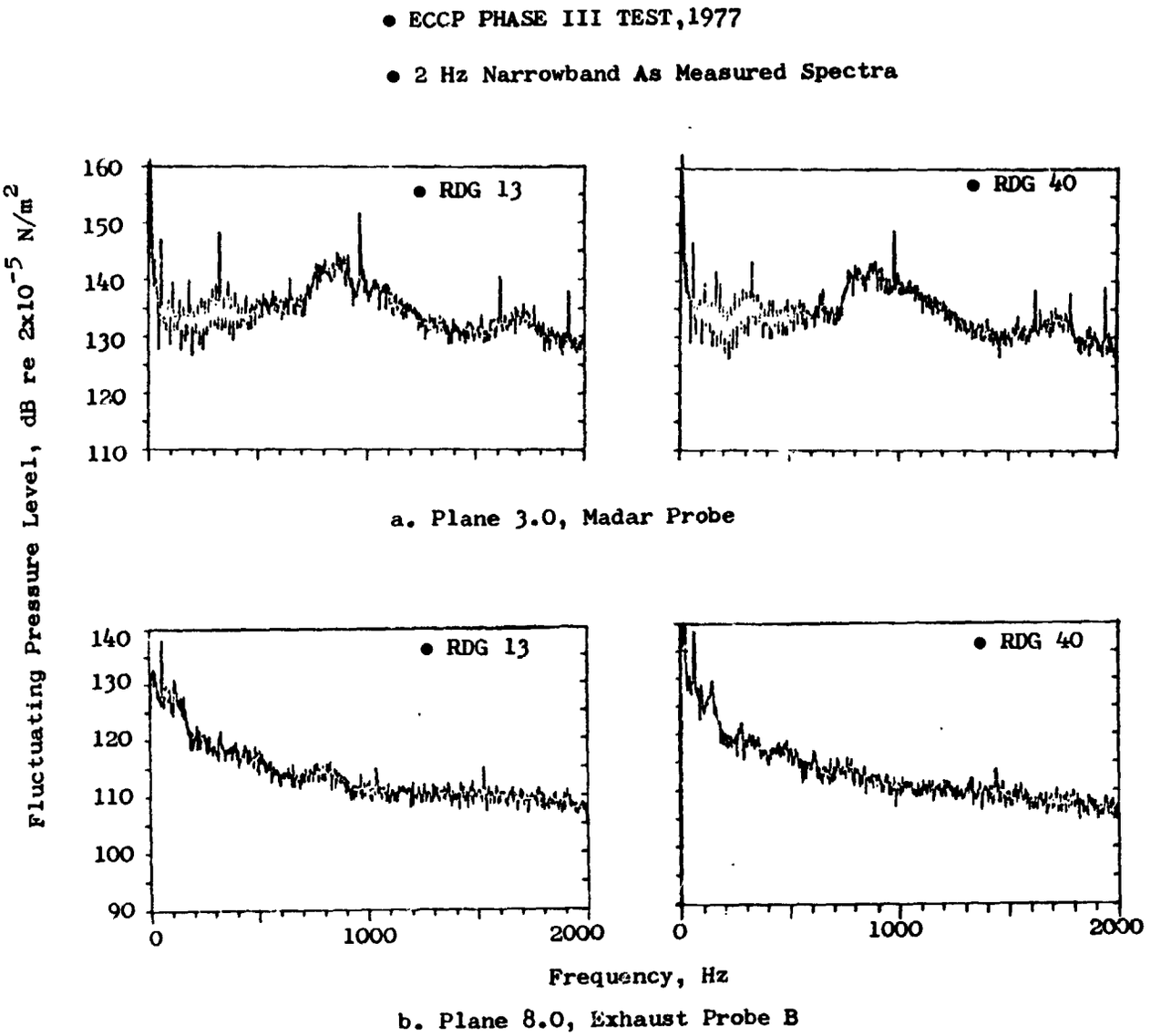

Figure 3-16. Comparison of Common Measurements For Repeat Readings at 64.6 Percent Thrust

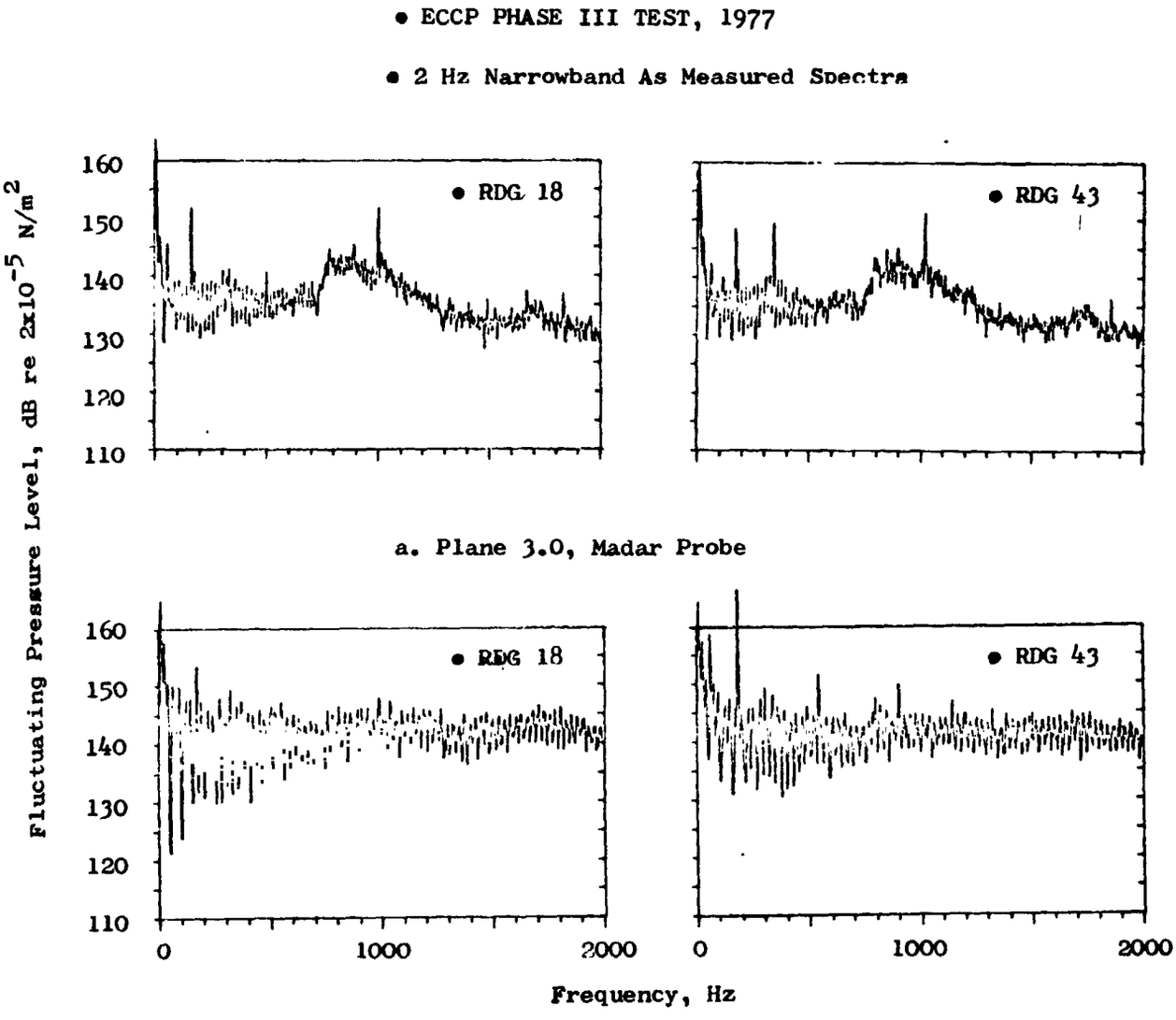

Figure 3-17. Comparison of Common Measurements For Repeat Readings at 82.0 Percent Thrust

4.0 ANALYSIS AND DISCUSSION OF RESULTS

4.1 SPECTRA COMPARISONS

Comparisons of the fluctuating pressure measurements at each measurement plane are discussed for the engine test. Results are based on the measured pressure data analyzed as 1/3 octave band and narrowband spectra. Frequency response corrections were applied to the 1/3 OBFPL, but not to the narrowband FPL.

The Double Annular combustor results from duct rig tests conducted during ECCP Phase I and II were compared to selected points from the ECCP Phase III engine tests.

4.1.1 Measurement Plane Comparisons of 1/3 Octave Band and Narrowband Spectra

The internal fluctuating pressure data acquired during the test of the Double Annular combustor in the CF6-50 engine were compared on both a 1/3 octave band a 2 Hz narrowband spectra basis. Comparisons were made to identify and investigate trends at each measurement plane for several test conditions covering the full operating range of the engine. The spectra encompass frequency ranges for core noise analysis from 50 to 2000 Hz in 1/3 octave band and from 0 to 2000 Hz in 2 Hz narrowband. The complete set of narrowband spectra for all test conditions is found in Appendix A. Similarly, the 1/3 octave band data is presented in both tabular and graphical form in Appendix B.

Five of the eight test conditions were selected for this analysis as representative of combustor operation over the engine operating line. These five conditions include the percent net thrust settings of 3.8 (idle), 19.7, 30 (approach), 64.6 and 94.7 (takeoff) percent. The first three conditions; 3.8, 19.7 and 30 percent net thrust are with pilot fuel only, while the 64.6 and 94.6 percent net thrust points are with fuel splits between pilot and main burner sections.

A common set of four sensors were used in the comparisons which were selected on the basis of measurement reliability and availability. The set included one probe at each measurement plane and consisted of the MADAR probe at Plane 3.0, the 282° borescope probe at Plane 3.5, the HPTN borescope probe at Plane 4.0 and the core exhaust probe, element B, on the sound separation probe located at Plane 8.0. The comparisons include the pilot fuel splits as a percentage of the pilot fuel to total fuel flows (PCT OUT).

Plane 3.0 - Compressor Discharge

The 1/3 octave band spectra comparison for the MADAR Probe in Figure 4-1 show a peaked shape at idle along with a predominate tone at 400 Hz. The fluctuating pressure level (FPL) increases uniformily by approximately 10 dB over the idle setting for 19.7 and 30 percent thrust points. The tone at 400 Hz is no longer a characteristic of the spectral shape at these conditions. At the higher power settings of 65 and 94.6 percent thrust the pressure levels increase by 4 to 5 dB over those at 30 percent thrust in the low frequencies, but show a significant increase of 10 dB at frequencies above 800 Hz. The FPL increase in the higher frequencies tends to flatten the spectra shape. The peaked spectra, characteristic of core noise dominated spectra, seem to be limited to power settings at approach and below.

The results of the 2 Hz narrowband spectra analysis of these conditions at Plane 3.0 are shown in Figure 4-2. The predominate tone at 400 Hz for the idle condition appears to be a low level resonance or combustor growl phenomenon which is not apparent at other conditions but is present at other planes for the idle condition. There is a slight reduction in combustor efficiency (see Table 5) of about one point at idle compared to the 19.7 and 30 percent thrust conditions with pilot fuel only. However, it does not appear that this amount of change would be sufficient to cause the large 400 Hz tone observed in the data. There is some electronic noise at 60 and 180 Hz. A "hay-stacked" tone is evident at 19.7 and 30 percent thrust occurring at approximately 700 Hz which corresponds roughly to the 5th per rev of the engine spool. A broad 5 to 7 dB plateau is also apparent between 700 and 900 Hz for these conditions. At the higher power settings the narrowbands appear quite similar and show an increase in the broadband above 1000 Hz which reflects the 1/3 octave band spectral results.

Plane 3.5 - Combustor Inlet

At the combustor inlet, Plane 3.5, the combustor borescope probe at the 282° position exhibits similar trends in the 1/3 octave band spectra (Figure 4-3) as were shown for the MADAR Probe at Plane 3.0. Peaked spectra (400 to 800 Hz) are evident for power settings of 30 percent thrust and below. The high power points show an increase in FPL of 5 to 10 dB above 1000 Hz and the 400 Hz tone at the idle condition is still apparent.

The narrowband analysis show spectra in Figure 4-4, for 3.8, 19.7 and 30 percent thrust which compare well with similar spectra for the Plane 3.0 probe in Figure 4-2. Large pressure fluctuations of ± 10 to ± 18 dB are seen below 500 Hz. There is evidence of electronic noise contamination at 60 and 180 Hz which does not compromise the quality of the data but might clarify a portion of these large fluctuations below 200 Hz. A possible explanation for the remainder might be due to the location of the probes. They are located in the pre-mix region of the combustor just aft of the fuel nozzle discharge where fuel injection and ignition take place which results in a high rate of energy release. Note that the spectra for 64.6 and 94.6 percent thrust points are flat in the high frequencies as opposed to the spectral drop off at lower power settings. This is consistent with the 1/3 octave band results.

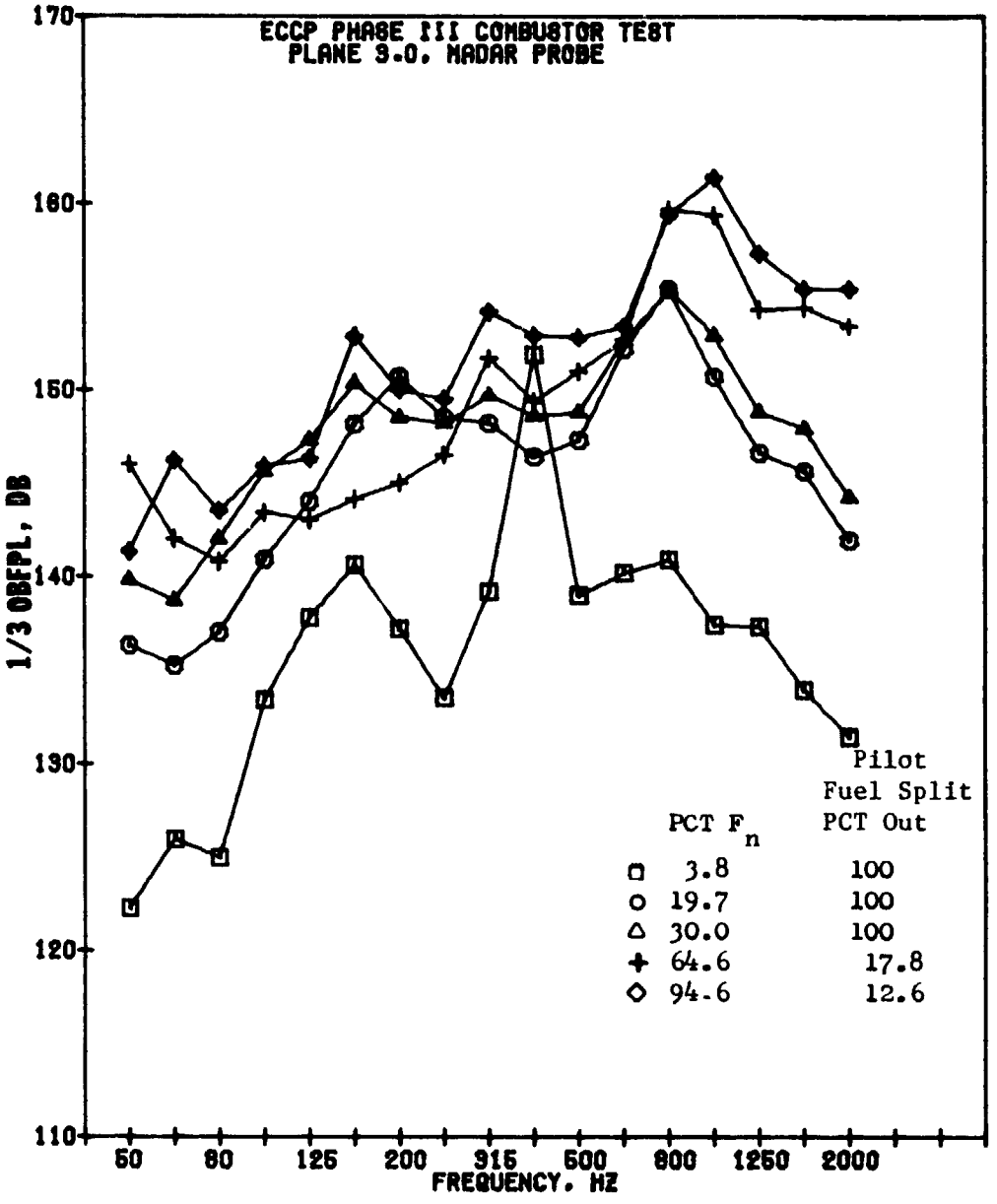

Figure 4-1. Plane 3.0 (MADAR Probe) 1/3 Octave Band Spectra Variation with Engine Speed

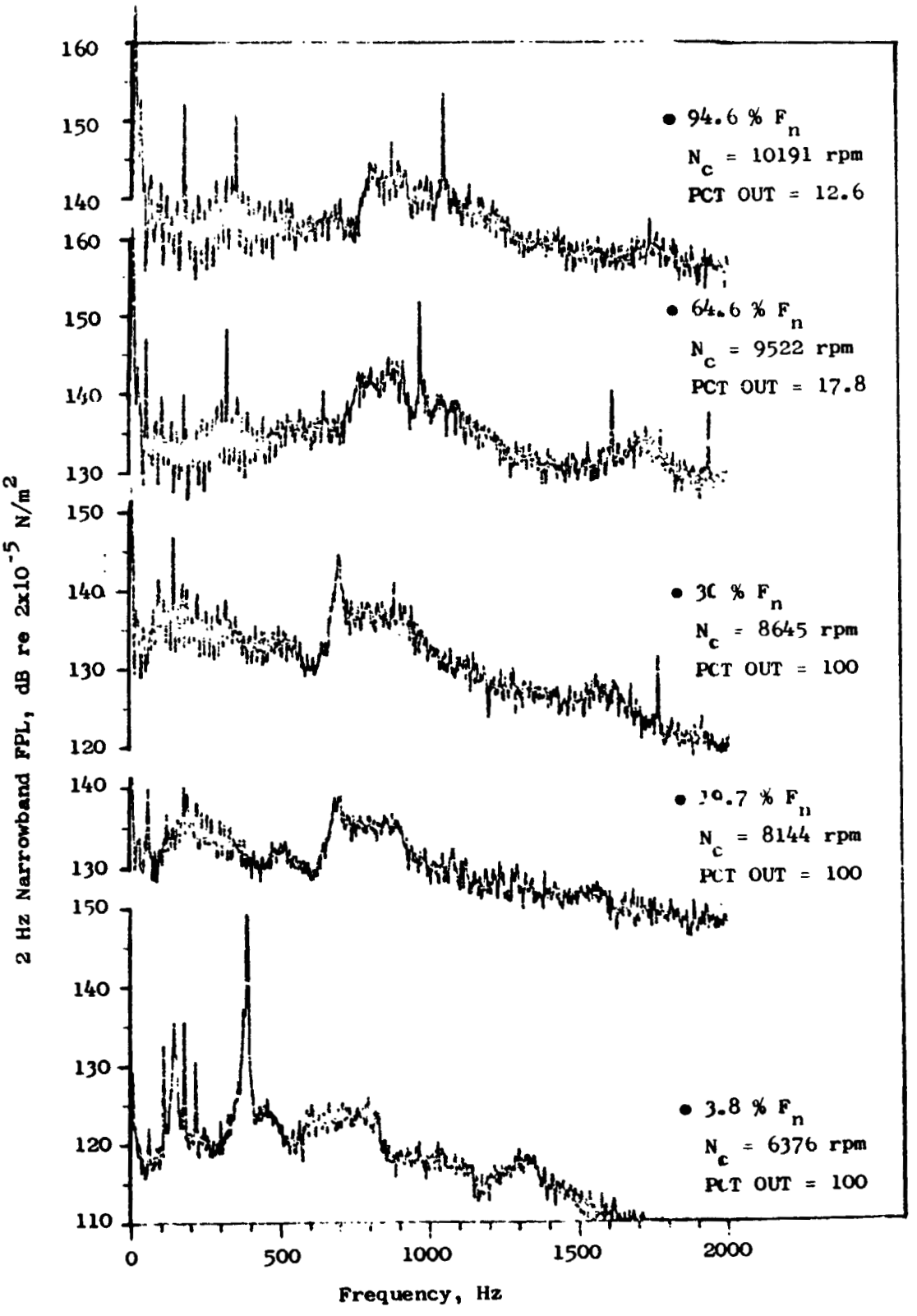

Figure 4-2 Plane 3.0 (MADAR Probe) Spectra Variation with Engine Speed

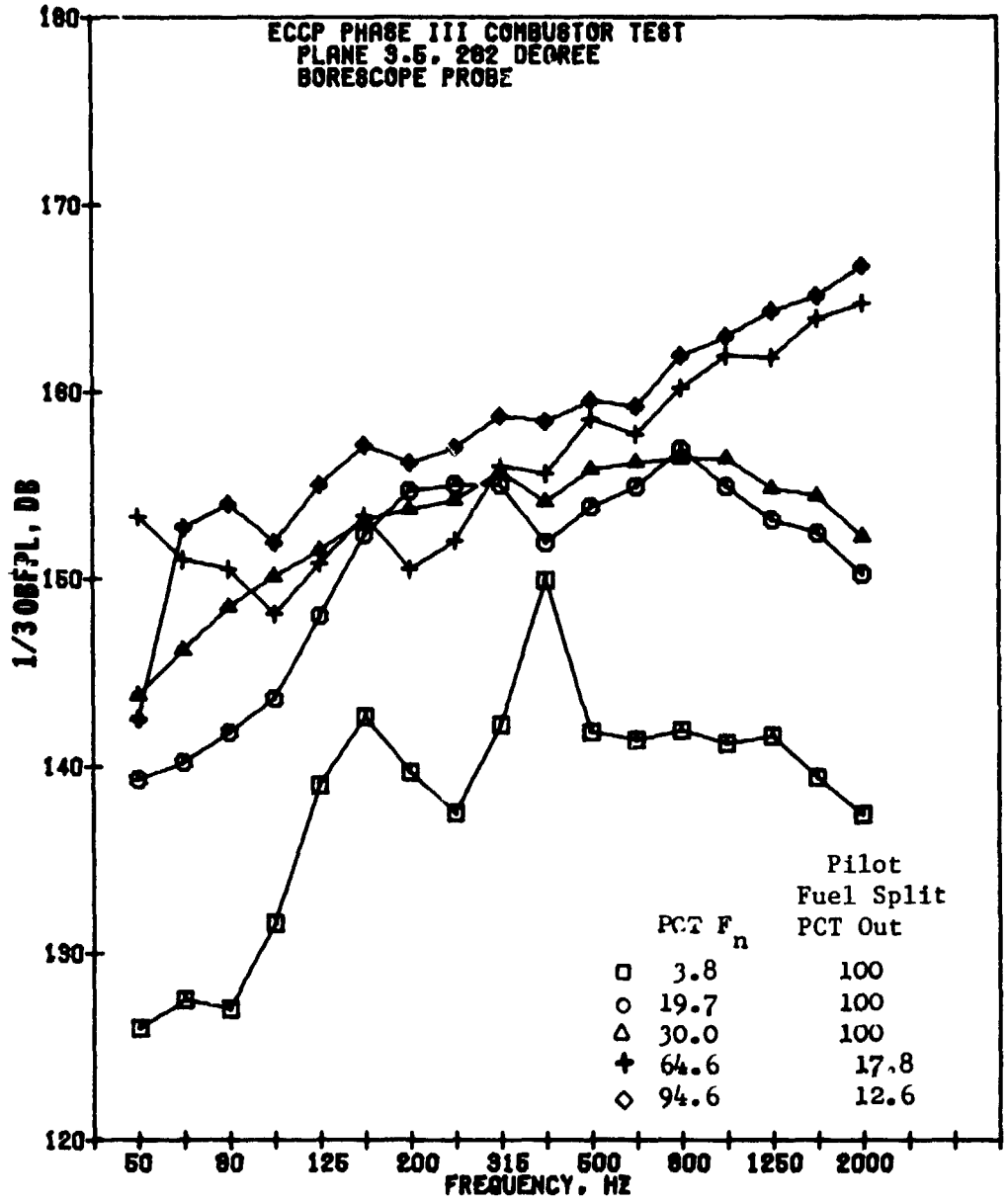

Figure 4-3. Plane 3.5 (282° Borescope Probe) 1/3 Octave Band Spectra Variation with Engine Speed

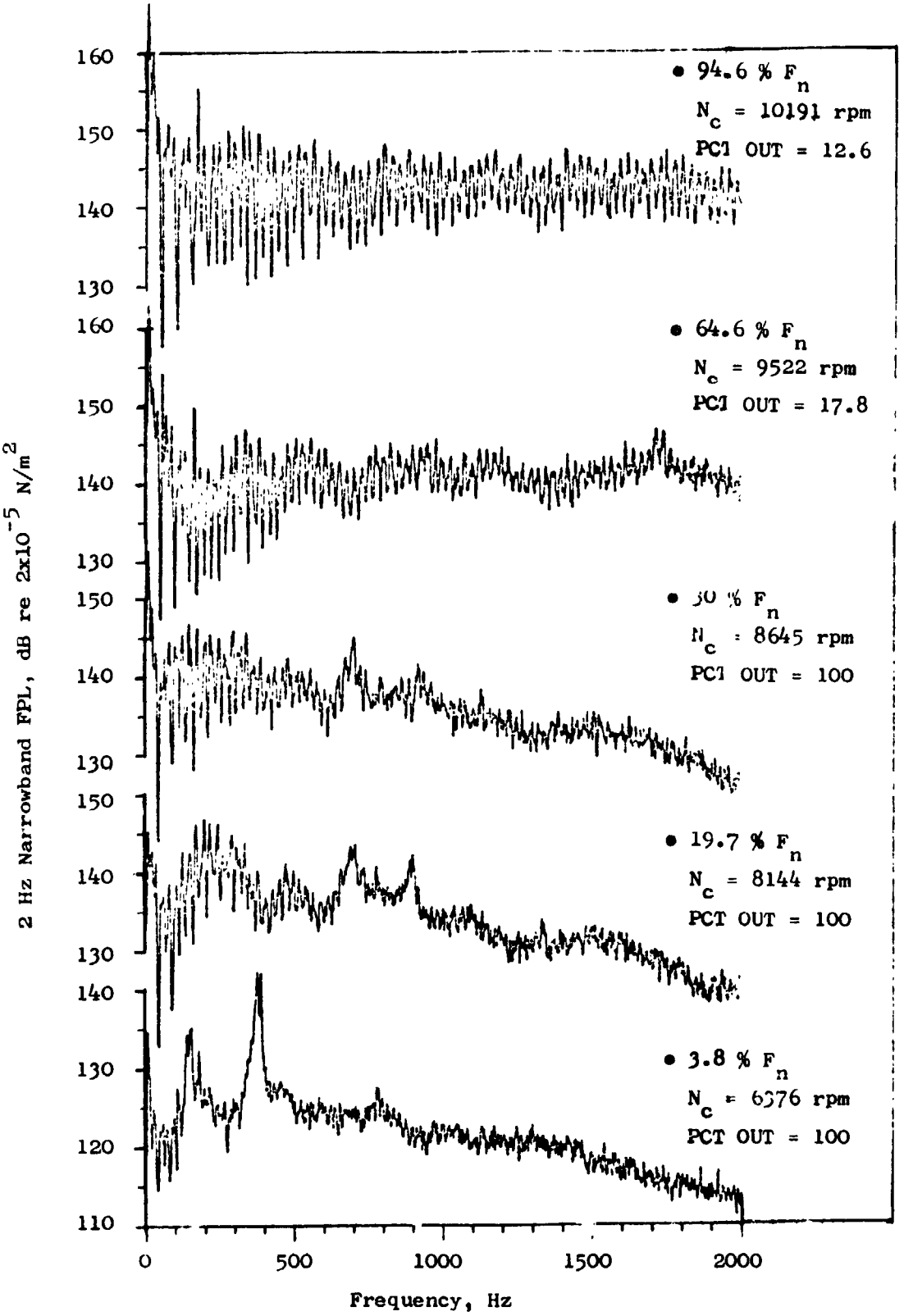

Figure 4-4 Plane 3.5 (282° Borescope Probe) Spectra Variation with Engine Speed

Plane 4.0 - Combustor Discharge

The HPTN borescope probe at Plane 4.0 exhibits increasing spectra for all conditions as shown in Figure 4-5. This sensor does not indicate a core noise spectrum shape at any of the test conditions and appears to be saturated with high frequency noise. This may be a consequence of the probe location between two vanes in the high pressure turbine nozzle diaphram.

The 2 Hz narrowband results presented in Figure 4-6 show flat spectra to 2000 Hz and high pressure fluctuations of ± 10 to ± 12 dB in the same region as the Plane 3.5 sensor. The highest levels are recorded at this probe location. This agrees with the physics of the combustion process which is culminated at the combustor exit after complete mixing and burning of the fuel-air mixture have taken place. It is at this plane that the maximum energy is available to do work on the turbine.

Plane 8.0 - Core Nozzle Discharge

The exhaust Probe B 1/3 octave band spectra shown in Figure 4-7 exhibit typical core noise shapes between 200 and 1250 Hz for the 3.8, 19.7 and 30 percent thrust points. At the higher power settings the high frequency noise (above 800 Hz) increased to produce an essentially flat spectrum at the takeoff condition. Below 200 Hz the FPL for all conditions, except idle, is generally about the same level, within ± 5 dB. This may be the result of low frequency turbulence generated off the centerbody of the factory plug nozzle.

The narrowband spectra for Probe B at the exhaust plane is shown in Figure 4-8. The 400 Hz tone at the idle condition is again clearly visible. The spectra below 30 percent thrust are dominated by the low frequencies (<1000 Hz). High frequency noise above 1000 Hz is increased at the power settings above 30 percent thrust as illustrated in Figure 4-8.

4.1.2 Double Annular Combustor Spectra Comparisons

Comparisons were made between the Double Annular combustor spectra measured on the engine test and the combustor spectra obtained from full annular duct rig tests conducted during Phase I and II of this program. The engine conditions at idle (3.8% F_n), approach (30% F_n with 100% pilot fuel and 29.7% F_n with 50% fuel split) and takeoff (94.6% F_n) were selected for comparison with the duct rig data.

A number of conditions approximating the above engine power settings were available for comparison from the duct rig data. The selection of the particular duct rig test points for comparison with the engine data was based on matching the inlet and discharge temperatures in conjunction with keeping $W\sqrt{T_3}/P_3$ constant for the approach and takeoff points. The idle set point selection was based on the inlet pressure and temperature match. Consideration was also given to matching the fuel-air ratios between duct rig and

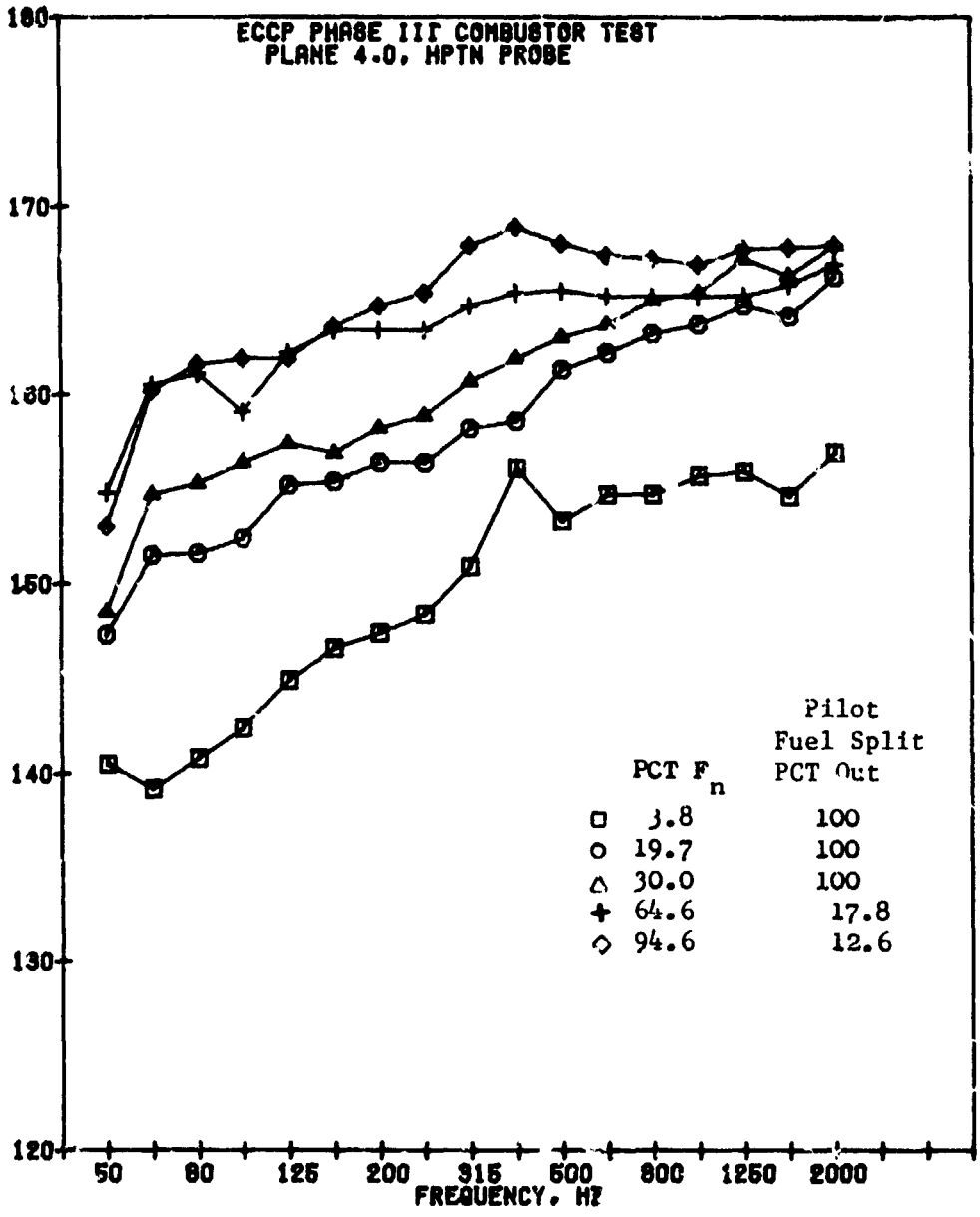

Figure 4-5. Plane 4.0 (HPTN Probe) 1/3 Octave Band Spectra Variation with Engine Speed

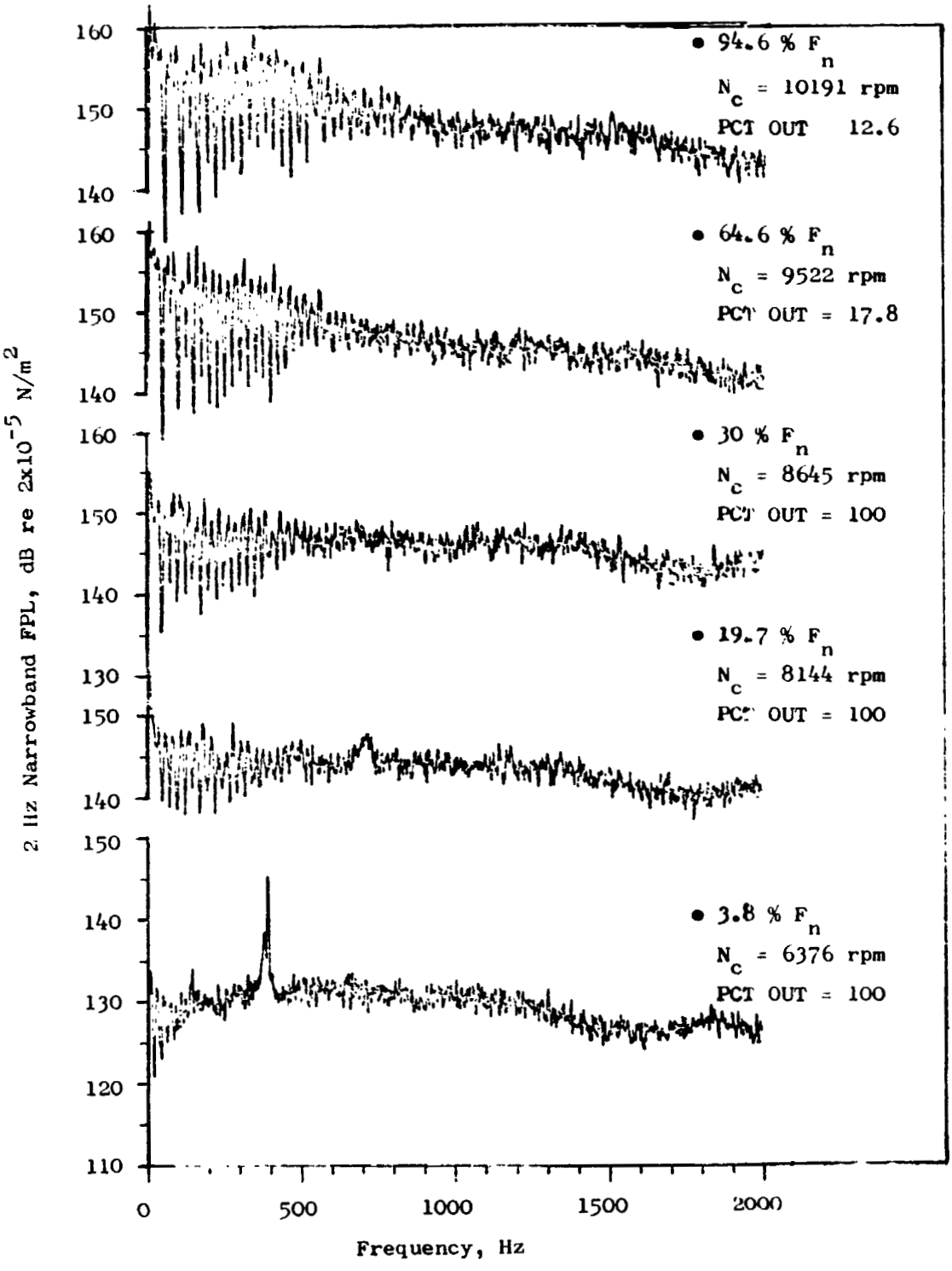

Figure 4-6 Plane 4.0 (HPTN Probe) Spectra Variation with Engine Speed

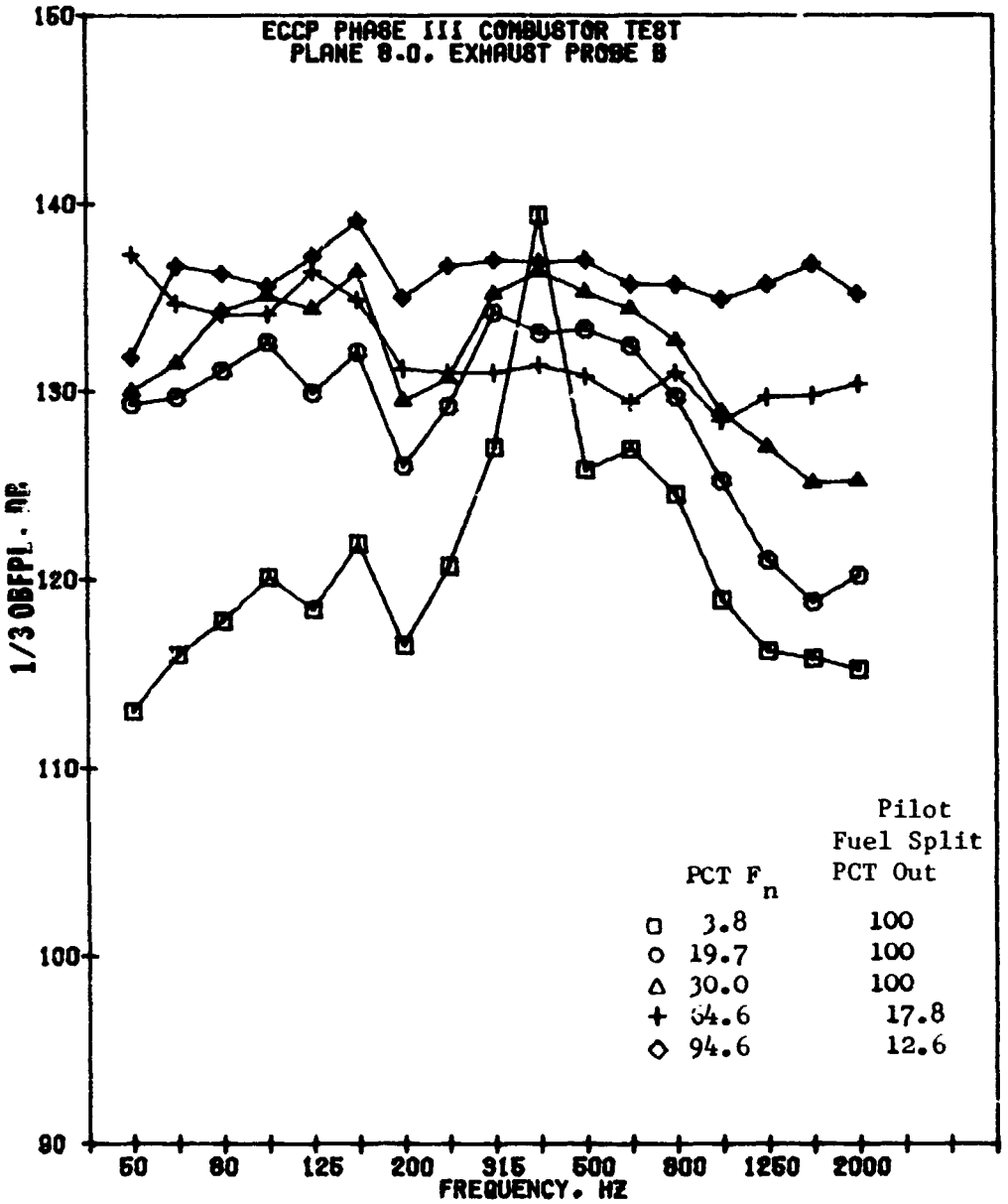

Figure 4-7. Plane 8.0 (Exhaust Probe B) 1/3 Octave Band Spectra Variation with Engine Speed

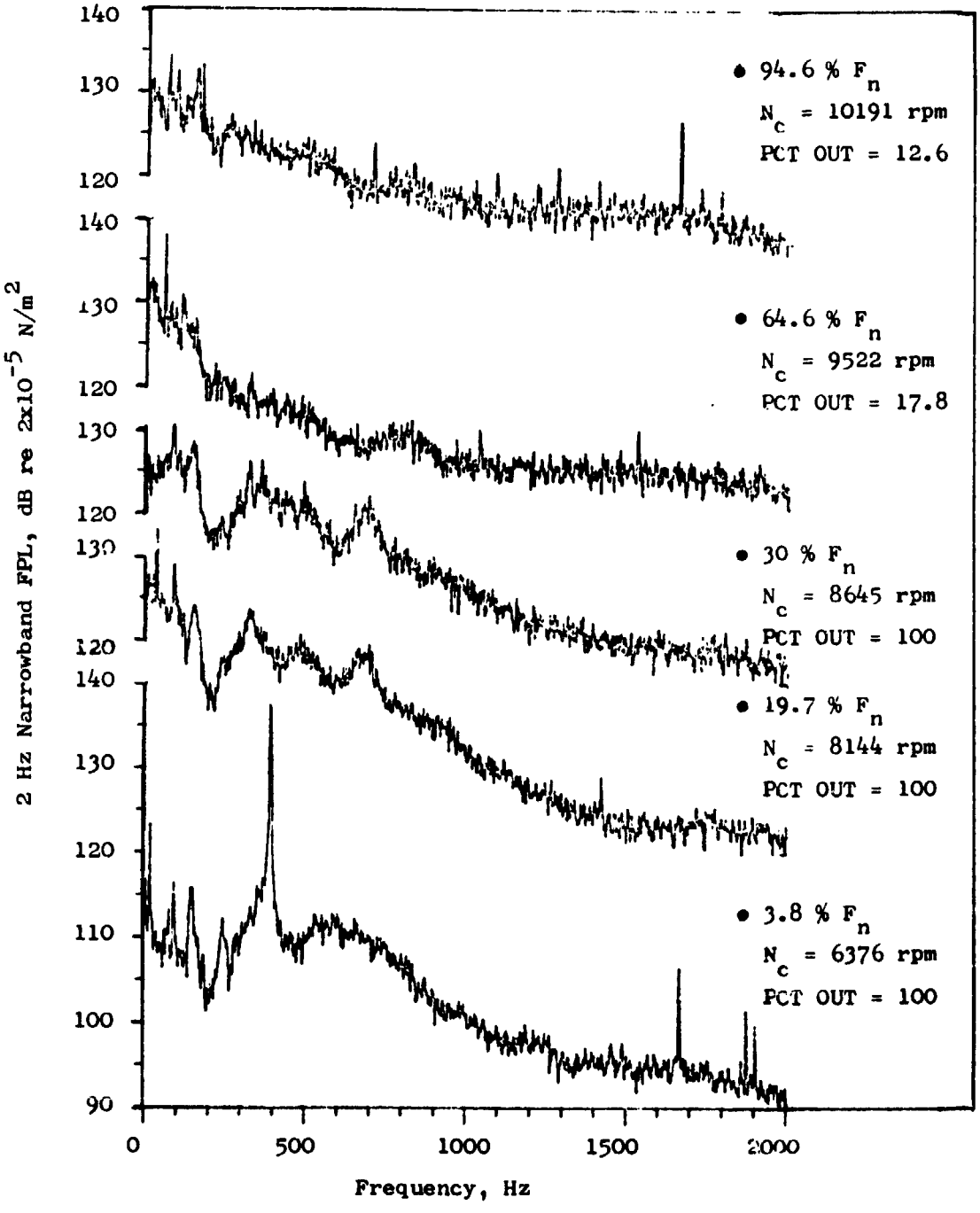

Figure 4-8. Plane 8.0 (Exhaust Probe B) Spectra Variation with Engine Speed

engine within the limits of data availability. Table 7 lists the compared test points for these conditions.

The set up for the duct rig tests is detailed in the ECCP Phase I and II final reports (References 3 and 5). The acoustic probe locations for these tests were as illustrated in Figure 4-9. The engine and duct rig acoustic measurement plane locations were not identical as noted in reviewing the engine plane locations in Figure 3-2.

The idle point 1/3 OBFPL spectral comparison is shown in Figure 4-10 for the combustor discharge sensors. No upstream probe measurements were available for the duct rig at this condition. The engine data are 17 to 20 dB greater than the duct rig data for the frequency range investigated.

Figures 4-11a and 4-11b present the combustor inlet and discharge fluctuating pressure level comparisons respectively for the approach condition. At the combustor inlet (Figure 4-11a), the Plane 3.0 engine probe shows results that are from 5 to 12 dB greater than the duct rig inlet probe for both the 100% pilot and fuel split approach condition. Larger differences are noted for the combustor discharge comparison in Figure 4-11b with the pilot only fuel than with the fuel split point. The engine Plane 3.5 sensor shows a characteristic core noise spectral shape peaking between 500 and 1000 Hz at both approach conditions.

At takeoff the Plane 3.0 engine and duct rig pressure level measurements in Figure 4-12a are within 1 to 4 dB at frequencies above 315 Hz. Below 400 Hz the engine measurements are 4 to 15 dB greater than those of the duct rig. The discharge Plane 4.0 measurements in Figure 4-12b show the same trends observed for the idle and approach point comparisons. The Plane 3.5 engine borescope spectrum shown in the figure is 10 to 15 dB greater than the duct rig data.

These engine to duct rig 1/3 OBFPL spectral comparisons indicate large level differences at both inlet and discharge measurement planes. The inlet plane comparisons are much closer (5 to 10 dB) than those at the discharge (15 to 20 dB). Some of the differences can be explained due to test condition differences as noted in Table 7. The local static pressures in the engine (Plane 4.0) are approximately 2.5 times greater than the duct rig static pressures for the conditions above idle.

In order to minimize these differences the duct-rig and engine 1/3 OBFPL spectra were converted to power spectra assuming all the measured signal was acoustic and plane wave propagation occurred at each measurement plane. The $FPWL_{meas}$ was calculated using Equation 5. Comparisons of the spectra from the fluctuating power level ($FPWL_{meas}$) showed much closer agreement between engine and duct rig data. Figure 4-13 shows the $FPWL_{meas}$ spectra comparison at Plane 4.0 for the idle condition. The engine spectra is approximately 8 dB above the duct rig results (solid symbols) for frequencies above 160 Hz where the spectral shapes are similar. The Plane 3.5 engine results (from the 282° borescope sensor) show good agreement from 160 to 500 Hz with the duct rig data. However, above 500 Hz the duct rig data is 6 to 10 dB higher than the engine data.

Table 7. Test Conditions for Comparison of ECCP Phase I, II and III Results.

Condition	Reading	ECCP Phase	f/a	P_{T3} atm	T_{T3} K	W_3 kg/sec	P_{T4} atm	T_{T4} K	$W\sqrt{T_{T3}}/P_{T3}$
Idle	713	II	0.0122	3.43	629.0	13.7	3.26	1077.0	100.2
	6	III	0.0156	2.95	442.8	12.5	2.85	1042.8	89.2
Approach	459	I	0.0175	3.58	664.0	15.3	3.35	1292.0	110.1
(100% Pilot)	23	III	0.0206	10.94	641.1	36.8	10.51	1374.4	85.2
(50% Pilot)	39	III	0.0166	11.48	642.8	45.0	10.98	1256.7	99.4
Takeoff	723	II	0.0230	9.53	816.0	33.3	9.01	1589.0	99.8
	33	III	0.0275	26.95	830.6	88.9	25.76	1733.3	95.1

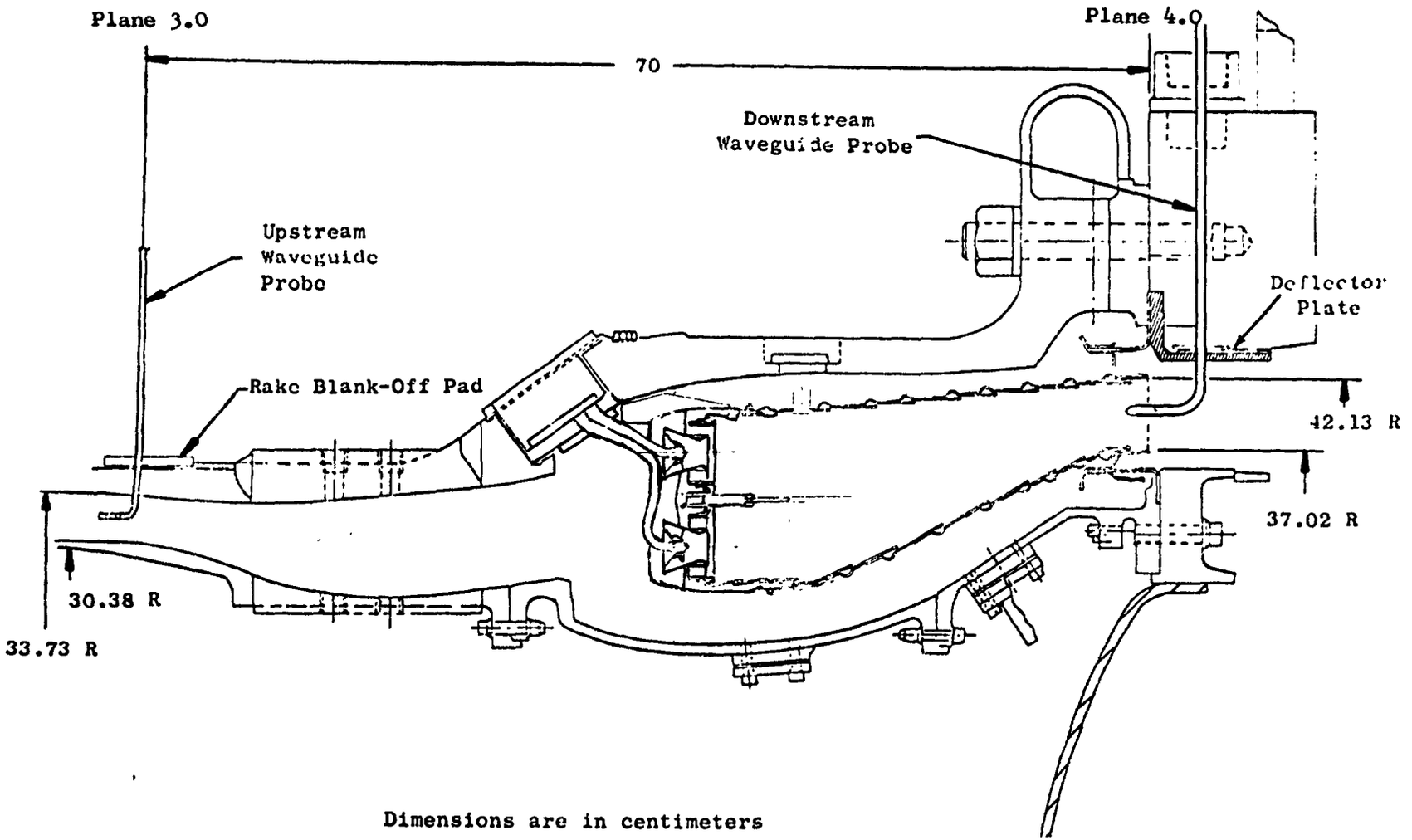

Dimensions are in centimeters

Figure 4-9. Acoustic Probe Locations for Duct Rig Test

Table 8. CF6-50 Turbine Attenuation Summary from ECCP Phase III Test Results.

- Results Based on Difference Between Coherent Spectra at Planes 4.0 and 8.0 Relative to Plane 3.5

Pct Thrust Aero/Tape Reading	3.8 147/6		19.7 149/16		30.0 151/23		29.7 119/39		45.4 154/28		64.6 163/40		82.0 156/18		94.6 107/33	
1/3 OB OASPL Frequency (Hz)	ΔSPL	ΔPWL	ΔSPL	ΔPWL	ΔSPL	ΔPWL	ΔSPL	ΔPWL	ΔSPL	ΔPWL	ΔSPL	ΔPWL	ΔSPL	ΔPWL	ΔSPL	ΔPWL
100	16	6.9	<19	< 4.2	18	1.4	>26	> 9.4	---	---	<19	<-1.3	>26	> 4.4	---	---
125	19	9.9	22.5	7.7	23	6.4	>23.5	> 6.9	>21	> 2.4	---	---	<16.5	< 5.1	---	---
163	19	9.9	26	11.2	20	3.4	28	11.4	<14	<-4.6	34	13.7	25	3.4	>32	> 9.5
200	<20	<10.9	30	15.2	<27	<10.4	<24	< 7.4	---	---	>35	>14.7	>30	> 8.4	---	---
250	25	15.9	19	4.2	23	6.4	---	---	---	---	---	---	---	---	---	---
315	<13	< 3.9	13.5	-1.3	19	2.4	23	6.4	27	8.4	---	---	>36	>14.4	30	7.5
400	14	4.9	<16	< 1.2	<18.5	< 1.9	29	12.4	---	---	---	---	<27	< 5.4	30	7.5
500	24	14.9	<22	< 7.2	25	8.4	---	---	35	16.4	37	16.7	<28	< 6.4	<29	< 6.5
630	<22.5	<13.4	31	16.2	27	10.4	39	22.4	30	11.4	35	14.7	---	---	---	---
800	<27.5	<18.4	30	15.2	31	14.4	<35	<18.4	30	11.4	34	13.7	33	11.4	31	8.5
1000	<33	<23.9	---	---	<34	<17.4	---	---	---	---	---	---	---	---	---	---
1250	<35	<25.9	---	---	---	---	---	---	---	---	---	---	---	---	---	---
1600	<31	<21.9	---	---	---	---	---	---	---	---	---	---	---	---	---	---
2000	---	---	---	---	---	---	---	---	---	---	---	---	---	---	---	---
Average ΔdB_{PWL}		13.9		9.1		7.5		11.8		10.0		14.7		7.4		7.9

Note: < Actual Attenuation is Less than Value Shown
> Actual Attenuation is Greater than Value Shown

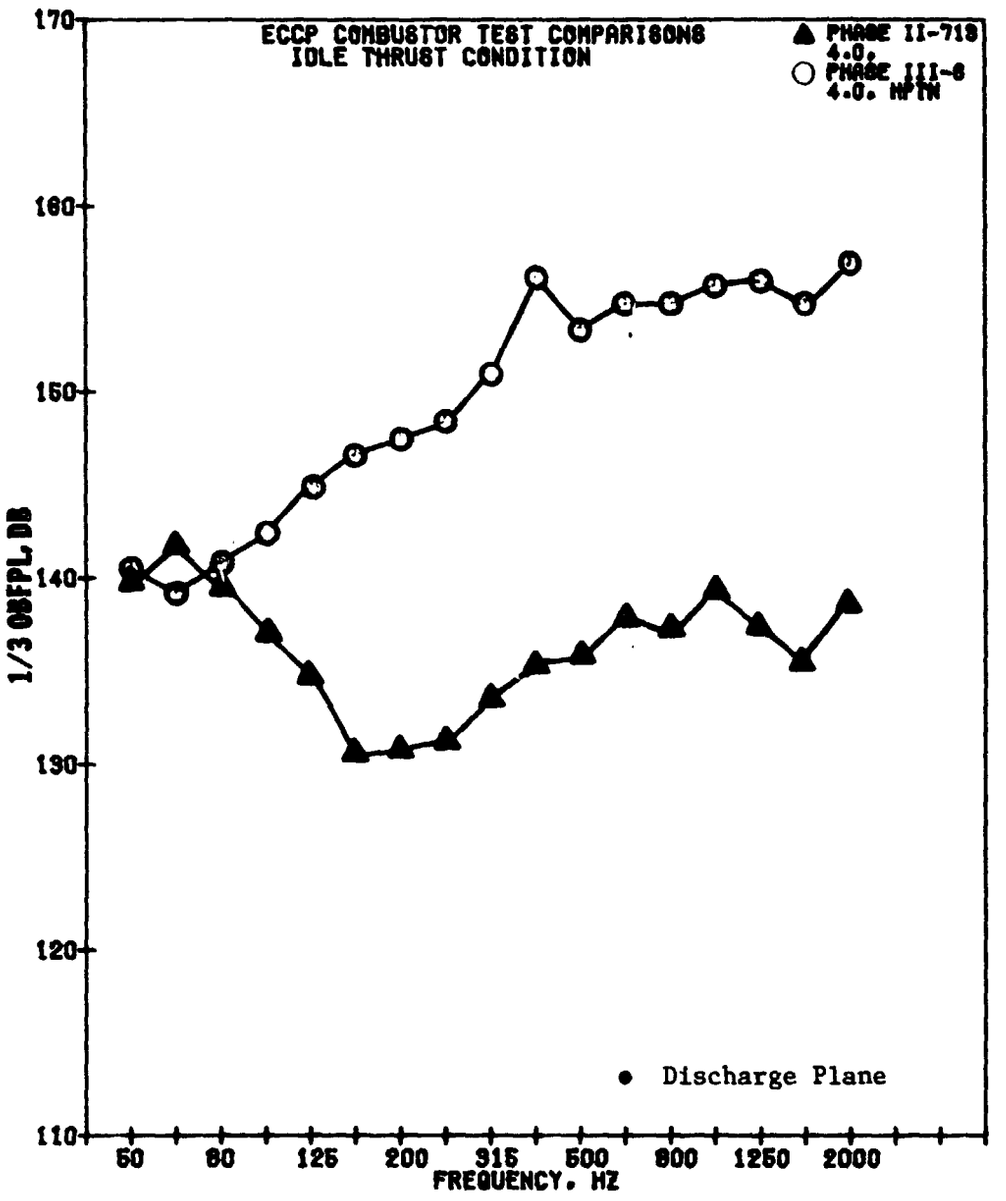

Figure 4-10. Engine-to-Duct Rig Pressure Spectra Comparison for Double Annular Combustor at Idle.

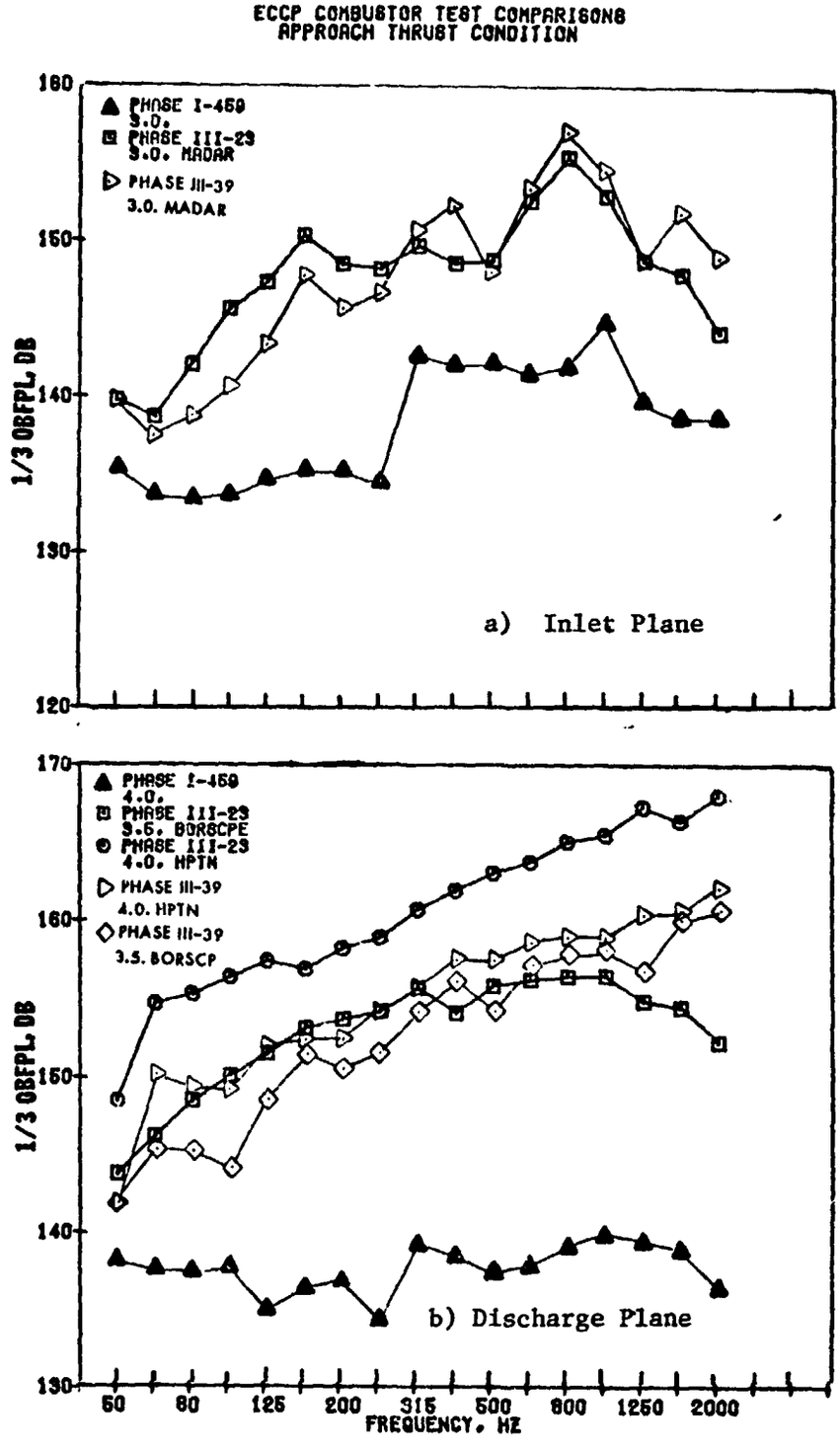

Figure 4-11 Engine-to-Duct Rig Pressure Spectra Comparison for Double Annular Combustor at Approach

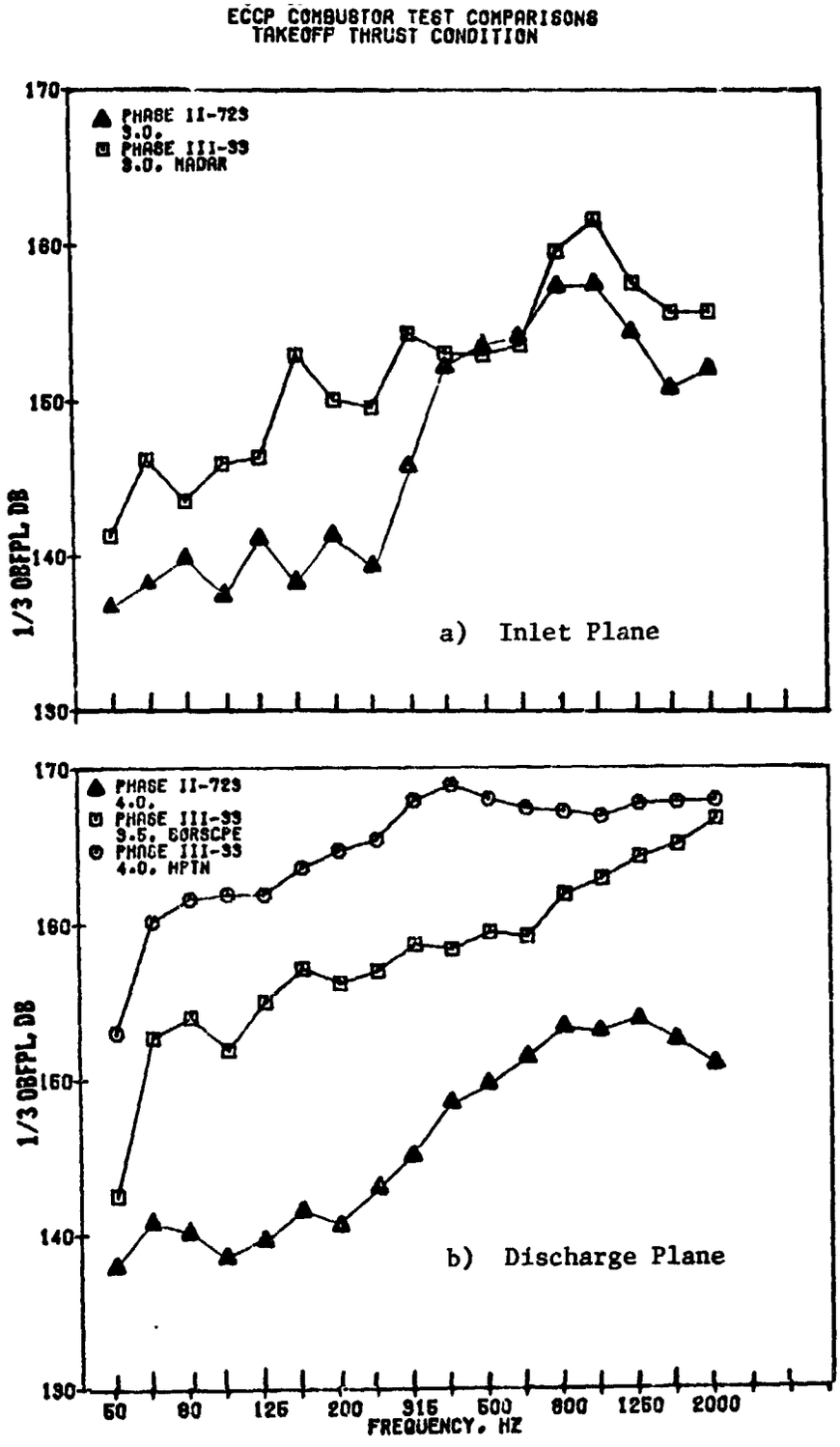

Figure 4-12 Engine-to-Duct Rig Pressure Spectra Comparison for Double Annular Combustor at Takeoff

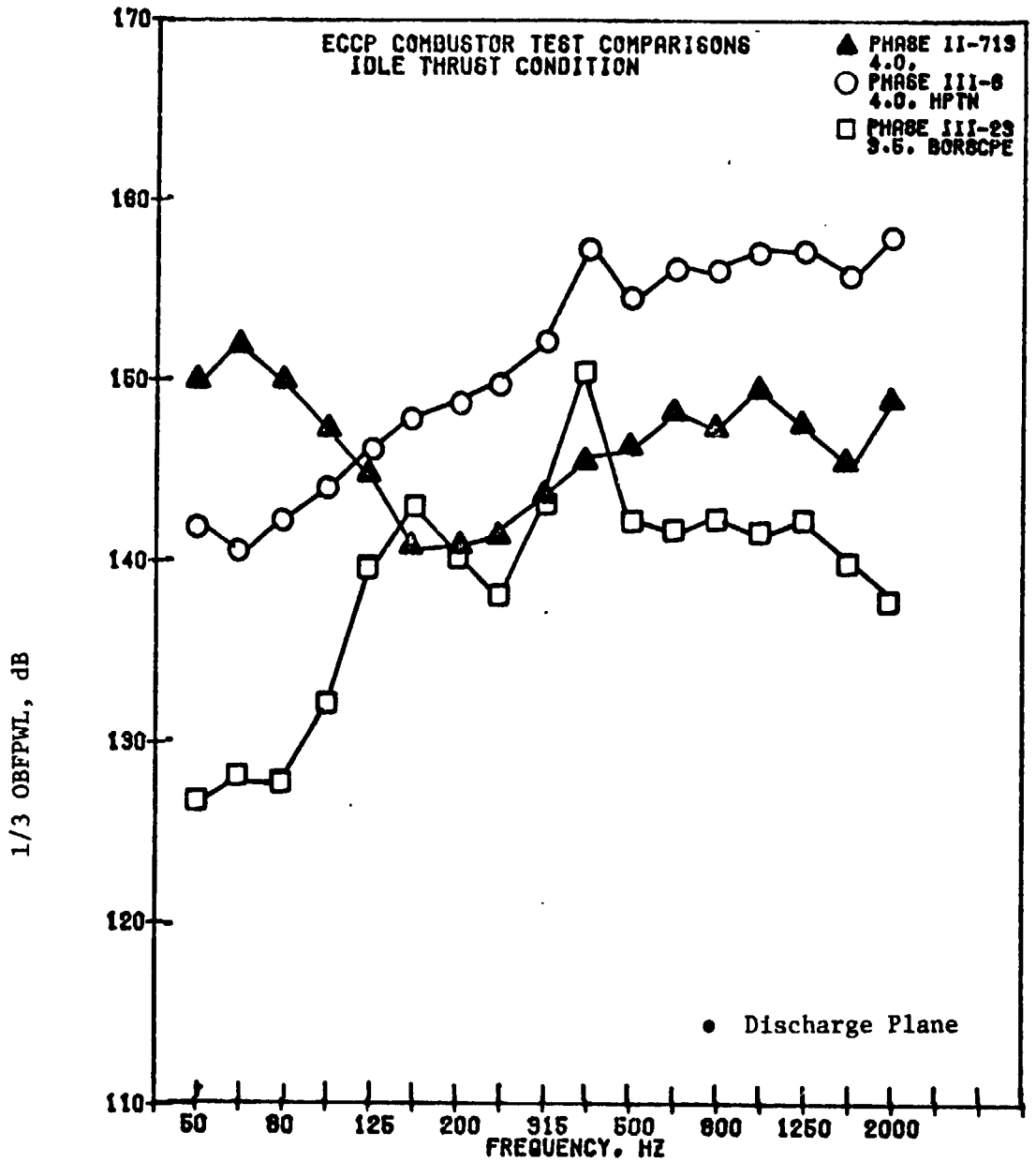

Figure 4-13 Engine-to-Duct Rig Power Spectra Comparison for Double Annular Combustor at Idle.

The approach power setting $FPWL_{meas}$ comparisons at the inlet plane are shown in Figure 4-14a. Agreement within 3 to 5 dB is apparent in frequency regions between 160 to 250 Hz and above 630 Hz for the duct rig results with both the 30% F_n (100% pilot fuel) and 29.7% F_n (50/50 fuel split) points.

The exit plane comparison for this approach condition shown in Figure 4-14b indicates good agreement in both spectral shape and level between the duct rig results and the engine Plane 3.5 data. The Plane 4.0 results from the engine are greater than the duct rig measurements by approximately 5 to 15 dB for the 30% F_n point and zero to 8 dB for this 29.7% F_n condition.

At takeoff, the inlet plane $FPWL_{meas}$ comparison in Figure 4-15a shows the duct rig data to be 10 to 12 dB higher than the engine Plane 3.0 power level above 400 Hz. The shape of the spectra appear quite similar over this full frequency range.

Figure 4-15b shows the exit plane comparison at the takeoff condition. The duct rig $FPWL_{meas}$ spectra matches the engine Plane 3.5 results below frequencies of 315 Hz, while at the higher frequencies the Plane 4.0 data appears to give a better match.

The comparisons of the engine and duct rig results on a fluctuating power level spectra basis show generally closer agreement than on a 1/3 OBFPL spectral basis as previously noted. The shapes of the engine spectra are very similar to the duct rig spectra at all planes investigated. The Plane 4.0 HPTN probe located in the engine turbine nozzle gives consistently higher fluctuating pressure levels than other engine probes. This may be due, in part, to the presence of the choked turbine nozzle diaphragm which supplies an entirely different end effect than the open plenum of the duct rig facility.

The differences in measurement plane location, the turbine nozzle diaphragm and the variations in test conditions all contribute to the differences in levels apparent between engine and duct rig. However, the overall engine-to-duct rig comparisons show good results.

A more controlled test, such as a one-on-one test between the engine and duct rig using the same combustor, dynamic instrumentation, instrumentation locations, and a turbine nozzle diaphragm configuration in the duct rig test would provide a better comparison.

4.2 TURBINE TRANSFER FUNCTION COMPARISON

The turbine acoustic transfer functions determined for the ECCP Phase III Double Annular combustor were calculated in the form of blade row attenuations across the turbine using coherence analysis techniques. Initially, attenuations were determined from the difference in the Plane 4.0 HPTN probe raw spectra with the coherent spectra of the Plane 8.0 core probe at the core nozzle discharge. This procedure proved unsuccessful due to the excessive amount of high frequency noise in the raw signal of the Plane 4.0 sensor which was incoherent with the downstream core probe signal. When the coherent

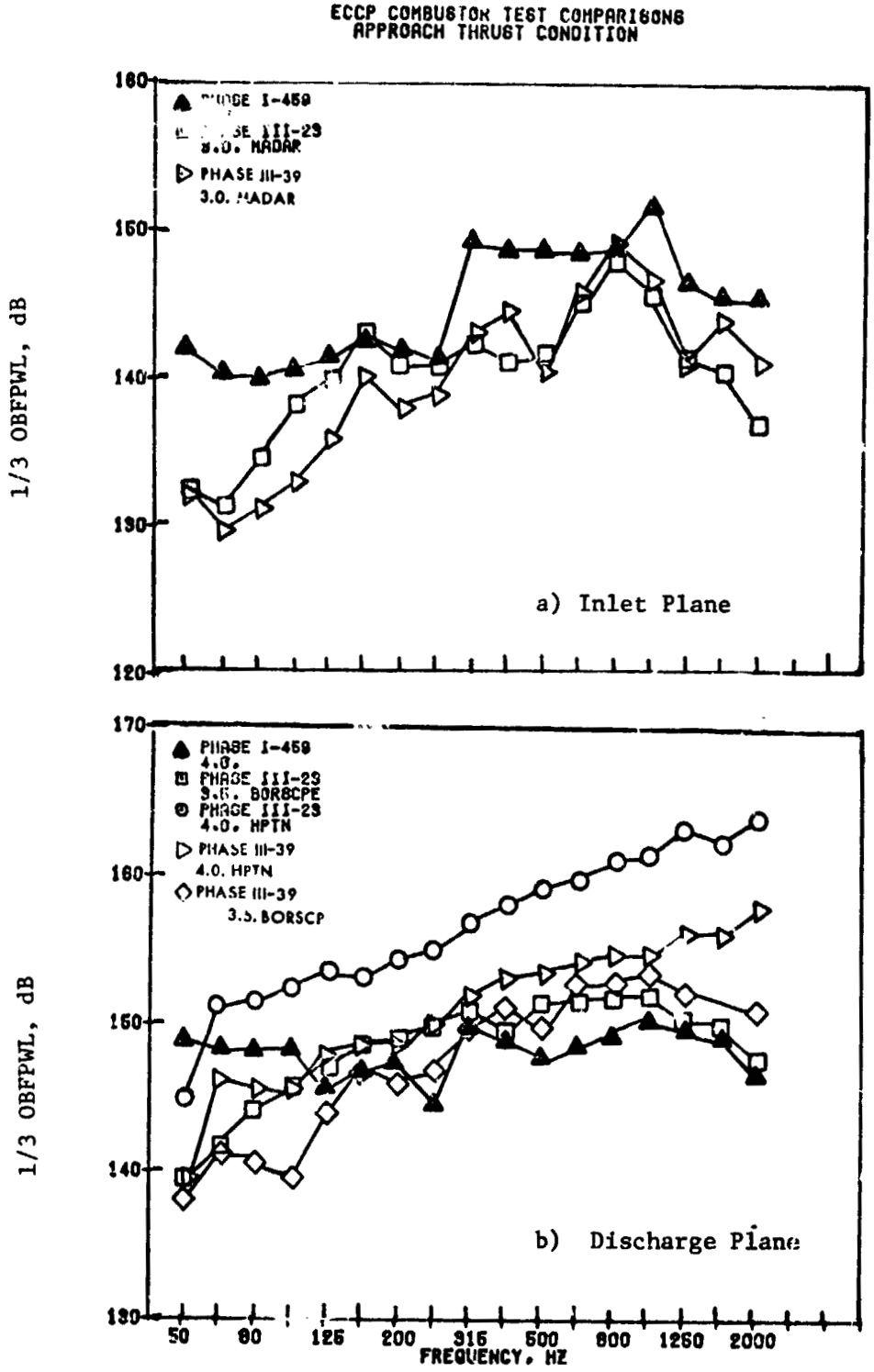

Figure 4-14 Engine-to-Duct Rig Power Spectra Comparison for Double Annular Combustor at Approach

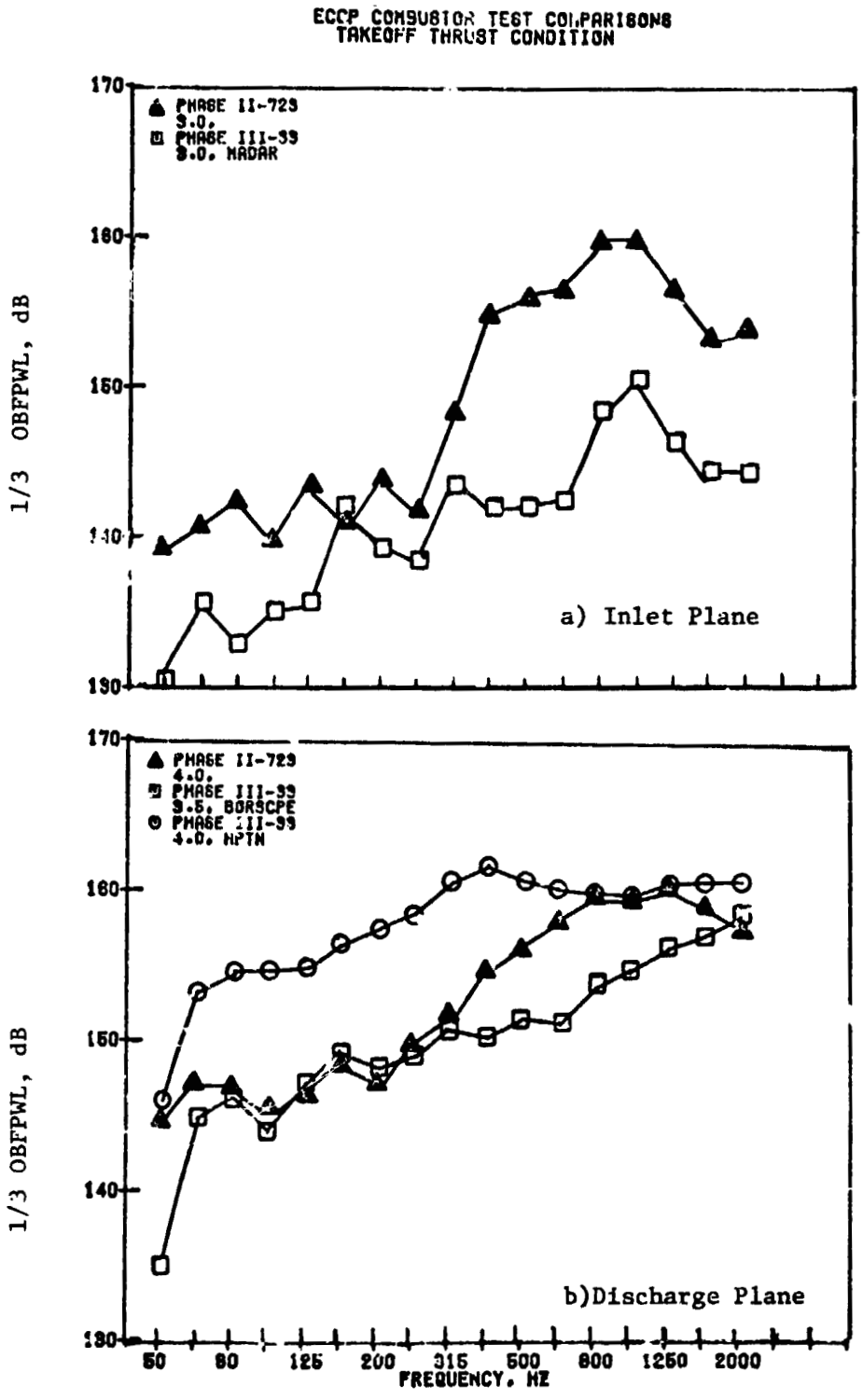

Figure 4-15 Engine-to-Duct Rig Power Spectra Comparison for Double Annular Combustor at Takeoff

spectra of the downstream probe was compared to the Plane 4.0 raw spectra the resulting attenuation amplitudes were excessive (in the order of 35 to 50 dB). The analysis technique employed did not lend itself to a direct comparison of the upstream raw signal with the downstream coherent spectra.

To minimize this effect, the attenuation was obtained from the difference in coherent 1/3 OBSPL spectra at Planes 4.0 and 8.0 relative to the upstream combustor signal at Plane 3.5. The coherent spectra between pairs of sensors incorporated positive time delays determined from cross-correlations to account for phase differences between sensors. In cases where negative time delays were observed (which indicated that the signals were traveling opposite to the assumed direction), a zero time delay was input. The error introduced by this procedure resulted in coherent spectra levels which were 0.1 to 0.6 dB higher than the true level. Adjustments were made to the resulting spectrum to account for these differences. The coherent spectra determined in this manner had some regions that were affected by the noise floor associated with the analysis procedure for determining the coherent spectra. This floor, based on sample length limitations which restricted the number of averages used in the analysis, was 18 dB down from the raw signal level. These regions were located in the higher frequencies above 800 Hz and in a low frequency region around the 250 Hz band at the higher test conditions above 30 percent thrust. Previous attenuation results (Reference 6) covered a range of frequencies from 100 to 1200 Hz.

4.2.1 Turbine Attenuation from Coherent Spectra

The attenuations determined for the ECCP Phase III data from the 1/3 OBSPL coherent spectra at Planes 4.0 and 8.0 relative to the borescope Plane 3.5 were converted to PWL attenuations to account for impedance changes, Mach number effects and area differences at the measurement planes.

For conditions above 30 percent thrust, the increased probe turbulence in the lower frequencies and incoherent high frequency noise produced coherent spectra at Plane 8.0 that were in the noise floor for several of the 1/3 octave bands. Consequently, turbine attenuations at these conditions were obtained at about 60 percent of the frequency bands up to 800 Hz. The attenuations determined from the differences in coherent spectra are summarized in Table 8 for each test condition. Both the coherent SPL and PWL attenuations are listed at the 1/3 octave band center frequencies from 100 to 2000 Hz. The missing attenuations indicate both coherent signals were in the noise floor. Where either one or the other spectrum was influenced by the noise floor, the attenuation listed is less than or greater than the value shown, as noted on the table. Appendix C presents the coherent spectra at Planes 4.0 and 8.0 relative to Plane 3.5 for each test condition used to determine the attenuation across the turbine.

Typically, the attenuation spectra show an S-shaped distribution as indicated in Figure 4-16 for 30 percent thrust. This is similar to component turbine attenuation results but includes any change in attenuation in propagating from the turbine exit to nozzle discharge. Average attenuations

computed from the arithmetic average of the ΔdB_{PWL}'s at each frequency for all conditions ranged from 7.4 to 14.7 dB as listed in Table 8.

4.2.2 Comparison of Engine Results with Component Tests

Component tests were conducted on a single stage high pressure turbine and on a low pressure turbine tested in both a 1- and 3-stage build. A siren was used to simulate combustor noise. The turbine attenuations obtained from these component tests conducted under another NASA Lewis sponsored program and reported on in Reference 6 were based on ΔdB_{PWL} determined from raw spectra upstream of the turbine to coherent downstream spectra. Average attenuations were obtained for each configuration in the same manner as the engine test. The frequency range for the average ΔdB_{PWL} was between 100 to 1200 Hz.

The average attenuation (ΔdB_{PWL}) for the 3-stage low pressure turbine ranged from 5.9 to 15.5 dB over the operating range tested as noted in the reference. These attenuations are of the same order of magnitude as determined from the engine test. The 3-stage low pressure turbine results used in the comparison were based on attenuations of siren tones at warm ambient inlet conditions to subambient conditions at discharge. The Phase III results are from an engine run at SLS operating line conditions.

The shape of the attenuation spectra for all component tests was similar and exhibited the same characteristic S-shape trend seen for the engine spectra. Figure 4-17 (from Reference 6) shows a typical example of the attenuations obtained from the component turbine test using siren tones. A comparison of this figure with Figure 4-16 shows close agreement between engine and component turbine attenuations, both in level and spectral shape. Variations of 3 to 5 dB in the component turbine attentuations based on tones at the same frequency were common in the previous test results. The engine attenuations, based on broadband results, match those of the component test with a similar data spread over the frequency range.

4.2.3 Comparison of Engine Results with Theory

The theoretical prediction of turbine transmission loss (attenuation) for supersonic blade rows as presented in Reference 9 was used to determine the attenuation for the 6-stage turbine on the CF6-50 engine. The takeoff design point condition was used in the analysis because of the availability of cycle conditions, but is considered representative of the other conditions since the turbine operates near choke for conditions above idle. The prediction program was set up following the recommendations noted in Reference 9 for the CF6-50 turbine. The attenuation results of the theoretical predictions are shown in comparison with the engine results on Figure 4-16. A maximum of 8.54 dB attenuation is recorded at 630 Hz after reaching the first cut-on frequency of 570 Hz. The attenuation drops off to 7.12 and 6.72 dB at 800 and 1000 Hz respectively. Prior to cut-on, no significant attenuation (1.43 dB) is computed.

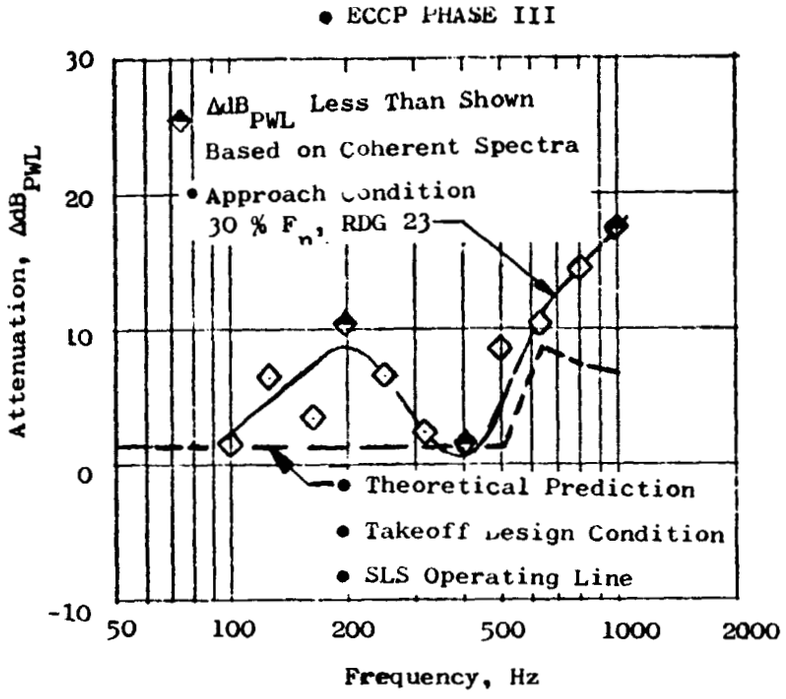

Figure 4-16 Measured Attenuation Spectrum and Predicted Results For CF6-50 Six Stage Turbine

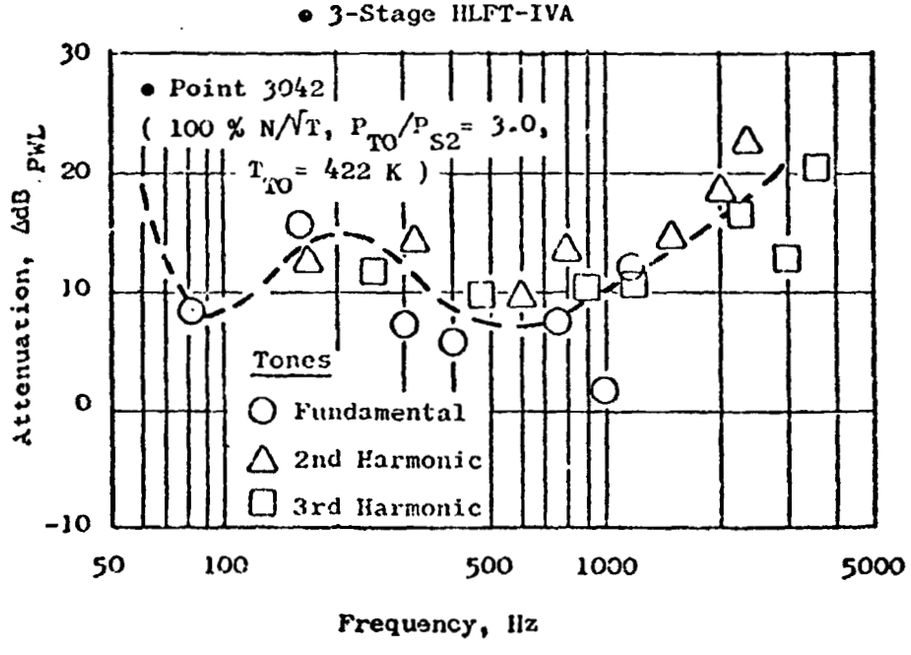

Figure 4-17 Attenuation Spectrum from 3-Stage Low Pressure Turbine

These results are similar to those obtained on the engine in that attenuations above 500 Hz are generally higher than those at the lower frequencies. The magnitude of the attenuations determined from the theoretical model are close to those obtained from the engine test. The engine results are 5 to 8 dB higher than the predicted attenuation in the region around 200 Hz. However, the effect of the cut-on frequency around 570 Hz is clearly seen in the engine data to follow the predicted results within 1.5 to 2 dB.

4.3 PRIMARY NOISE SOURCE LOCATION

Cross-correlation analysis was used in an attempt to identify primary noise source locations within the combustor. Pairs of sensors combined for this analysis included those at:

- Compressor exit (Plane 3.0, MADAR Probe) to combustor inlet (Plane 3.5, 102° or 282° borescope probe)
- Compressor exit (Plane 3.0) to combustor exit (Plane 4.0, HPTN probe)
- Combustor inlet (Plane 3.5) to combustor exit (Plane 4.0)
- Compressor inlet (Plane 3.0) to core exhaust (Plane 8.0, Exhaust Probe A or B)
- Combustor exit (Plane 4.0) to core exhaust (Plane 8.0)

Comparisons were also made between the 102° and 282° borescope probes located at Plane 3.5 for a few of the low thrust settings.

The data for the cross-correlations used 25 averages in the analysis and were high pass filtered above 80 Hz to remove a test cell resonance and eliminate some 60 Hz electronic noise in the data.

In general good cross-correlations were obtained for all conditions between pairs of internal combustor sensors. At approach power and below, internal combustor signals correlated well with the core exhaust probe sensor. Little or no correlation was observed between internal combustor sensors and the core exhaust probe above 30% F_n, however. This was due to increased turbulence on the probe and uncorrelated noise in the high frequencies. The signal between Plane 3.5 to 4.0 was observed to be uncorrelated at conditions of 82 and 94.6% F_n.

A review of the detailed results for the approach condition (30 percent thrust) is presented for illustration. Similar results were obtained at the lower power settings at all measurement planes. The higher power setting results were also similar for the internal combustor sensors, but the low signal correlation between the combustor sensors and the core probe limited these results.

Coherent spectra derived from the cross-correlations were used to compliment the cross-correlation results and are also presented where appropriate.

4.3.1 Combustor Internal Sensor Comparison

The internal sensors were paired for cross-correlation analysis using the upstream sensor as the sender and the downstream sensor as the receiver. The time delays of the maximum peaks associated with the cross-correlations between Planes 3.0 to 3.5 as seen in Figures 4-18 and 4-19 are negative (-1.5 msec) and correspond to a velocity of 490 m/s which was computed using the point-to-point distance in Table E-1, Appendix E. The average acoustic velocity between these planes is around 482.5 m/s at the approach condition which indicates the peak represents an acoustic wave traveling upstream against the flow. Similar results are observed in Figure 4-20 for the cross-correlation between Planes 3.0 and 4.0. In this instance, the negative time delay corresponds to a velocity of 581 m/s which is very close to the average acoustic velocity of 566 m/s between these planes at this condition.

The cross-correlation between the 102° borescope sensor at Plane 3.5 with the Plane 4.0 probe (Figure 4-21) shows a zero time delay for the peak, indicating the acoustic signal is reaching both sensors simultaneously. The cross-correlations between the 282° borescope sensor at Plane 3.5 with Plane 4.0 shows a negative time delay for the peak in Figure 4-22 which is similar to those observed in Figures 4-18, -19, and -20.

The internal combustor sensor comparison is completed with a cross-correlation at Plane 3.5 between the 102° and 282° borescope probes. Two peaks are observed from the resulting cross-correlation in Figure 4-23, having equal time delays of opposite sign (±2.0 msec) which correspond to velocities of ±634 m/s. The speed of sound at this plane is 482.5 m/s. Acoustic signals at this plane appear to be traveling in a spiral pattern across the sensor and moving in a generally forward direction against the flow as indicated by the time delays obtained from cross-correlations between the Plane 3.5 sensors with the sensor at Plane 4.0 (see Table E-1 in Appendix E).

4.3.2 Combustor Internal to Core Nozzle Sensor Comparisons

A similar analysis conducted between the internal combustor sensors paired with the downstream core probe showed positive time delays for the major peaks of the cross-correlations as noted in Figures 4-24 and 4-25. The Plane 3.0 to Plane 8.0 (element A) cross-correlation in Figure 4-23 shows a positive time delay of +5 msec for the largest positive correlation peak. This time delay corresponds to a velocity magnitude of 553 m/s which is comprised of both acoustic and flow velocities. A negative correlation peak is also observed in the figure which is similar to the result obtained by Karchmer and Reshotko (Reference 10). The Plane 3.0 to Plane 8.0 (element B) cross-correlation in Figure 4-25 shows similar results.

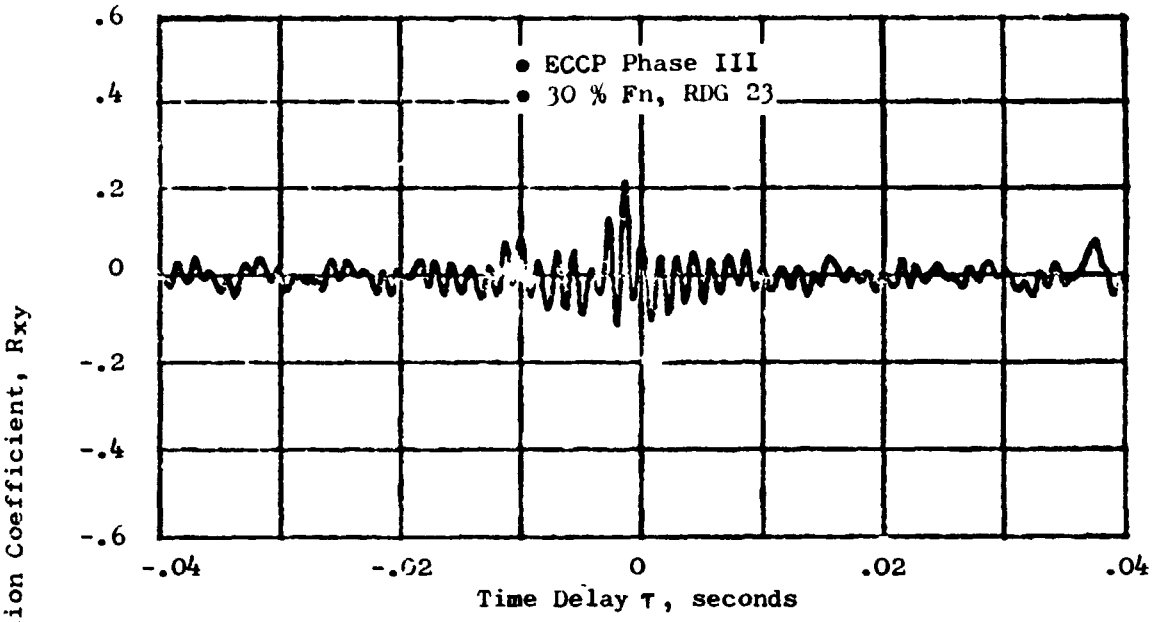

Figure 4-18. Cross-Correlation of Plane 3.0 to Plane 3.5 (102° Probe)

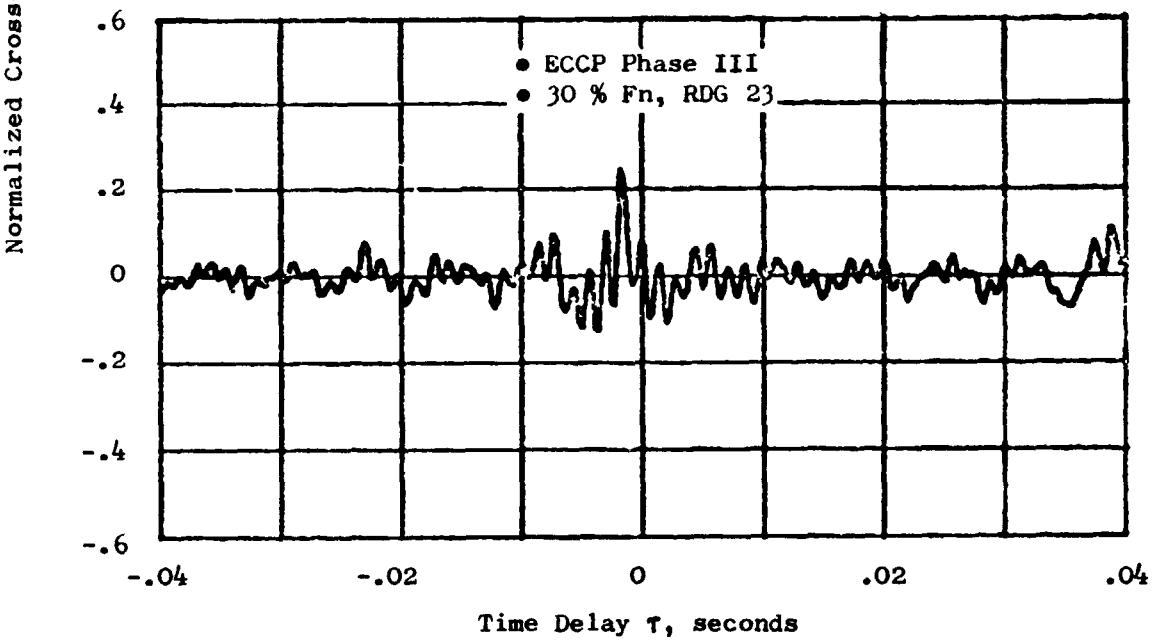

Figure 4-19. Cross-Correlation of Plane 3.0 to Plane 3.5 (282° Probe)

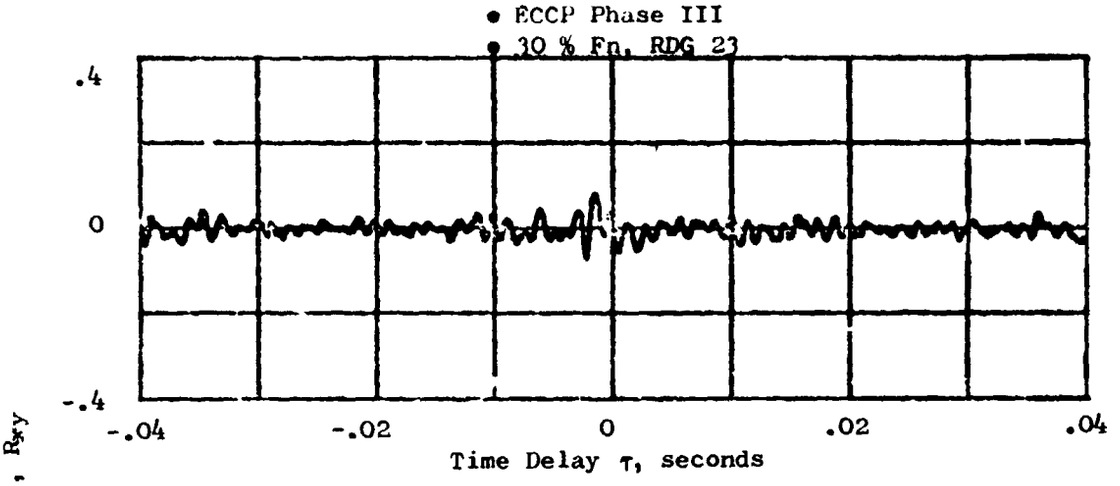

Figure 4-20. Cross-Correlation of Plane 3.0 to Plane 4.0

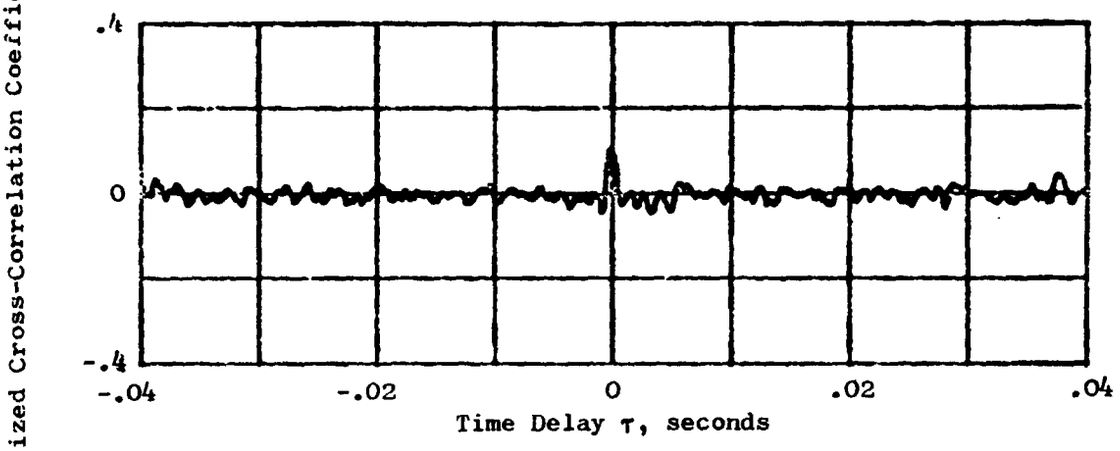

Figure 4-21. Cross-Correlation of Plane 3.5 (102° Probe) to Plane 4.0

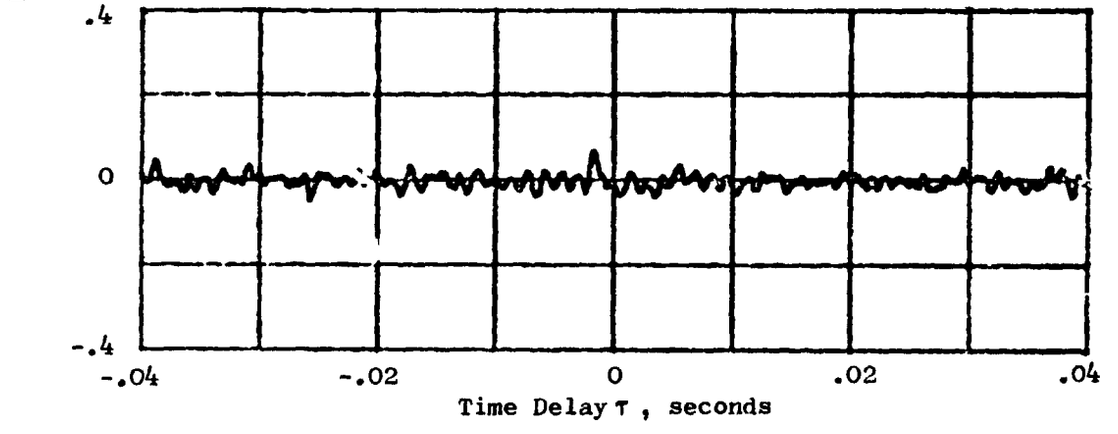

Figure 4-22. Cross-Correlation of Plane 3.5 (282° Probe) t Plane 4.0

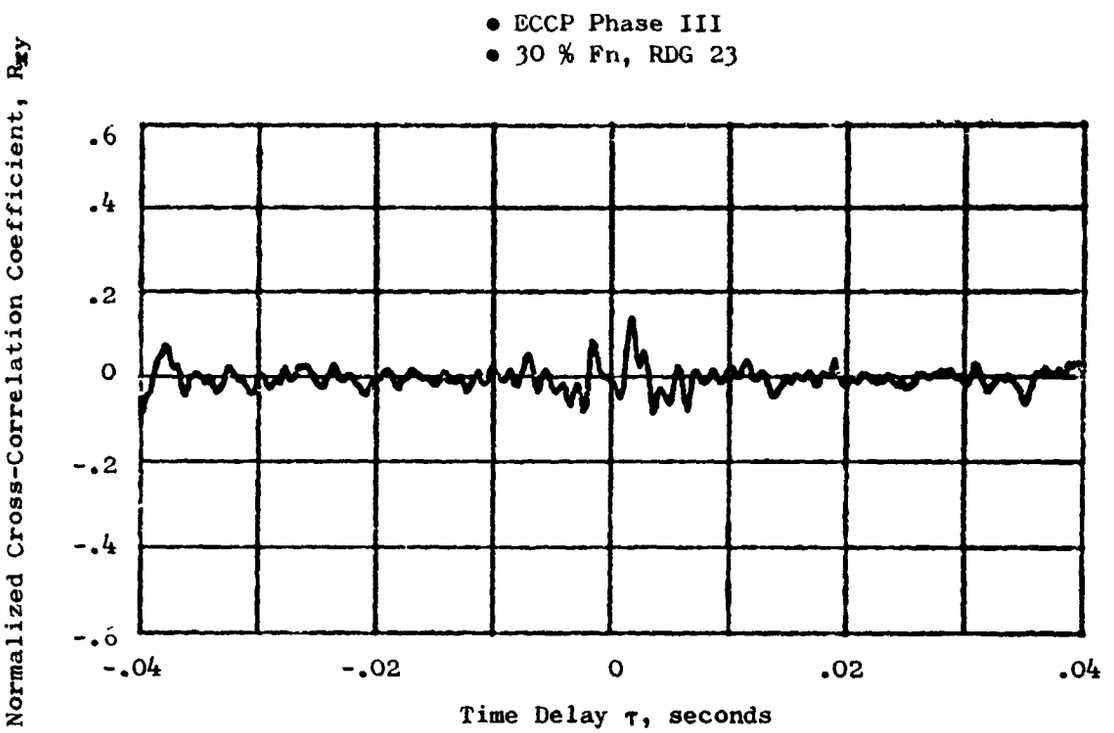

Figure 4-23. Cross-Correlation at Plane 3.5 Between 102° to 282° Sensors

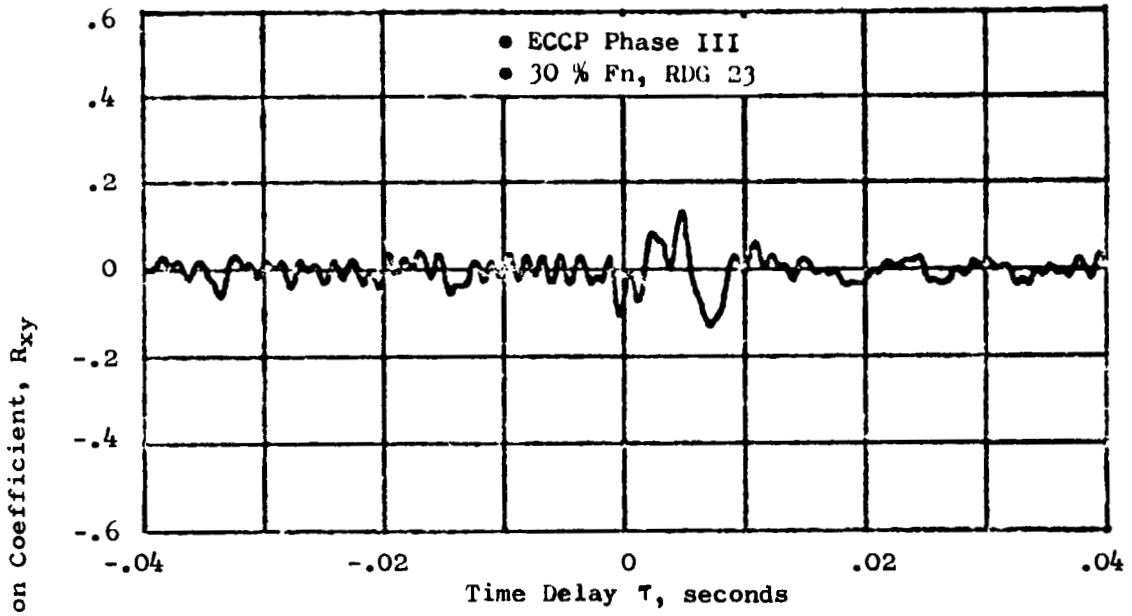

Figure 4-24. Cross-Correlation of Plane 3.0 Probe to Plane 8.0 Probe Element A

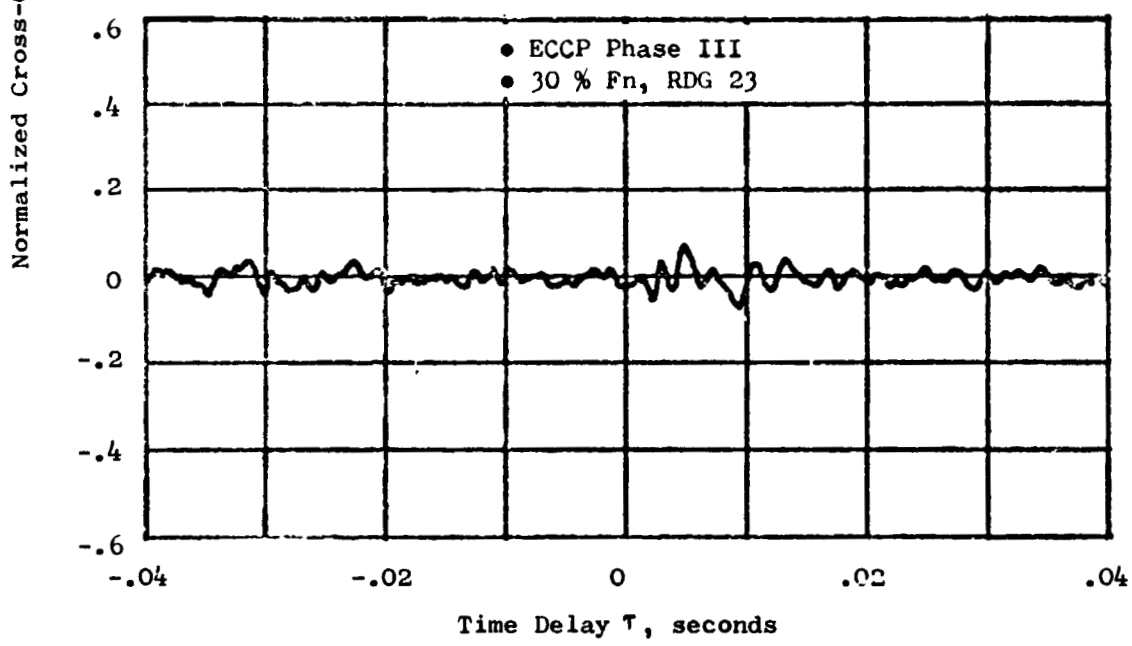

Figure 4-25. Cross-Correlation of Plane 3.0 Probe to Plane 8.0 Probe Element B

The amplitudes of the cross-correlation peaks give an indication of the amount of correlation existing between signals. In the previous results the amplitudes of the normalized correlation coefficient, R_{xy} ranged from +0.25 to +0.075. Complete signal correlations are obtained when R_{xy} is equal to 1.0. Therefore, the degree of signal correlation for the sensor pairs previously discussed is low.

A cross-correlation determined for the forward to aft sensors on the downstream core probe in Figure 4-26a shows a high degree of signal correlation (+0.74) with zero time delay. This result is presented for the approach condition but is representative of the other lower power settings. The high degree of correlation and zero time delay indicates that the majority of the signal is acoustic. A closer look at the cross-correlation between the core exhaust probe A and B Kulites with an expanded time scale of 2 msec per division and increased sample rate is shown in Figure 4-26b. Delay times corresponding to the calculated acoustic and flow velocities for this condition are 0.25 msec and 0.6 msec respectively. The correlation coefficient, R_{xy}, of approximately 70% is seen for a zero time lag peak, which corresponds approximately to the acoustic signal at the probe location. No peak due to turbulence is observed, even with the time resolution increased 25 times the strength of the acoustic signal appears to override any signal due to turbulence at the location. The resulting coherent spectra for this condition are, therefore, considered to be primarily acoustic. The coherent spectrum resulting from this cross-correlation is shown in Figure 4-27 to confirm this since there is almost complete coherence over the frequency range of 250 Hz to 800 Hz, which is the core noise region of interest.

4.3.3 Primary Noise Source Summary

The cross correlation of the internal pressure measurements obtained on the ECCP combustor in the CF6-50 engine were reviewed to determine the maximum time delay attributed to acoustic propagation. Vectoring of the time dalays from each of the cross-correlations gave an indication of the direction of acoustic signal travel between sensors. Amplitudes of the peaks were compared to those of the time delays associated with the flow velocity in order to evaluate the strength of the acoustic signal. A tabulation of the amplitudes and time delays for these cross-correlations is found in Appendix D. This procedure, performed at each test condition, indicated acoustic signals were traveling upstream between pairs of sensors in the combustor region (Planes 3.0, 3.5 and 4.0). A downstream traveling signal was apparent for all vectoring done between the combustor sensors and the core exhaust probe.

The cross-correlation between the 102° and 282° sensors at Plane 3.5 shows positive and negative time delays corresponding approximately to acoustic velocity and of nearly equal amplitude. This suggests that circumferential traveling waves are also present in the combustor.

The forward traveling signals occur between Planes 3.0 to 3.5, 3.0 to 4.0, and 3.5 to 4.0. This result suggests that the primary noise source is located near the combustor discharge since the highest energy level is in this

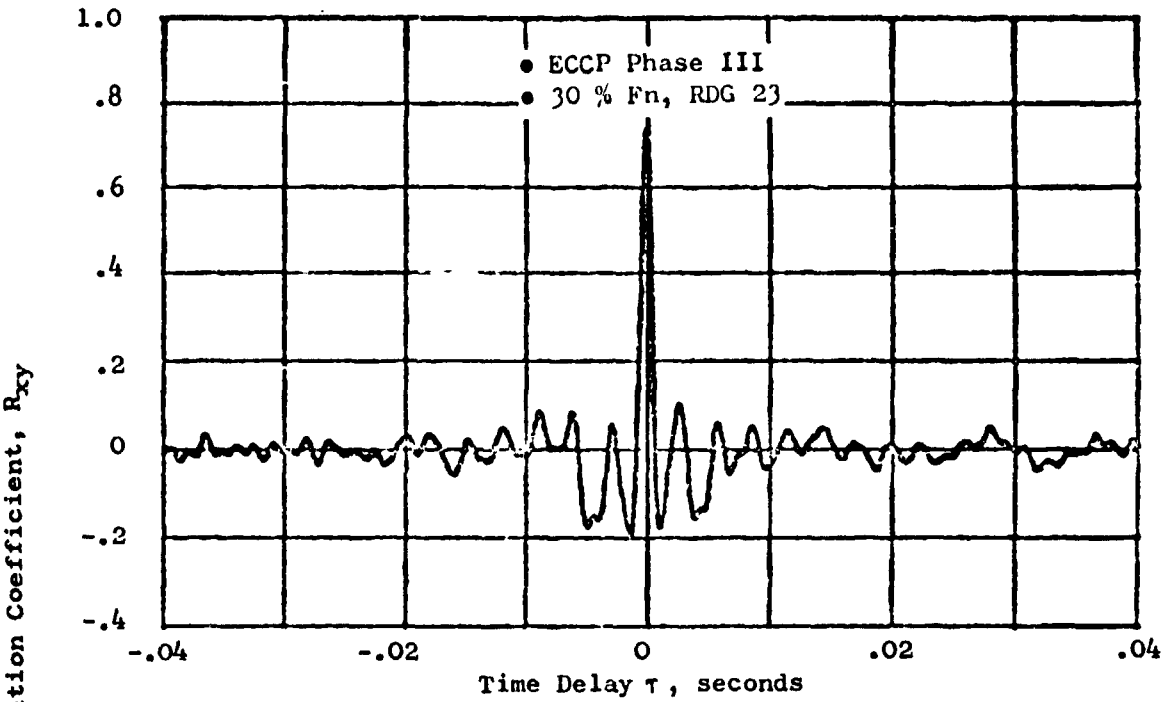

Figure 4-26.a. Cross-Correlation of Core Probe Element B With Element A

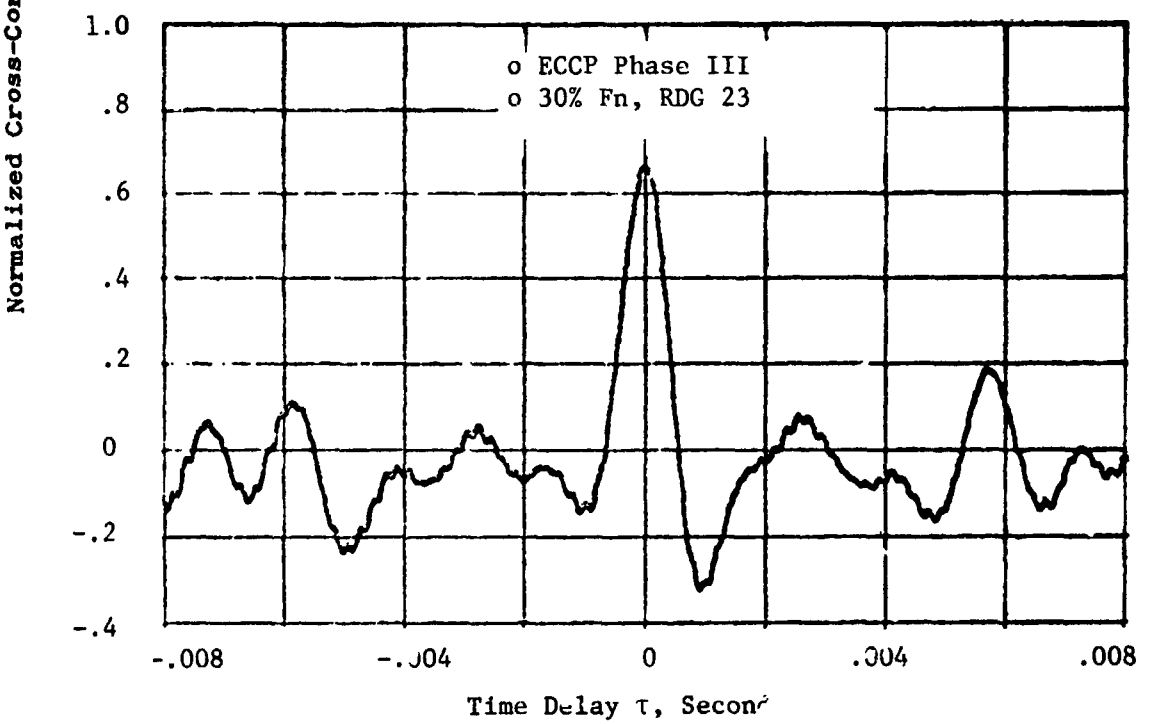

Figure 4-26b. Cross-Correlation of Core Probe Element B with Element A, On Expanded Scale

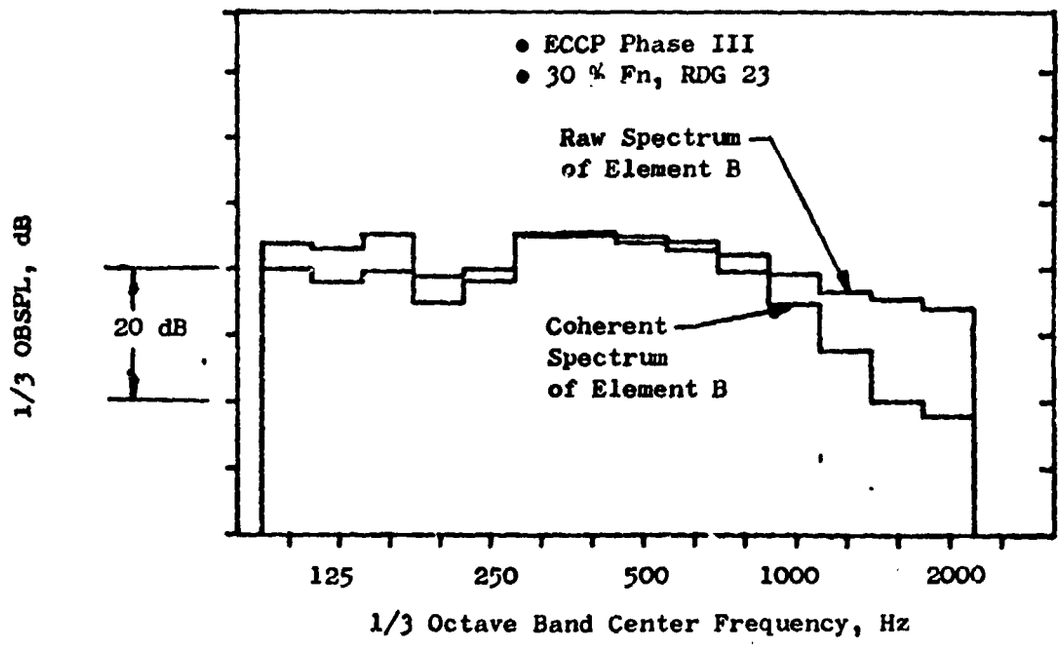

Figure 4-27. Coherent Spectrum at Core Nozzle Discharge, Plane 8.0

area. The cross-correlations for conditions below 45% F_n between the combustor sensors and the exhaust probe indicate the sound is traveling aft.

A review of the cross-correlation analysis results indicates the combustor environment is a highly turbulent flow field with numerous noise sources. The entire combustor region might be considered as a source since the wave lengths of predominate concern for core noise are from 0.914 to 1.524 meters long at the engine operating conditions and the distances between probes average 0.304 to 1.219 meters.

4.4 OVERALL POWER LEVEL COMPARISONS

Comparisons were made at the core nozzle discharge plane with the overall sound power level computed from probe raw spectra and with coherent spectra considered to be mostly sound.

Overall power level comparisons were made between the measured results ($FPWL_{meas}$) and the General Electric component (PWL_{GE}) and engine (PWL_{GEFAA}) correlating parameters used for OAPWL predictions. The measured results assume that the measured pressure is entirely made up of acoustic plane waves both in the combustor and core nozzle.

4.4.1 Acoustic Power Level in Exhaust Duct

The power level in the engine core exhaust duct was calculated from pressure measurements made with the Plane 8.0 sound separation probe. The probe was traversed to five radial immersions located on centers of equal annulus areas. The FPL 1/3 octave band spectra from 50 to 2000 Hz obtained at each immersion were compared for similarity. Figure 4-28 shows this comparison for both Kulites on the probe at the 30% F_n approach power setting. It indicates close agreement in spectral shape and content for all immersions except the inner immersion (5) which is near the turbulent region of the plug nozzle centerbody. This result in general, typifies comparisons of these measurements at other conditions. Because of the close agreement at all immersions the pitchline immersion (3) was the primary immersion used in all measurement comparisons with upstream sensors. Cross-correlation analysis was performed between the "A" and "B" Kulites on the core probe at each immersion for all test conditions. A high degree of correlation between Kulite signals was apparent at all immersions for power settings of 30% F_n (100% pilot fuel) and below.

Coherence analysis performed on these sensors at these conditions showed good coherence between the forward and aft sensors on the probe in the frequency range between 315 to 630 Hz which is the primary region for core noise. Figure 4-29a and -29b illustrate the cross-correlation and coherence analysis results for the 30% F_n point (with 100% pilot fuel) at immersion four. The correlation coefficient R_{xy}, is 0.75, as seen in Figure 4-29a. Note that the probe 1/3 octave band coherent spectrum (frequency range of 100

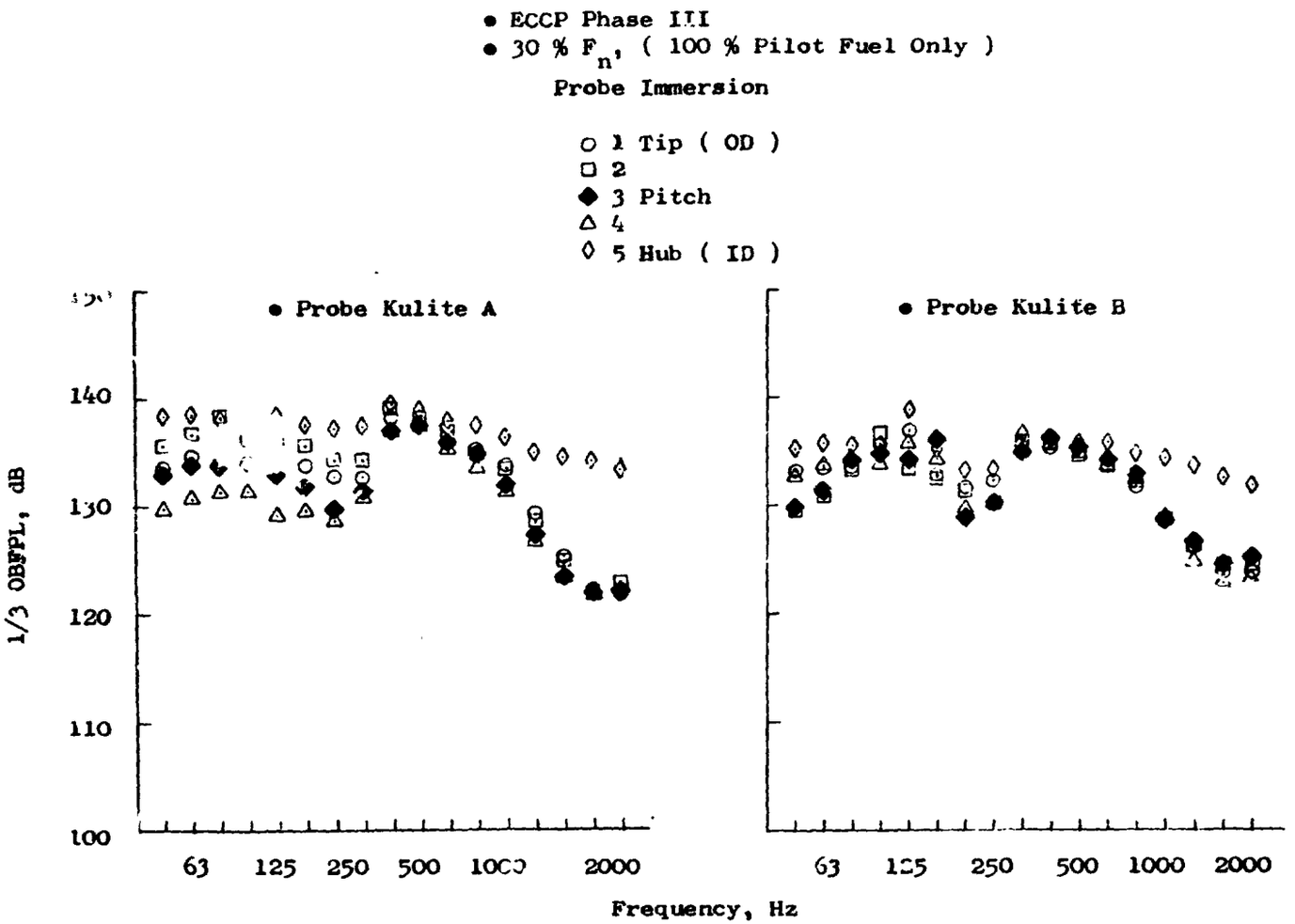

Figure 4-28. Comparison of Core Probe Spectra [illegible] Immersion

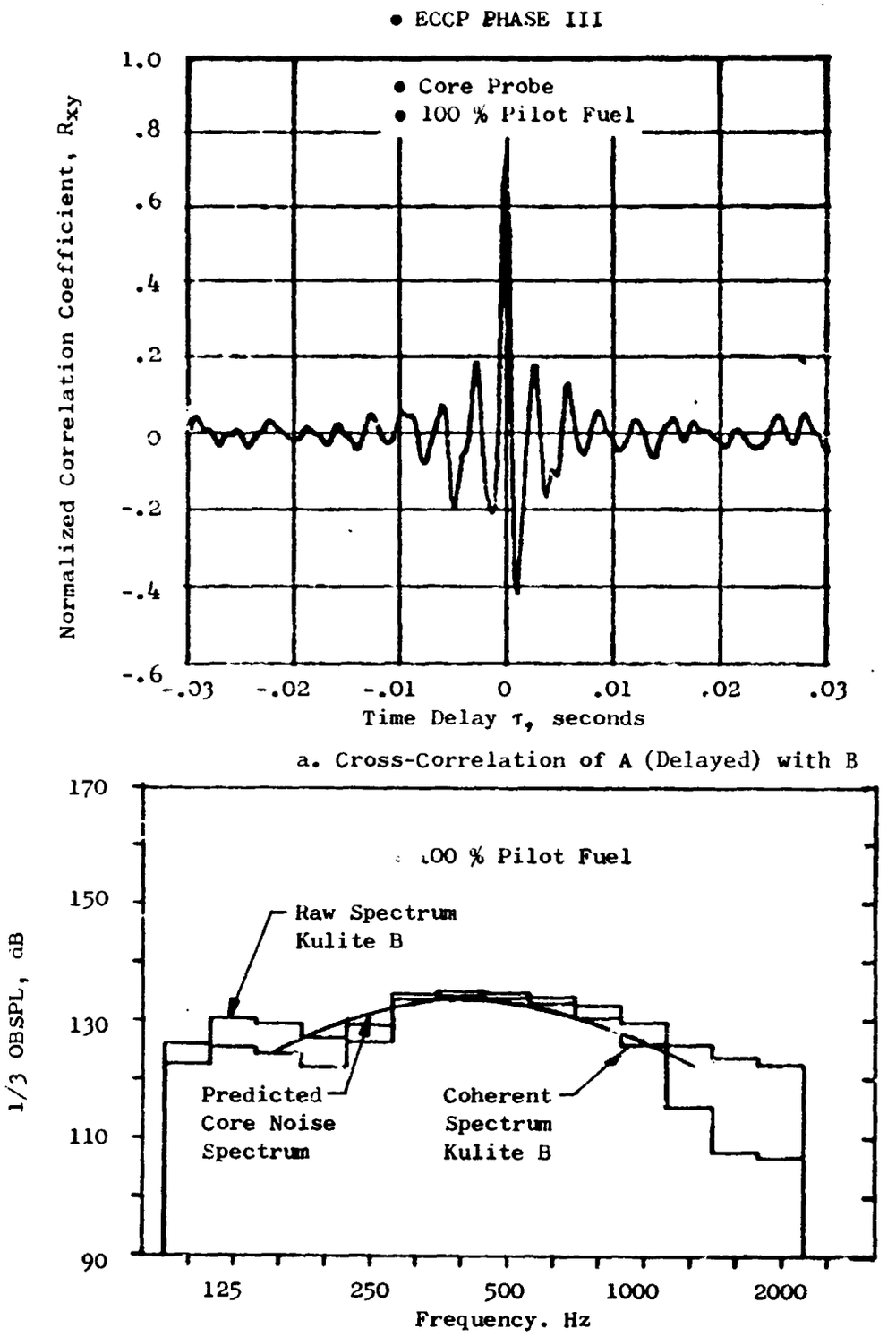

Figure 4-29. Core Probe Immersion 4 at 30 Percent Thrust

through 2000 Hz) in Figure 4-29b, with its peak at 400 Hz, fits almost exactly, with the GE core noise predicted spectrum shape (Reference 11), the level of which was shifted to agree with the coherent spectral level at 400 Hz. Similar results for the 19.7% F_n point with 100% pilot fuel are presented in Figures 4-30a and -30b. A level of 0.55 is observed for the correlation coefficient. The predicted core noise spectrum is again, in very good agreement with the coherent spectrum in the region of high coherence, indicating the sound observed is predominantly core noise.

The approach power setting at 29.7% F_n with a near 50/50 fuel flow split between pilot and main burner stages shows a lesser degree of correlation (below 0.2) than for the 100% pilot fuel condition. The higher power settings which operate on a split fuel flow schedule also showed a much lower correlation between signals at all immersions. The coherence analysis of these conditions showed a reduction of the coherent portion of the spectrum to between 315 to 500 Hz. The amount of coherence between the core probe signals for these mixed fuel flow points was less than for the 100% pilot fuel points. Figures 4-31a and b illustrate the results obtained from the cross-correlation and coherence analysis of the approach point at 29.7% F_n (with 46.9% pilot fuel). The coherent spectrum at this condition still retains the core noise shape but there is less agreement with the core noise predicted spectrum. This is characteristic of the results obtained at the high thrust, split fuel flow conditions, as illustrated by Figures 4-32a and b which show results for 64.6% F_n with 17.8% pilot fuel. The amount of correlation is again low (the level of the normalized correlation coefficient is 0.2), and the amount of coherence between the raw and coherent spectra is less than at the lower power settings with 100% pilot fuel.

Average overall pressure levels were determined for all conditions from selected immersions. The immersions selected were based on those with the higher degree of correlation and the least noise floor of the coherent spectra.

The overall pressure levels determined from the core probe immersion averaged raw signal levels and the coherent spectra (which are considered to be mostly sound) were compared on a corrected core speed basis. The results of this comparison in Figure 4-33 shows the effect of the operation with pilot fuel only, and with a fuel split to the pilot and main burner systems on the overall sound pressure level in the core exhaust. A reduction in OASPL is realized when operating in the split fuel flow mode. This reduction at approach is seen to be as much as 7.5 dB with the raw spectra to 9 dB with the coherent spectra.

The acoustic power level in the core nozzle is clearly dominated by core noise at approach conditions and below. These conditions which operate with the pilot burner only also show a high OASPL. At higher power settings which operate with fuel flow splits to the pilot and main stage burners the OASPL is less than the low power settings. The effect is most dramatic at the approach condition with and without the fuel flow split.

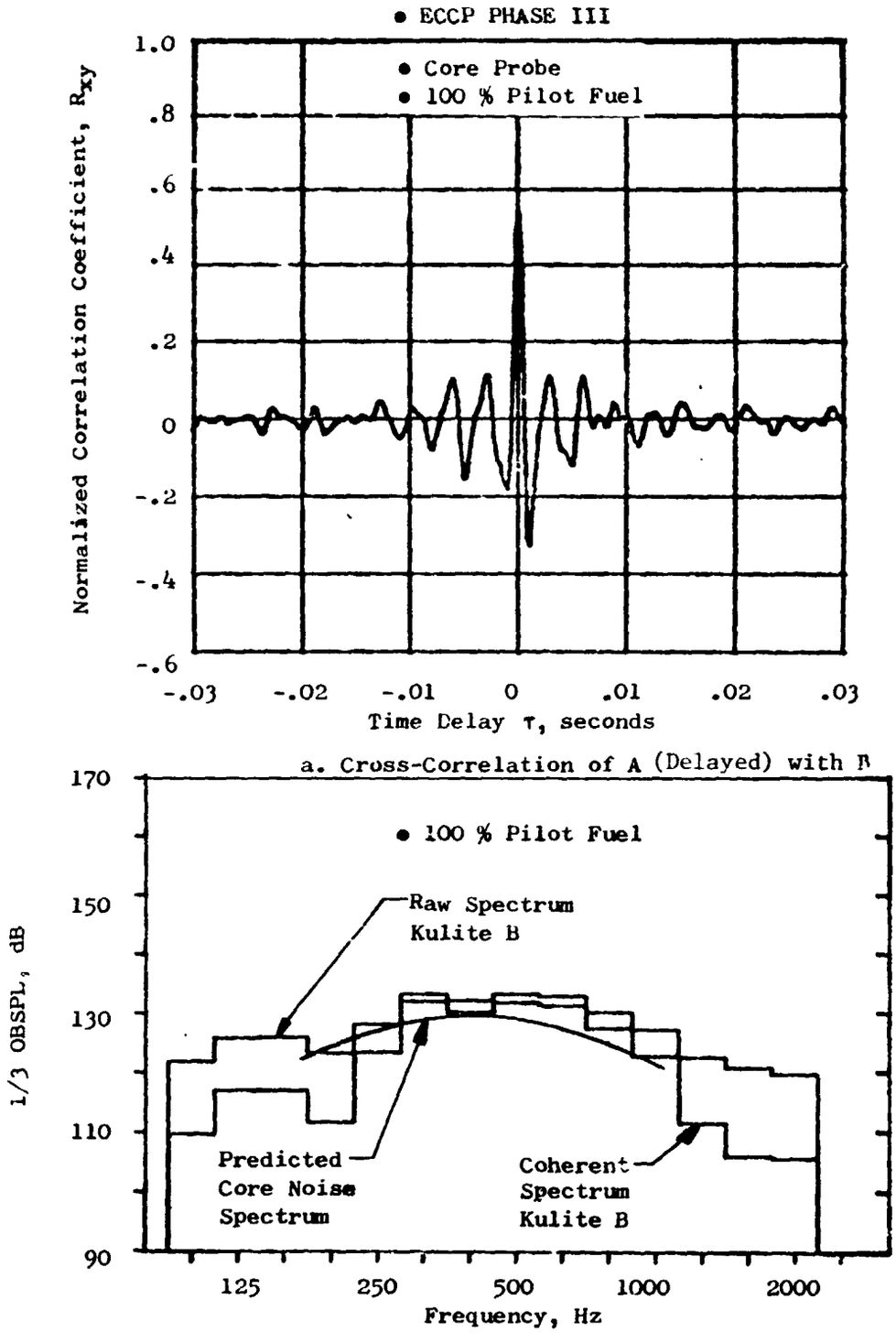

Figure 4-30. Core Probe Immersion 4 at 19.7 Percent Thrust

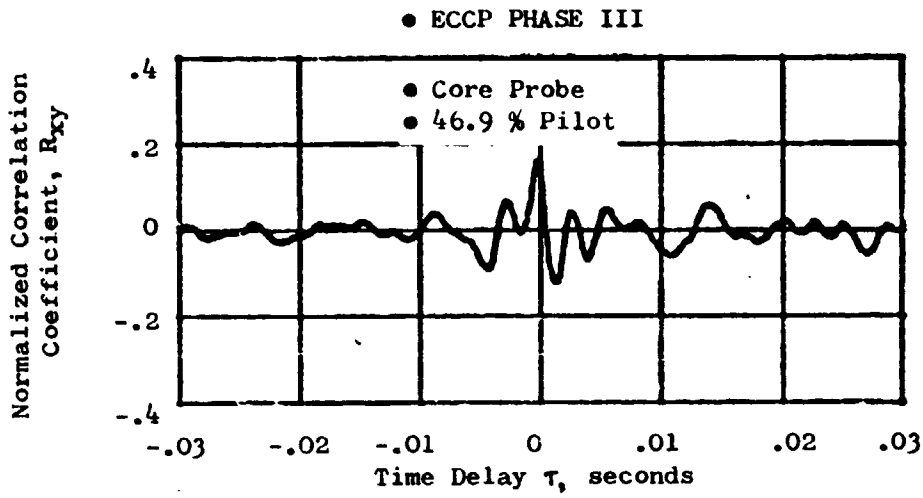

a. Cross-Correlation of A (Delayed) with B

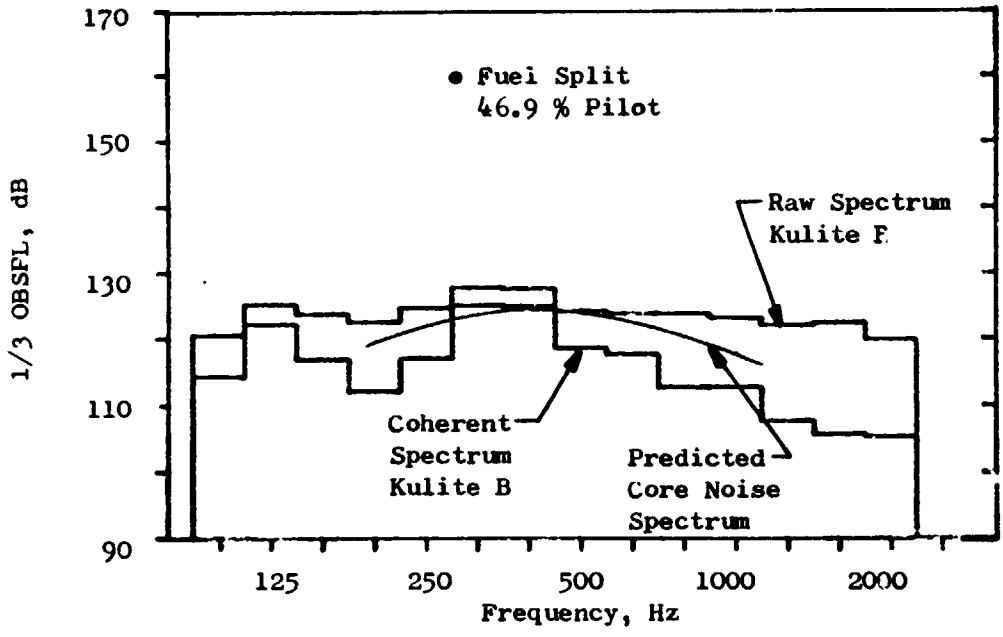

b. Coherent Spectrum of Element B

Figure 4-71. Core Probe Immersion 4 at 29.7 Percent Thrust

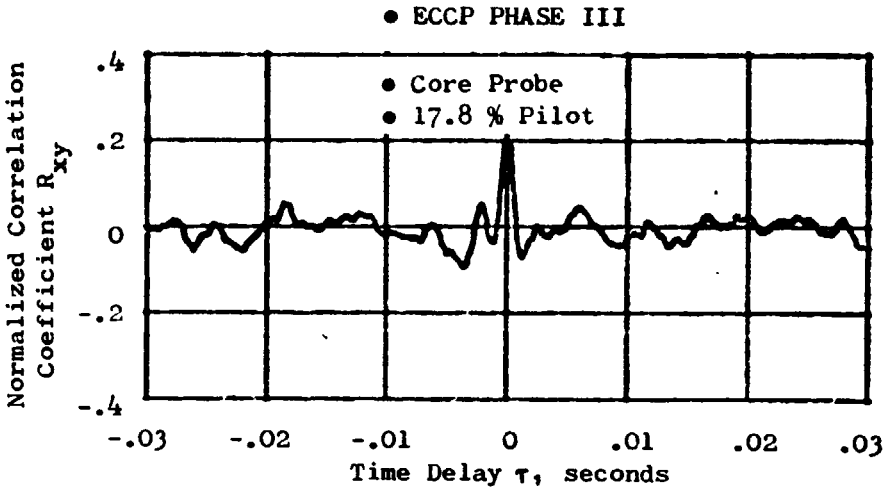

a. Cross-Correlation of A (Delayed) with B

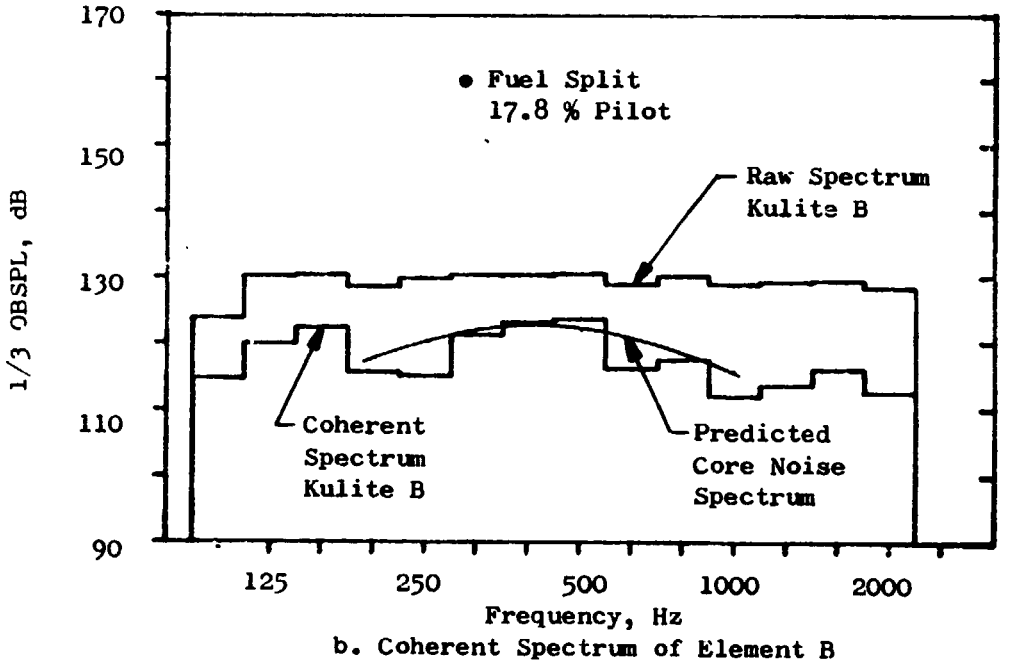

b. Coherent Spectrum of Element B

Figure 4-32. Core Probe Immersion 4 at 64.6 Percent Thrust

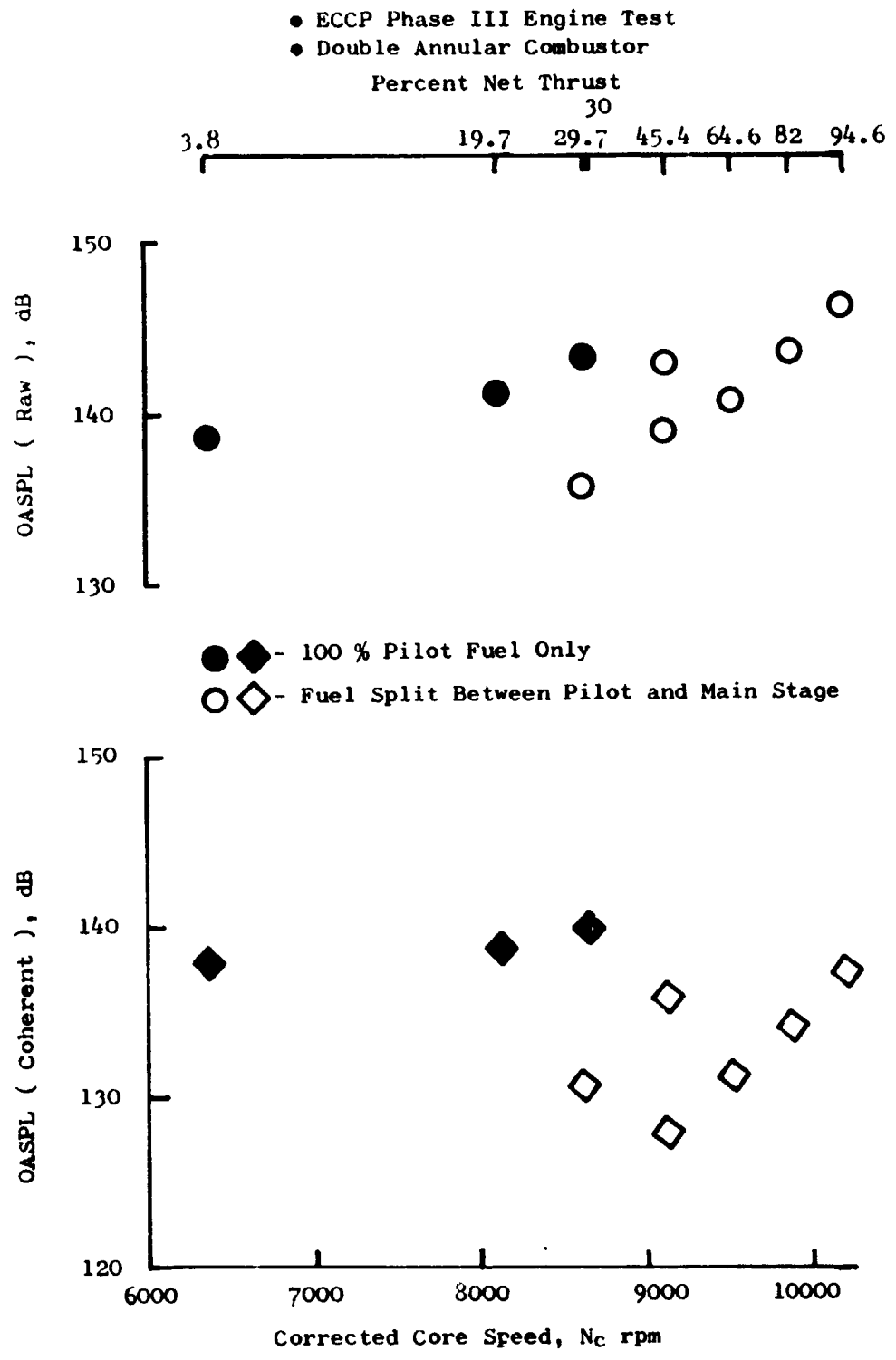

Figure 4-33. Comparison of Raw and Coherent OASPL with Core Speed

4.4.2 Comparison of Measured Power Level with Component and Engine Predictions

The component and engine overall power level predictions were based on corrections derived from tests conducted under the GE Core Engine Noise Investigation Program, Reference 11.

Component (PWL_{GE}) Comparison

The component prediction is based on the correlation derived from component tests conducted in Reference 11. The overall power level PWL_{GE} is calculated from:

$$PWL_{GE} = 83.6 + 10 \log \left[(P_{T3}/T_{T3})^{1.5} V_r^{3.5} (T_{T4}-T_{T3}) \right] , \text{ re } 10^{-13} \text{ watts} \qquad (7)$$

where P_{T3} = Combustor inlet total pressure, kN/m^2

T_{T3} = Combustor inlet total temperature, K

T_{T4} = Combustor exit total temperature, K

V_r = Reference velocity defined as

$$= \frac{W_{36} R T_{T3}}{P_{T3} A_{ref}} , \text{ m/s}$$

W_{36} = Total combustor air flow, kg/sec

A_{ref} = Combustor reference area, m^2 (for CF6-50 A_{ref} = 0.37287 m^2)

The aero parameters used in calculating the PWL_{GE} values are found in Table 5 (Section 3.7).

The measured results were based on an overall power level determined from the internal fluctuating pressure measurements reduced to 1/3 octaveband spectra and corrected for frequency response loss. The overall levels determined from these pressure measurements (considered to be acoustic plane wave signals) were converted to power level accounting for impedance changes due to differences in test conditions, Mach number effects, and area differences at each measurement plane as described in Section 3.7. The resulting power level was designated $FPWL_{meas}$ with units in dB re 10^{-13} watts. The parameters used in the conversion to $FPWL_{meas}$ are found in Table 6.

Figure 4-34 shows the comparison of $FPWL_{meas}$ to PWL_{GE} for the internal combustor sensors at Planes 3.0, 3.5 and 4.0. The Plane 3.0 $FPWL_{meas}$ is 5 to 15 dB lower than the $FPWL_{meas} = PWL_{GE}$ line at conditions above idle giving a flatter trend to the data. The FPL measured at Plane 3.0 is in the compressor discharge region prior to the start of combustion.

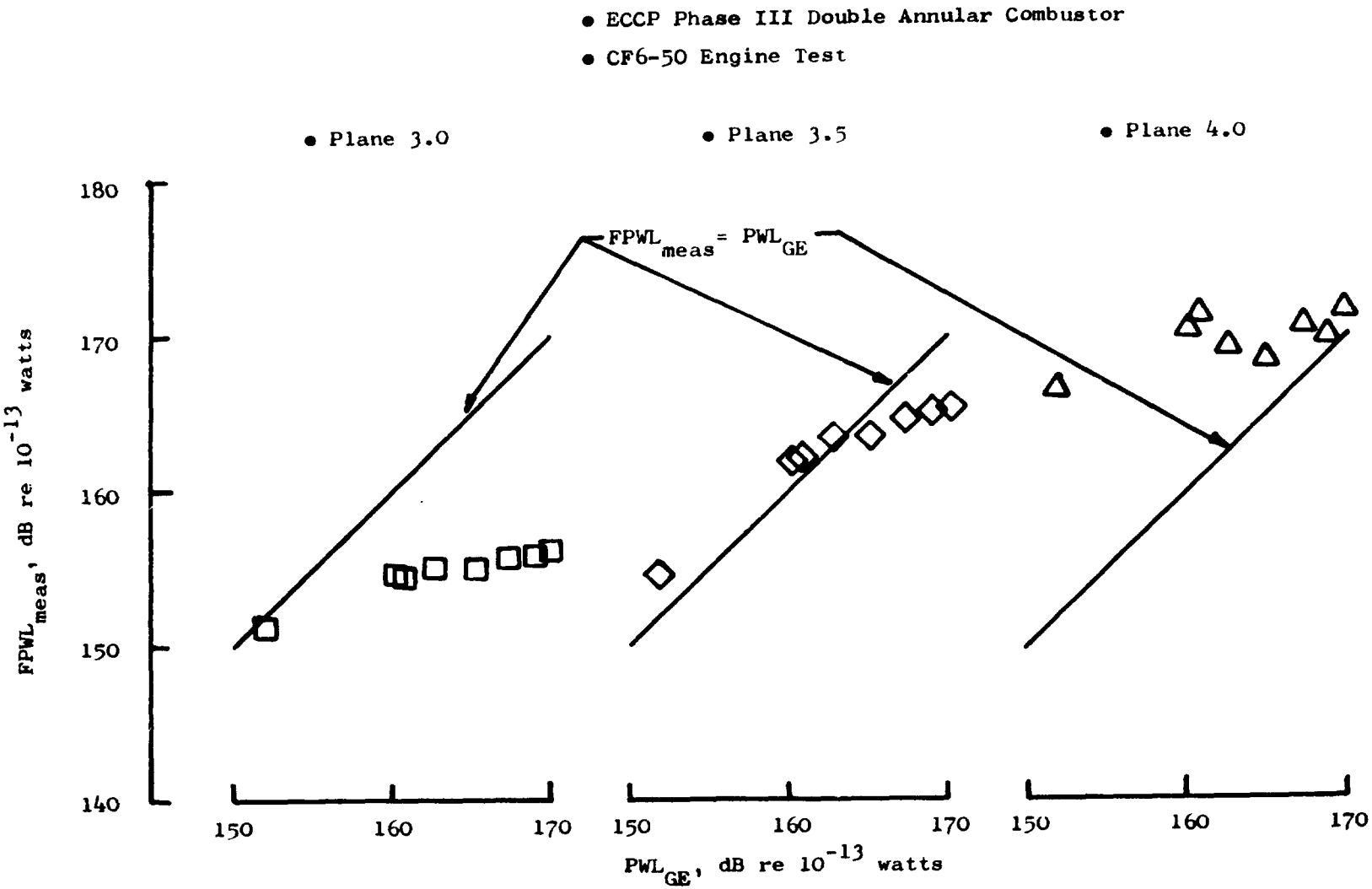

Figure 4-34. Comparison of $FPWL_{meas}$ to PWL_{GE} for Internal Sensors

The $FPWL_{meas}$ at Plane 3.5 agre ell with the predicted PWL_{GE} at all test conditions except at the extre .s. Plane 3.5 is in the pre-mix region of the combustor aft of the fuel nozzles. Ignition takes place at this plane to start the combustion process.

At Plane 4.0, the $FPWL_{meas}$ is higher than predicted at the lower half of the test conditions by 15 to 5 dB and gives a similar data trend as seen for Plane 3.0. The FPL at this plane is determined from measurements in the borescope port located between two vanes in the high pressure turbine nozzle diaphragm. As previously discussed, this region, which operates at a near constant Mach number of 0.55, contains a large amount of high frequency noise at all test conditions.

The best comparison with PWL_{GE} of the engine $FPWL_{meas}$ from FPL measurements appears to be at Plane 3.5 for virtually all test conditions.

Engine (PWL_{GEFAA}) Comparison

The PWL_{GEFAA} engine prediction is based on a correlation derived from engine farfield data and core probe results obtained during tests conducted under the Core Engine Program, Reference 11. The overall power level from the engine correlation is calculated from

$$PWL_{GEFAA} = 169.3 + 10 \log W_{36}(T_{T4}-T_{T3})^2(\rho_3/\rho_o)^2 - 40 \log (T_{T_4}-T_{T_5})_{Design}$$

re 10^{-13} watts (8)

where the nomenclature is described above and $(T_{T4} - T_{T5})_{Design}$ is the total temperature drop across the high and low pressure turbines at the cycle design point.

The comparison with the measured power level is based on the pressure measurements taken with the sound separation probe in the core nozzle. The power level determined from the as measured fluctuating pressure measurements in the core exhaust was higher than the predicted power level from the engine correlation. To more accurately compare the ECCP Phase III data with the engine correlating parameter, the coherent part of the probe Kulite B spectra with the probe Kulite A signal was used to compute the PWL_{meas}. An average OASPL obtained from the individual immersions was used in conjunction with the PWL calculation procedure noted in Section 3.7.

Figure 4-35 shows the comparison of PWL_{meas} computed from coherent spectra as discussed with the engine prediction parameter PWL_{GEFAA}. The solid symbols are for the lower power settings using 100% pilot fuel, while the open symbols are for split fuel flow conditions. The idle point was highly contaminated with a large 400 Hz sinusoidal tone, as previously discussed. A tone correction of 7.9 dB brought this point in agreement with the other 100% pilot points (dark symbols) which then paralleled the equal PWL line. The

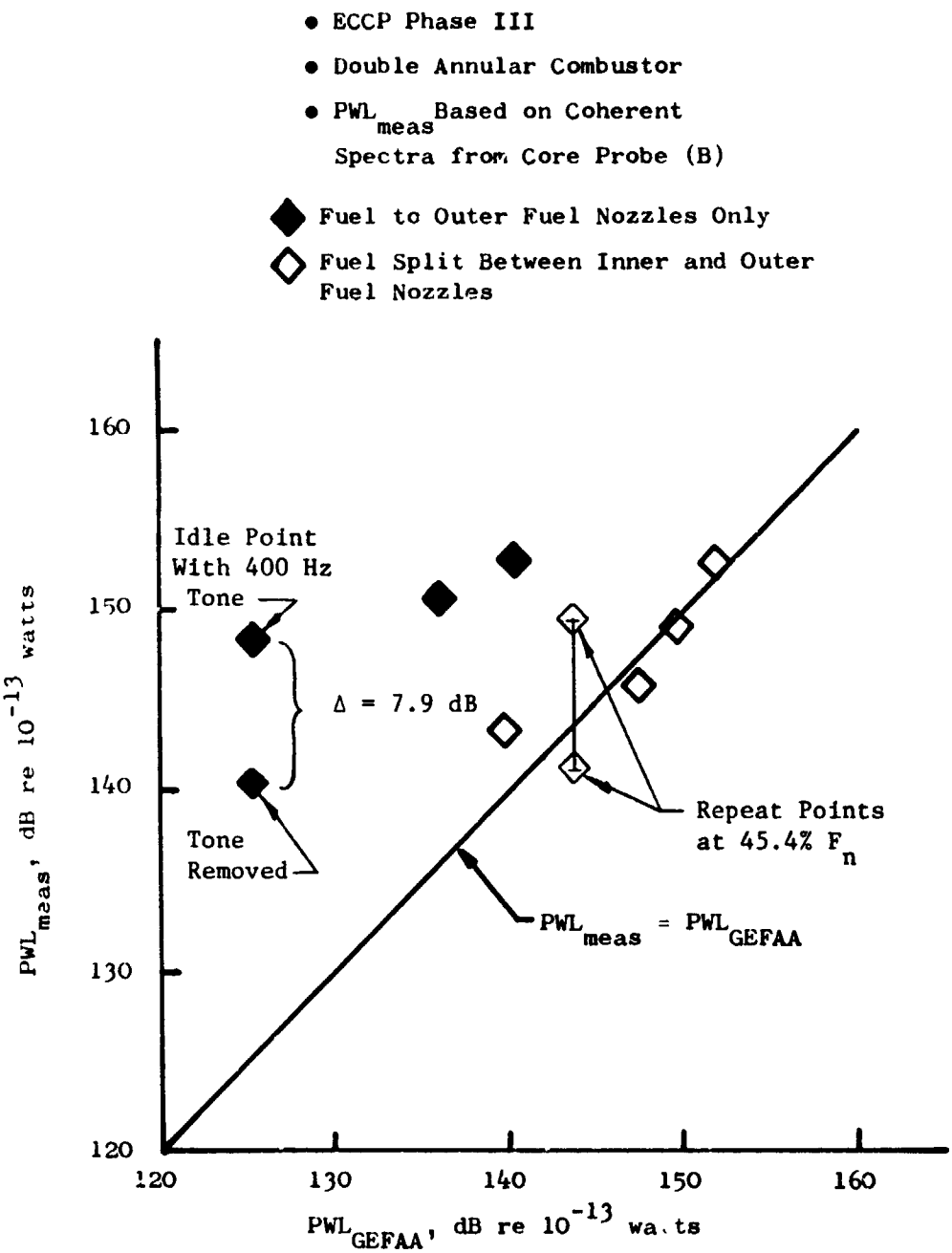

Figure 4-35. Comparison of PWL_{meas} to PWL_{GEFAA}

tone correction was applied to the OASPL from the 1/3 OBSPL coherent spectra at each immersion. An average "tone corrected" OASPL was then obtained and converted to PWL_{meas}. This figure clearly shows the effect of burning in the outer pilot stage only as resulting in higher overall power levels by about 15 dB. The split flow conditions, however, agree with the correlation as repeat readings at 45.4% F_n fall above and below the equal PWL line. The approach point at 30% F_n (100% pilot fuel) is 9 dB above the same condition at 29.7% F_n with a fuel split of about 50%.

Operating the combustor with the outer ring of 30 fuel nozzles only, at the power settings of approach and below is desirable from an emissions standpoint as discussed in Reference 1. With fuel to the pilot stage only the 24% of the total combustor air that passes through the outer burner mixes with the total amount of fuel added. The main burner air flow (49% of the total combustor air flow) may be considered to act as cooling or dilution air which mixes with the other 29% of W_{36} used for liner cooling, etc. This has the effect of increasing the local fuel-air ratio and results in hot flow in the outer annulus with a higher velocity, while the flow in the inner annulus remains relatively cool and has a lower velocity. Mixing of these two dissimilar regions may result in noise generation due to shear layer interaction between the hot and cool streams. There is, of course, no way of determining this from the present scope of work.

With both pilot and main stage burning, the temperatures in both streams are in much closer agreement and consequently, the stream velocities are more nearly equal, thus reducing any shear layer interaction noise. Pressure measurements taken at Plane 4.0 at 30% F_n with the 100% pilot fuel and at 29.7% F_n with both pilot and main stages fueled show a difference of approximately 6 dB lower level with the 60 fuel nozzles in both stages burning.

Agreement with the engine correlation is obtained for the 100% pilot fuel only points in Figure 4-36 when an effective temperature, $T4_p$, is computed from the fuel-air ratio determined for the percentage of the total combustor airflow that passes only though the outer pilot burner annulus. The fuel-air ratio for these 100% pilot only points is considerably higher since only the pilot air enters into the calculation. The main stage air in this case, is considered to act only as cooling and dilution air and does not enter the combustion process.

The higher $T4_p$ obtained from the increased fuel-air ratio results in a greater PWL_{GEFAA} which shifts the 100% pilot points at 30, 19.7% F_n and the tone corrected idle condition within the data correlation region.

Results of the ECCP Phase III tests have shown a significant increase in overall sound power level (9 dB) at approach with 100% pilot fuel, compared to an approximate 50/50 fuel split between stages. Consideration must, therefore, also be given to the influence of noise on the operation of the Double Annular combustor system during approach power, in addition to the emission tradeoffs.

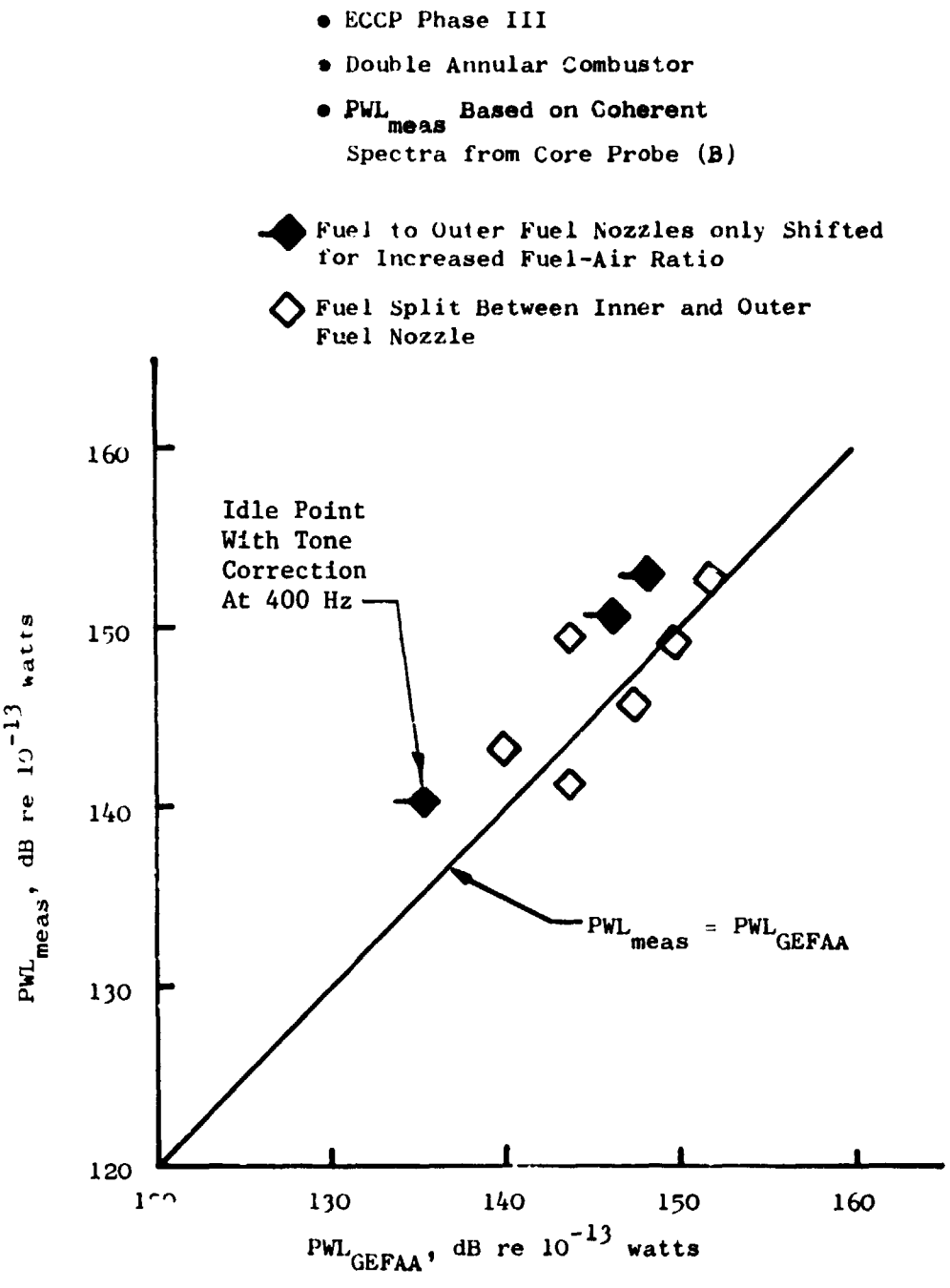

Figure 4-36. Comparison of PWL_{meas} to PWL_{GEFAA} Using Adjusted Fuel-Air Ratio for 100 % Pilot Points

5.0 CONCLUSIONS

This was the first time internal pressure measurements were acquired on the CF6-50 engine with a Double Annular combustor. The significance of this engine test was to establish a base for comparison with component data and provide an understanding of the operation of a Double Annular combustor system in an engine environment.

5.1 DOUBLE ANNULAR COMBUSTOR SPECTRA COMPARISONS

The resulting spectra from the internal combustor measurements indicate that conditions at the lower power settings (30% F_n and below) are more characteristic of core noise spectra. The Plane 3.5 1/3 octave band spectra are peaked in this frequency range between 250 and 1000 Hz for those lower power points, which is typical of core noise. The measurements at this plane are more representative of combustion noise than either the compressor discharge, Plane 3.0 or combustor discharge, Plane 4.0. Values of $FPWL_{meas}$ computed from the Plane 3.5 measurements match the predicted values of PWL_{GE} from the component correlation.

The core probe measurements at these conditions match the empirical combustor shape, peaking at 400 to 600 Hz. Levels of PWL_{meas} computed from the core probe average OASPL from coherent spectra (which were mostly sound) obtained from as many as five radial immersions showed good agreement with the engine PWL_{GEFAA} correlation for the approach power setting and higher points operated with fuel splits to the inner and outer rings of fuel nozzles. The power levels from the approach condition and lower points operated with 100% fuel to the outer pilot ring of fuel nozzles were higher than predicted. Adjusting the T_{T4} to account for the increased fuel-air ratio in the outer annulus with pilot fuel only increased the PWL_{GEFAA} and shifted the lower power points within the region of data correlation.

The results from this Double Annular combustor test show a significant increase in overall power level (9dB) at approach with 100% pilot fuel, compared to an approximate 50/50 fuel split between pilot and main stage. Considerations must therefore be given to the noise impact as well as the emissions trades in selecting approach power operating fuel schedules.

The transmission loss across the CF6-50 turbine and nozzle computed from the difference between spectra which were predominately acoustic matched component test results and theoretical predictions.

5.2 NOISE SOURCE LOCATIONS

The results of the cross-correlation analysis showed negative time delays for the internal combustor sensors paired upstream to downstream,

indicating forward sound wave propagation, opposite to the direction of flow. The internal combustor to core nozzle Kulite pairs gave positive time delays, indicating acoustic signals traveling aft. Circumferential waves were also identified between the Planes 3.5 sensors at 102° and 282°.

The predominate time delays between all the Kulite sensor pairs are listed in Table E-1 of Appendix E. As seen in the table, positive time delays are recorded for combustor sensors paired with the sensors on the probe in the core exhaust, Plane 8.0. Negative time delays are observed between any combination of internal combustor sensors paired upstream to downstream. The time delay for cross-correlations between Plane 3.5 (102°) with Plane 4.0 is zero (at 30% F_n) or very near zero (-0.3 msec at 19.7% F_n) for the limited data available, indicating the source may be between Plane 3.5 (102°) and Plane 4.0. However, the positive time delays associated with Plane 4.0 to Plane 8.0 and the other combustor sensor planes with the core exhaust suggest the presence of another source downstream of the turbine that was not of a propagating acoustic nature until after passing through the turbine.

5.3 ENGINE TO DUCT RIG COMPARISONS

The comparison of the engine-to-duct rig measurements made on the Double Annular combustor during this program showed large differences of 10 to 25 dB on a pressure level spectra basis between both inlet and discharge measurement planes. The power level comparisons showed considerably closer agreement with differences in levels of about 3 to 8 dB over the frequency range. The spectral shapes of the engine and duct rig measurements are very similar.

Some of the differences in level are concluded to be the result of the difference in static pressure between engine and duct rig at the high power points, measurement plane location differences, and the presence of the choked nozzle diaphragm in the engine which is absent from the duct rig. Another factor is the difference due to combustor operation with pilot fuel only for the low power settings on the engine as opposed to operation with fuel splits to the pilot and main stage burners in the test rig for the Phase I and II noise measurements.

APPENDIX A - 2 Hz NARROWBAND SPECTRA RESULTS

The 2 Hz narrowband spectra results presented in this Appendix are based on fluctuating pressure levels (FPL's) from the raw internal measurements on the CF6-50 engine with the ECCP Phase III Double Annular combustor. The FPL spectra plots cover the frequencies up to 2000 Hz and are presented for the available sensors at each of the eight test conditions including repeat points.

- ECCP Phase III Combustor Test, 1977
- 2 Hz Narrowband Spectra
- Reading 6

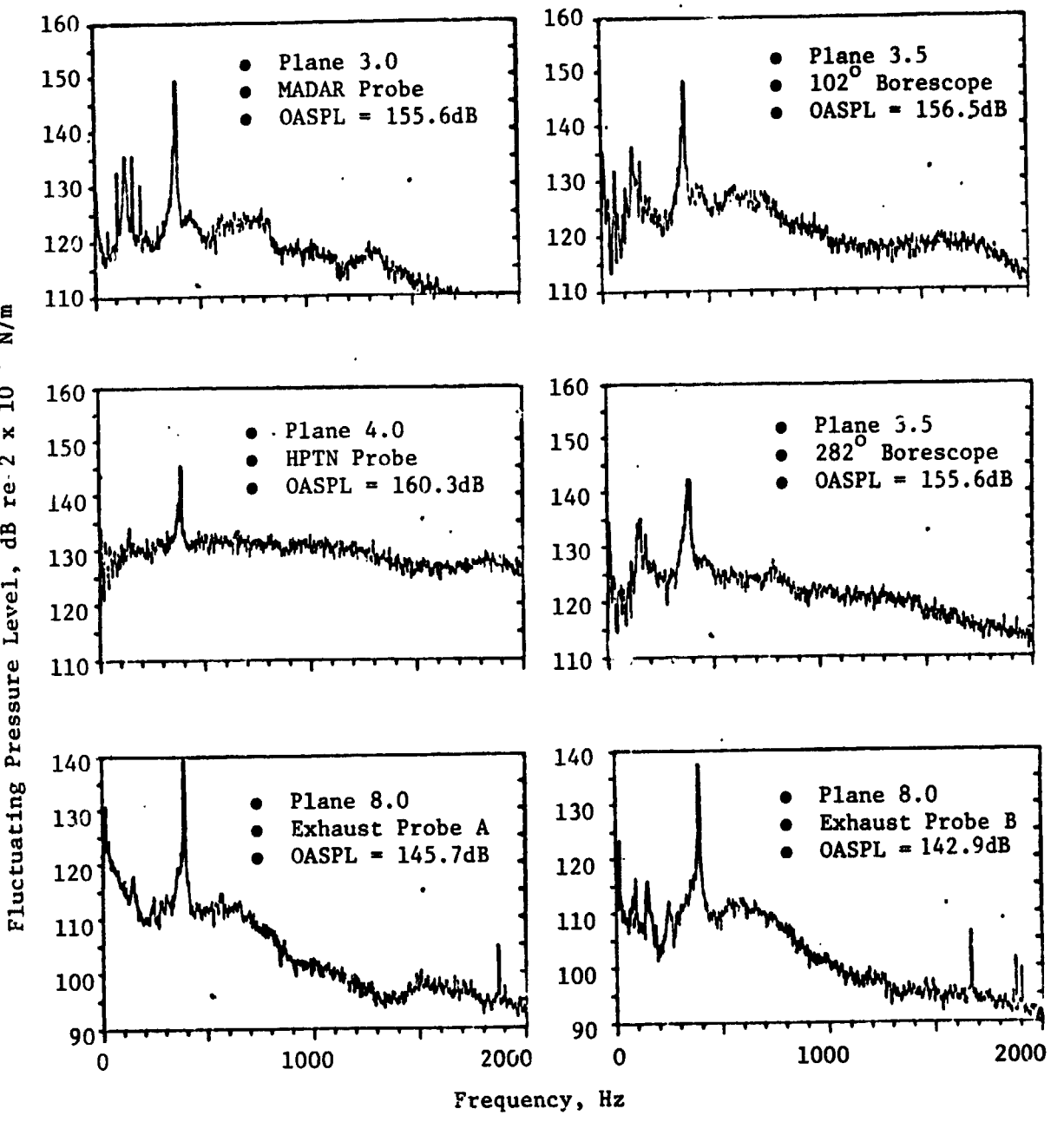

Figure A-1. As Measured Narrowband Spectra for CF6-50 Engine Condition at 3.8 Percent Thrust, Reading 6 (Idle)

- ECCP Phase III Combustor Test, 1977
- 2 Hz Narrowband Spectra
- Reading 16

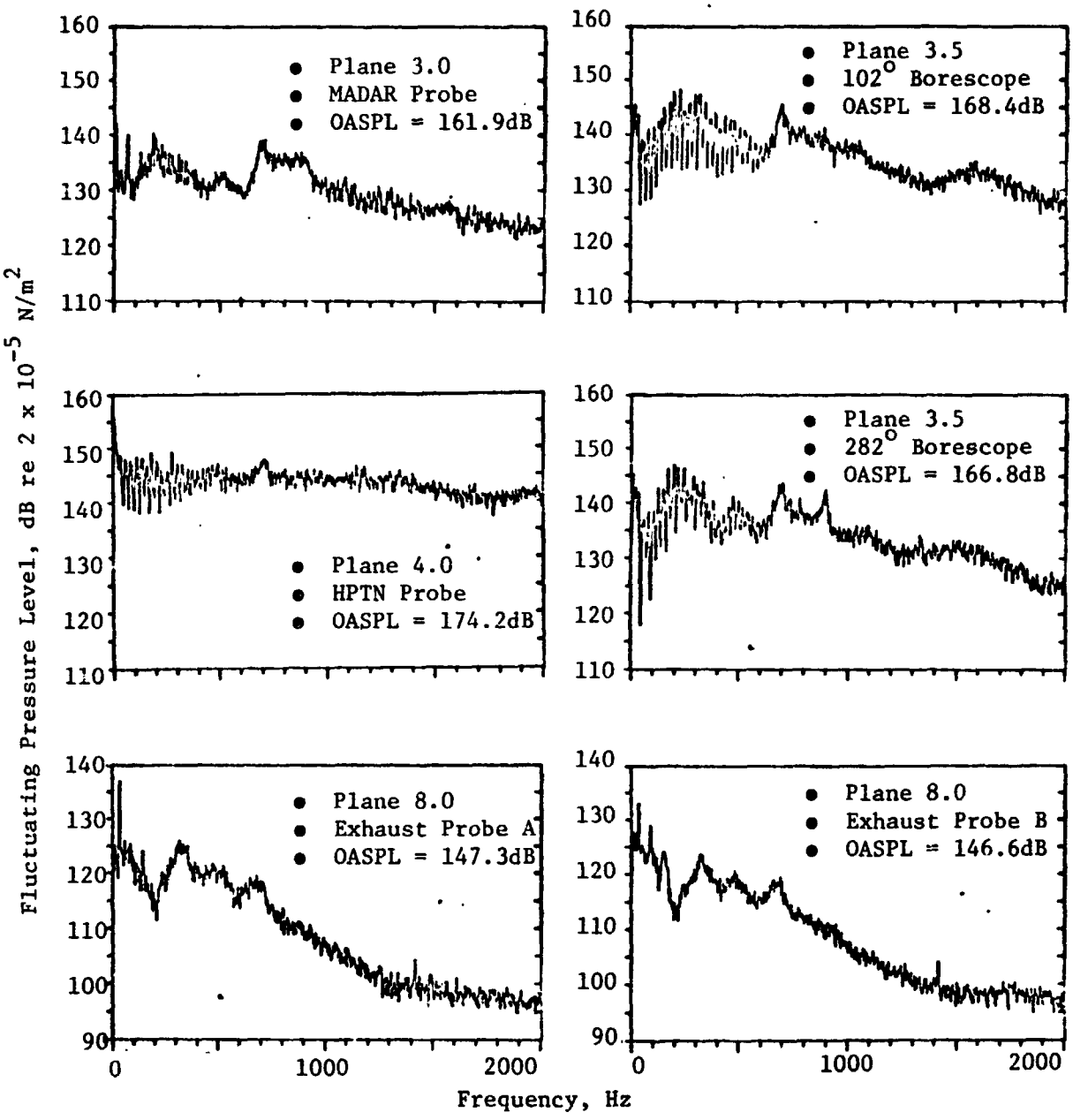

Figure A-2. As Measured Narrowband Spectra for CF6-50 Engine Condition at 19.7 Percent Thrust, Reading 16

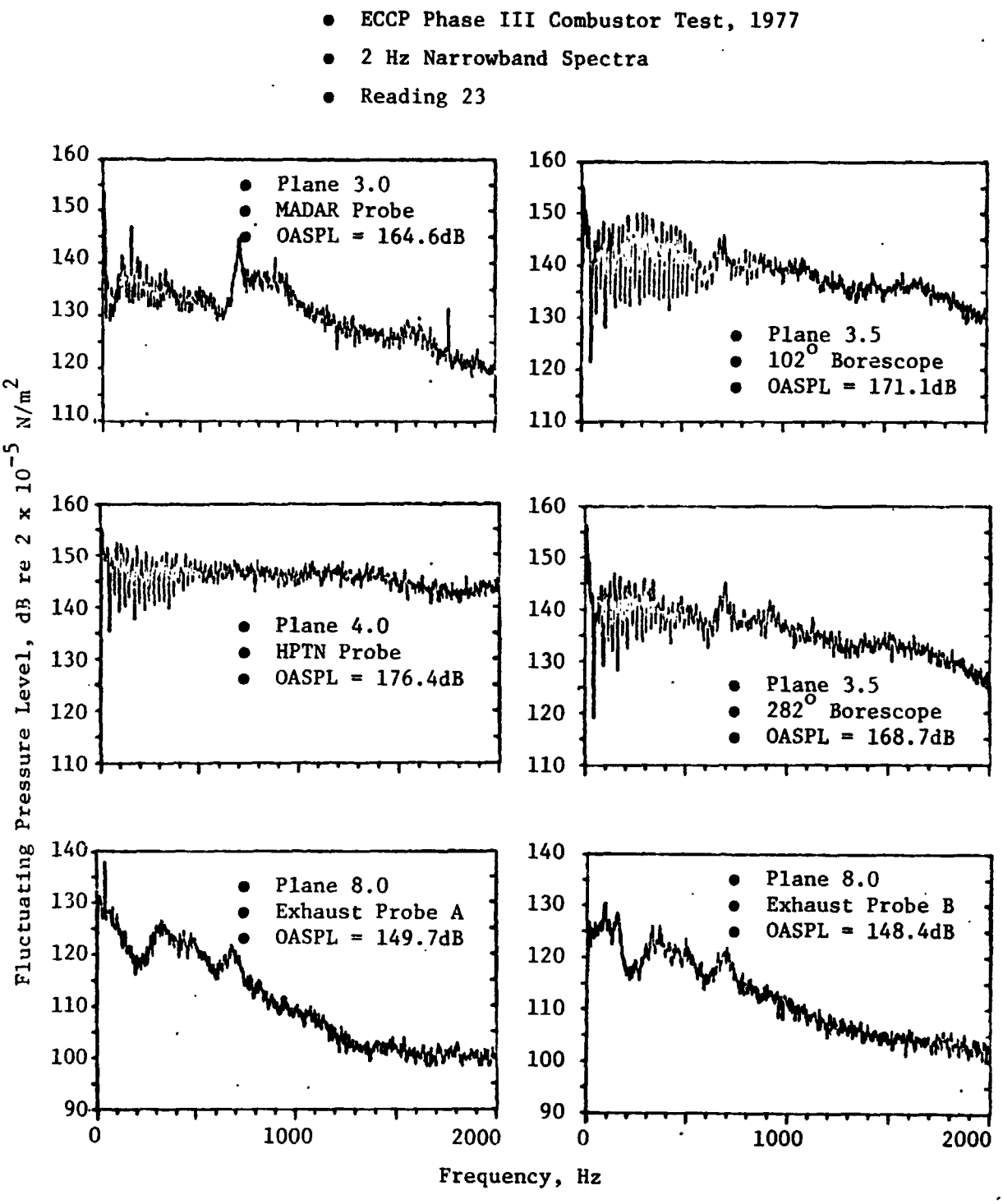

Figure A-3. As Measured Narrowband Spectra for CF6-50 Engine Condition at 30 Percent Thrust, Reading 23 (Approach Power with 100 Percent Pilot Fuel)

- ECCP Phase III Combustor Test, 1977
- 2 Hz Narrowband Spectra
- Reading 39

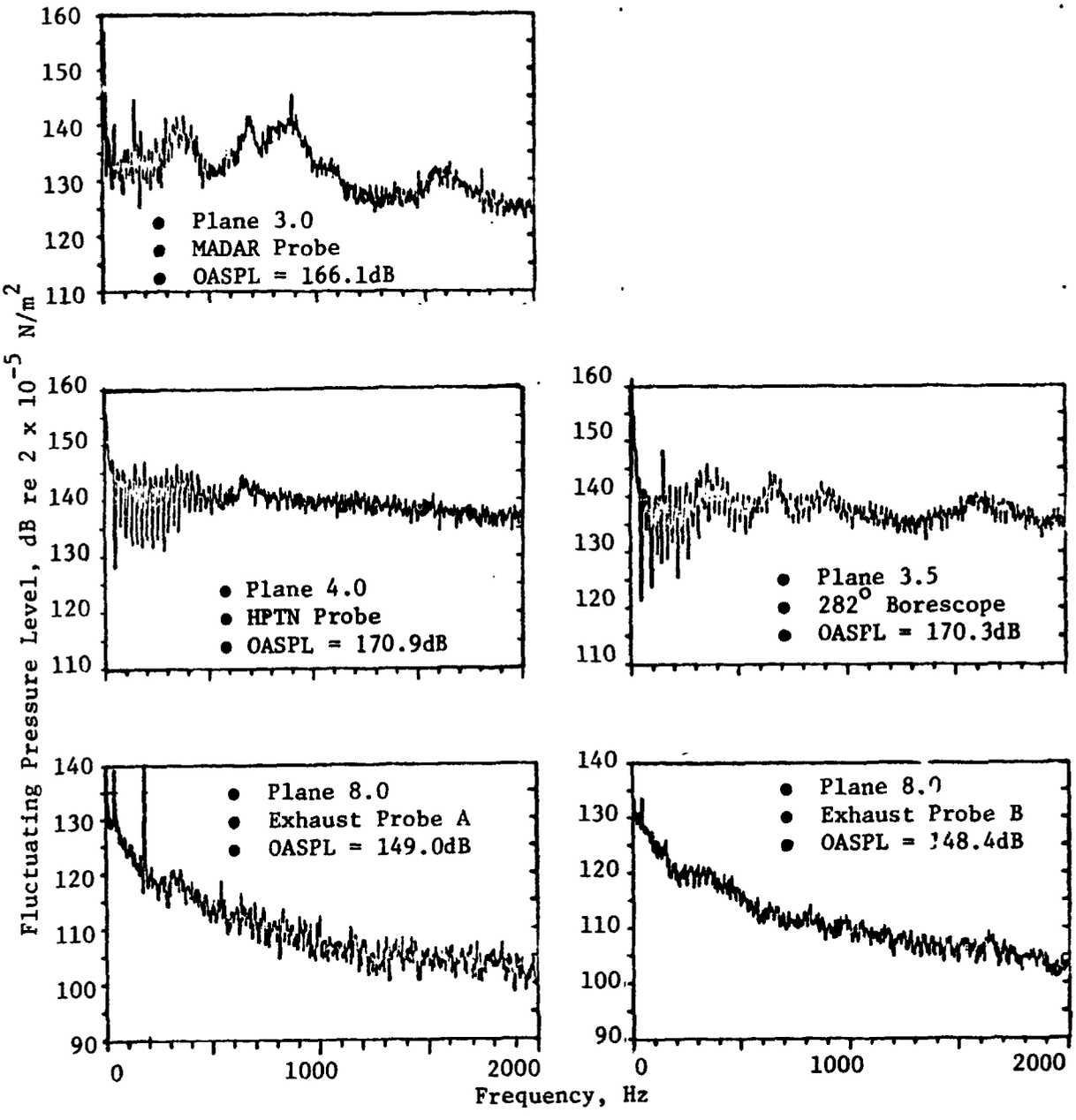

Figure A-4. As Measured Narrowband Spectra for CF6-50 Engine Condition at 29.7 Percent Thrust, Reading 39 (Approach Power with 50/50 Fuel Split)

- ECCP Phase III Combustor Test, 1977
- 2 Hz Narrowband Spectra
- Reading 34

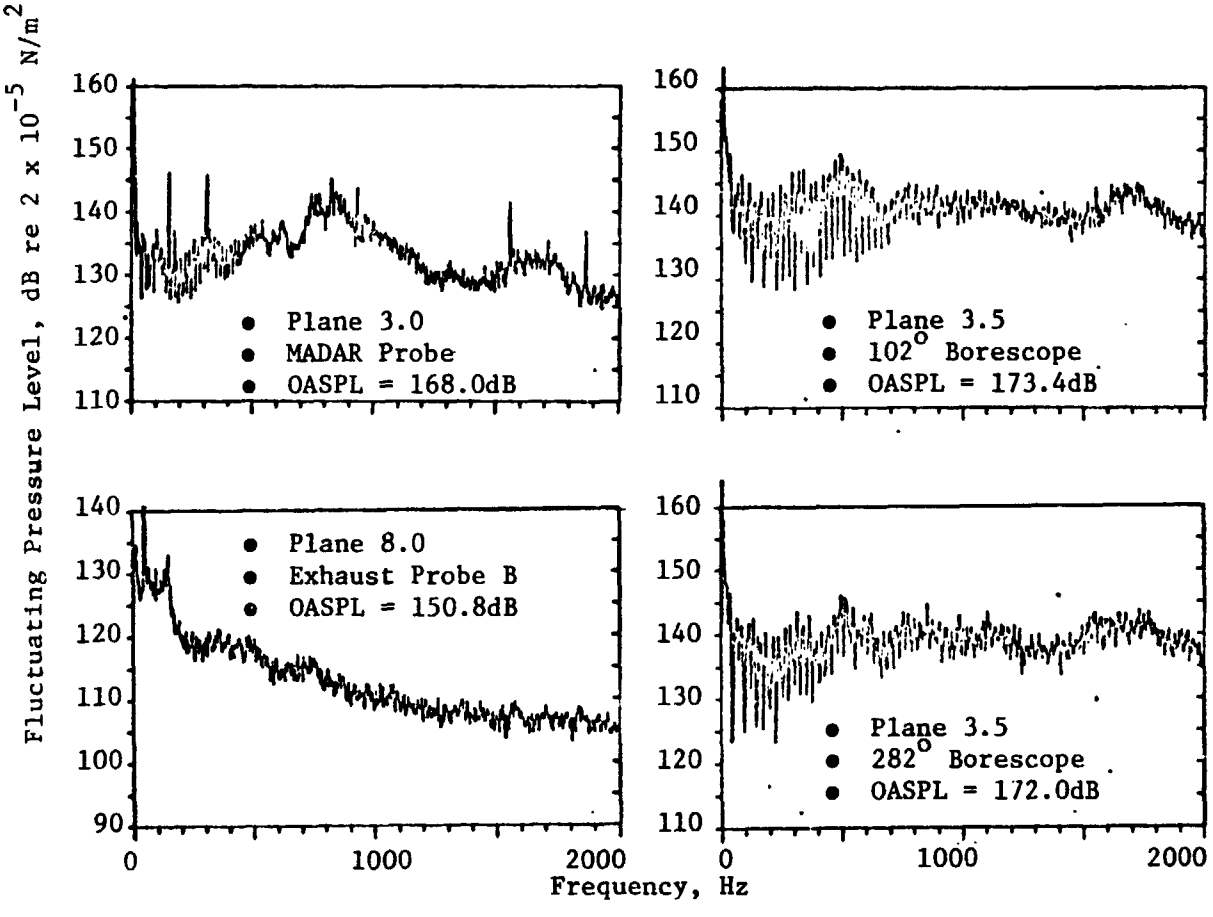

Figure A-5. As Measured Narrowband Spectra for CF6-50 Engine Condition at 45.4 Percent Thrust, Reading 34

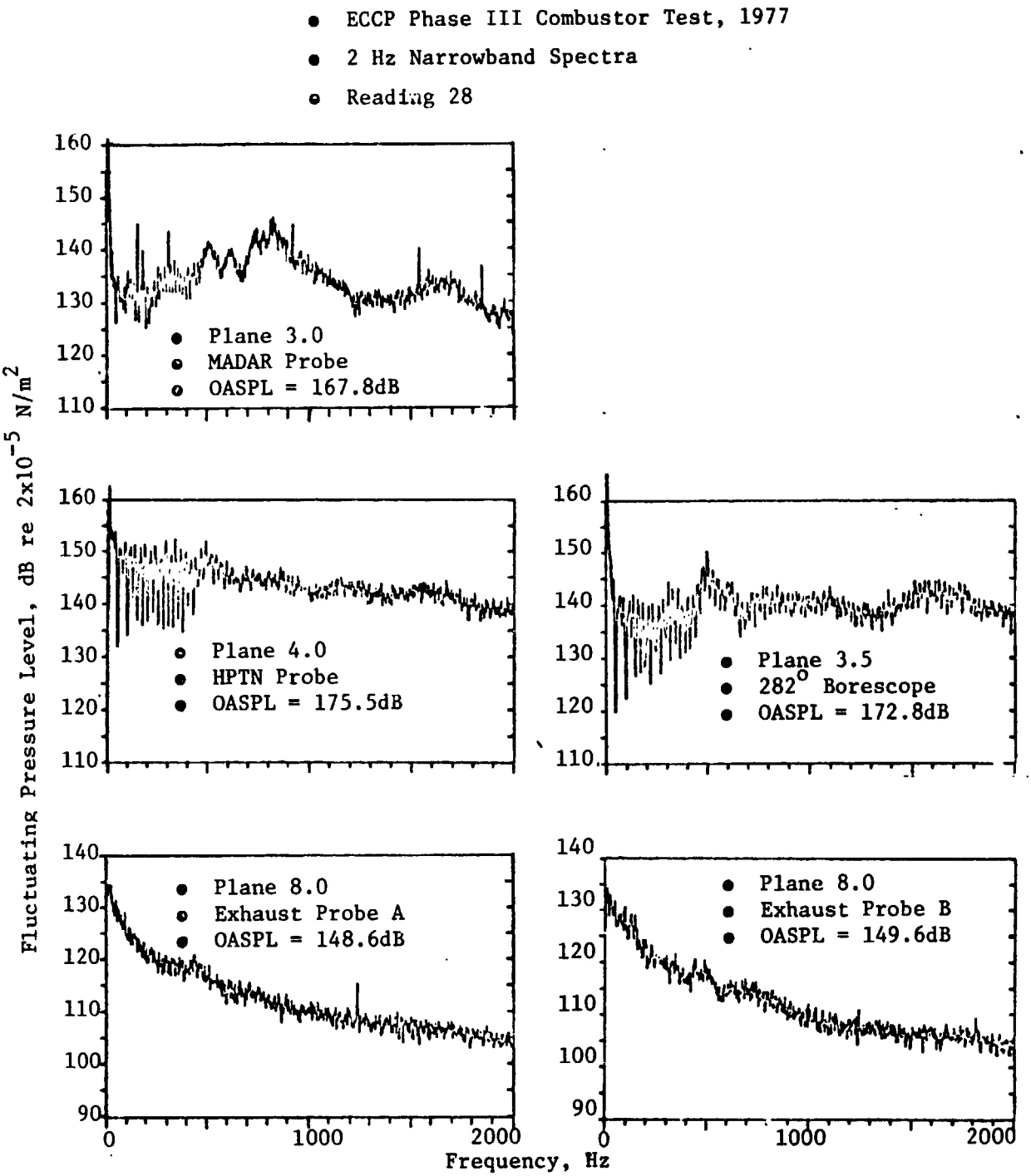

Figure A-6. As Measured Narrowband Spectra for CF6-50 Engine Condition at 45.4 Percent Thrust, Reading 28

- ECCP Phase III Combustor Test, 1977
- 2 Hz Narrowband Spectra
- Reading 40

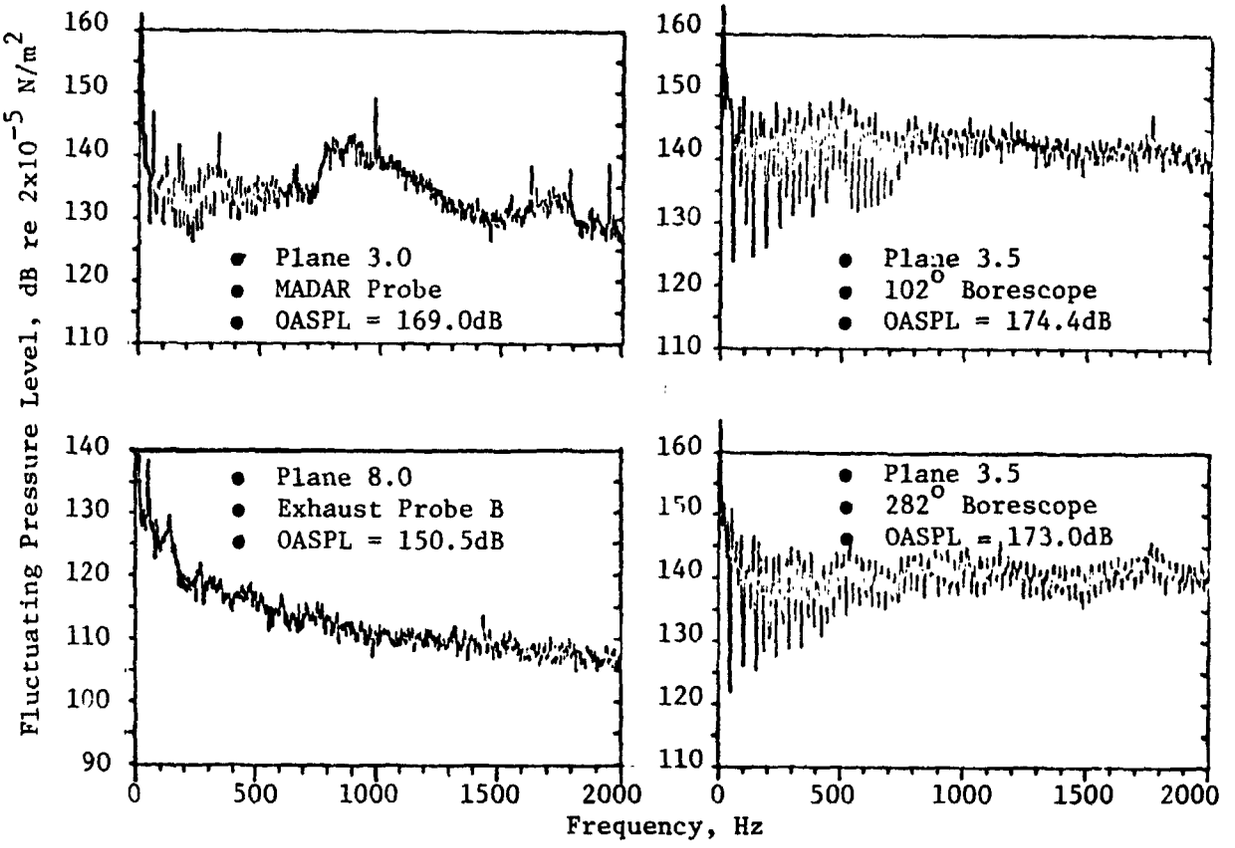

Figure A-7 As Measured Narrowband Spectra for CF6-50 Engine Condition at 64.6 Percent Thrust, Reading 40

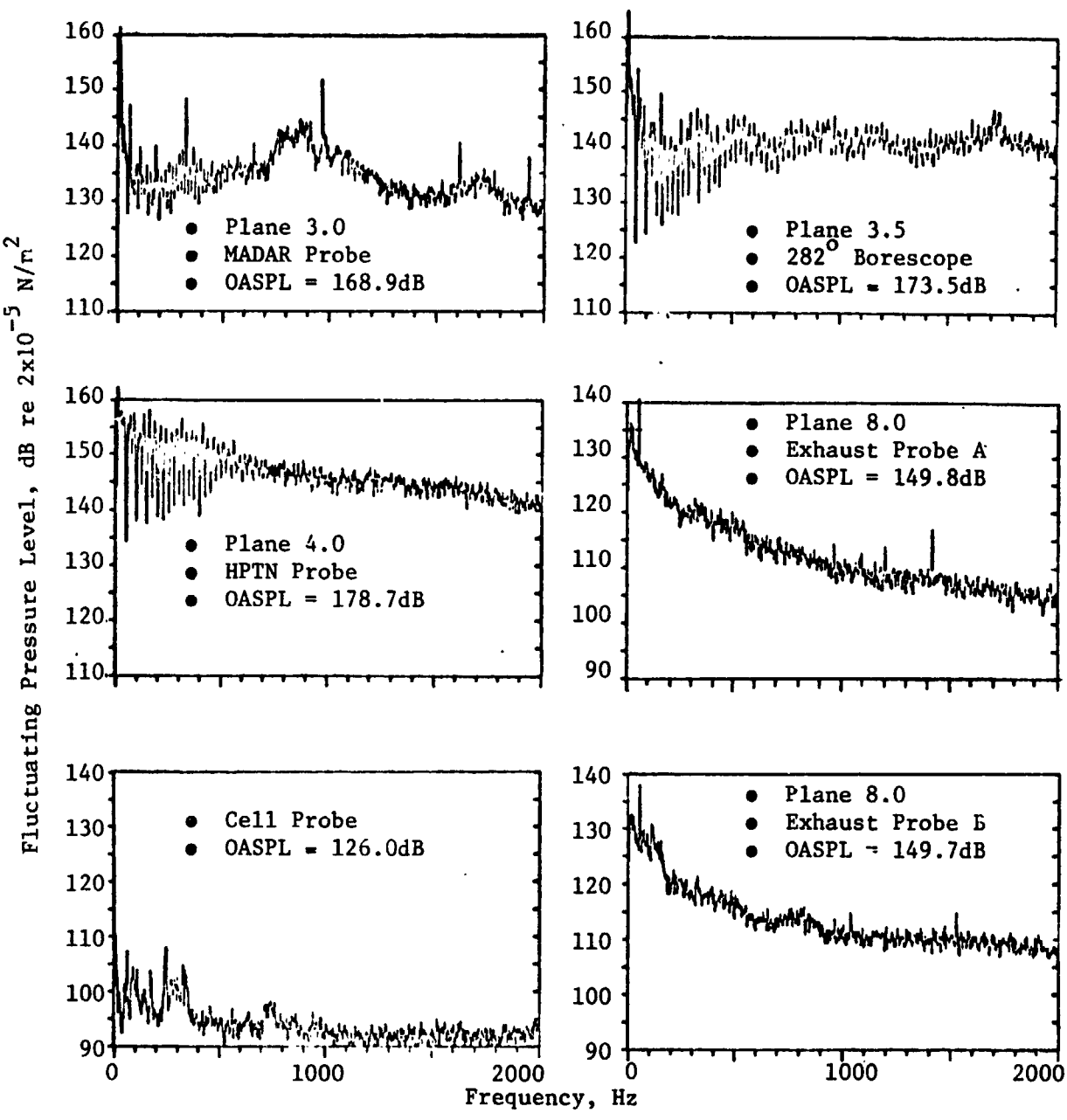

Figure A-8. As Measured Narrowband Spectra for CF6-50 Engine Condition at 64.6 Percent Thrust, Reading 13

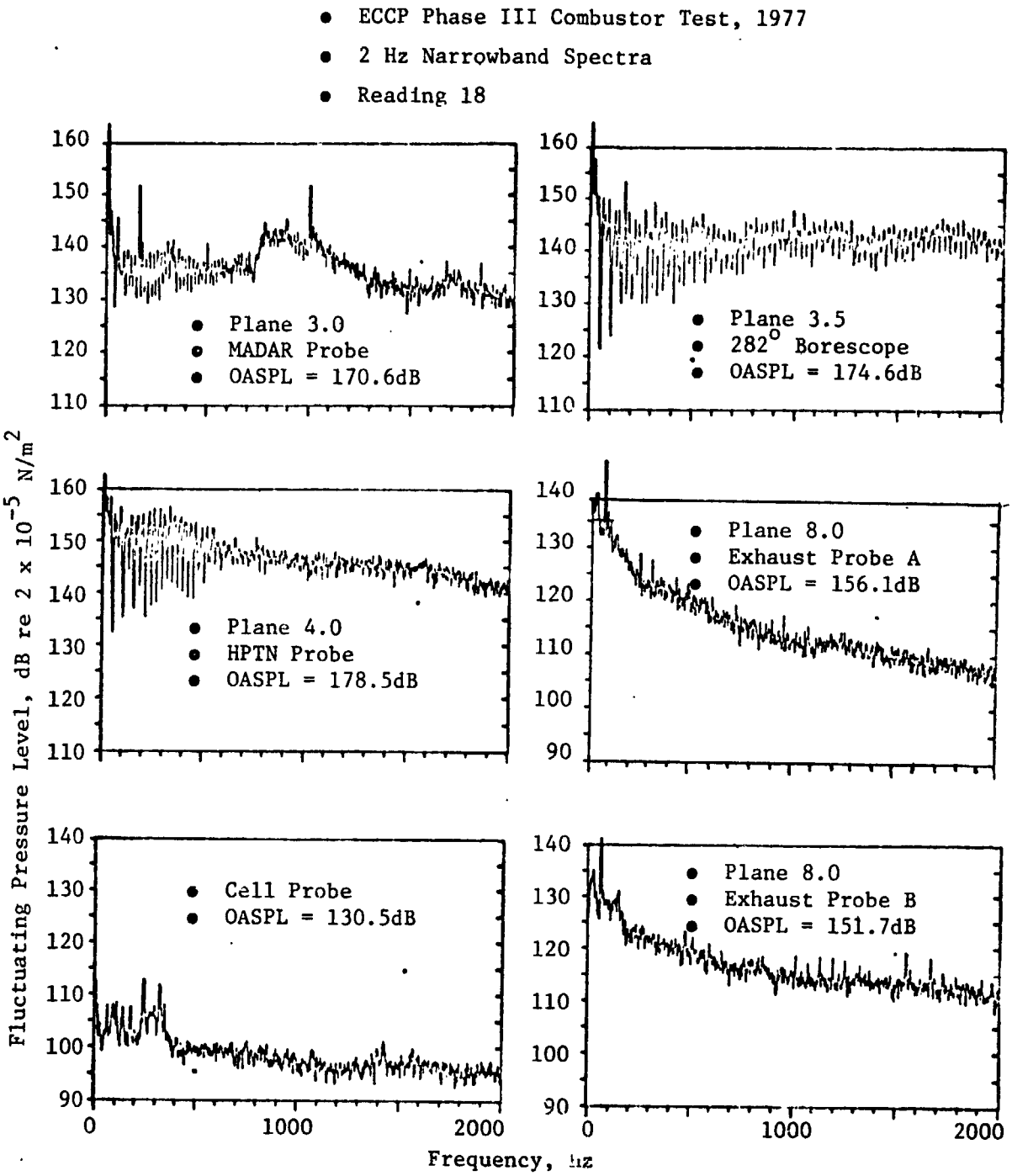

Figure A-9. As Measured Narrowband Spectra for CF6-50 Engine Condition at 82 Percent Thrust, Reading 18

- ECCP Phase III Combustor Test, 1977
- 2 Hz Narrowband Spectra
- Reading 43

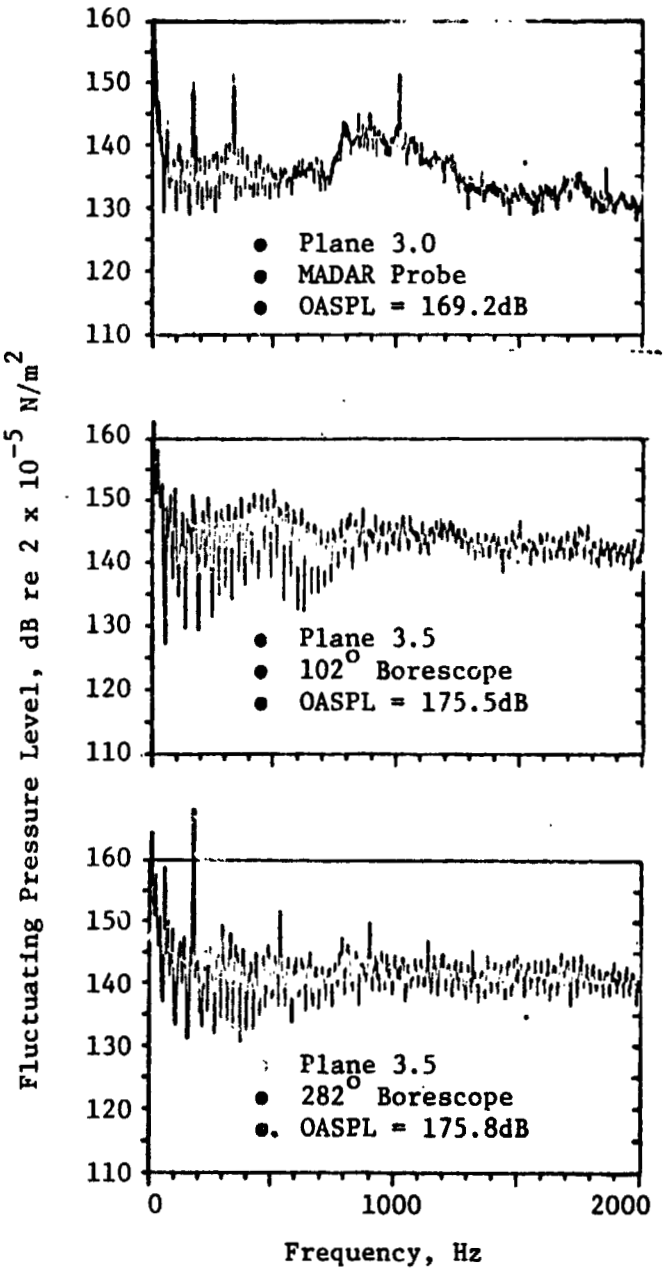

Figure A-10. As Measured Narrowband Spectra for CF6-50 Engine Condition at 82 Percent Thrust, Reading 43

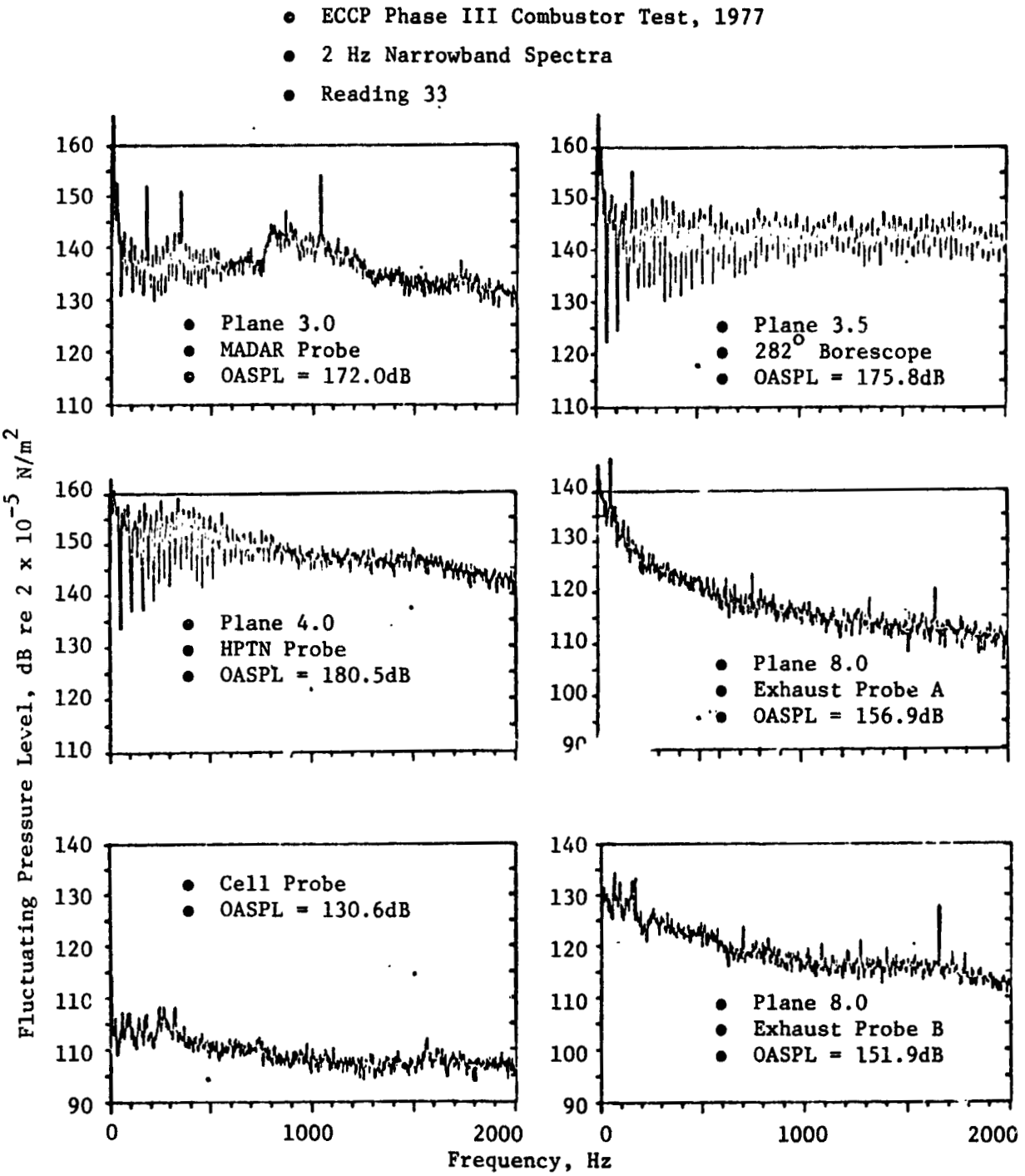

Figure A-11As Measured Narrowband Spectra for CF6-50 Engine Condition at 94.6 Percent Thrust, Reading 33

APPENDIX B - 1/3 OCTAVE BAND SPECTRA RESULTS

This Appendix contains the 1/3 octave band spectra results from 50 to 2000 Hz in both tabular and graphical form for the eight test conditions noted in the acoustic test matrix. The data presented is the measured internal spectra with corrections for ambient frequency response loss.

Table B-1. One-Third Octave Band Spectra from ECCP Phase III CF6-50 Engine Test.

Frequency (Hz)	a) 3.8% F_n (Idle)						b) 19.7% F_n					
	3.0	3.5 (102°)	3.5 (282°)	4.0	8.0 (A)	8.0 (B)	3.0	3.5 (102°)	3.5 (282°)	4.0	8.0 (A)	8.0 (B)
50.	122.3	128.0	126.0	140.5	124.8	113.0	136.3	140.0	139.3	147.3	126.3	129.3
63.	126.0	133.0	127.5	139.2	124.2	116.0	135.2	142.7	140.2	151.5	126.5	129.7
80.	125.0	128.0	127.0	140.8	123.3	117.8	137.0	143.8	141.8	151.6	126.8	131.1
100.	133.4	132.4	131.6	142.4	123.1	120.1	140.9	145.9	143.6	152.4	126.4	132.6
125.	137.8	139.0	139.0	144.9	123.9	118.4	144.0	149.0	148.0	155.2	125.9	129.9
160.	140.6	142.4	142.6	146.6	125.4	121.9	148.1	152.1	152.4	155.4	125.6	132.1
200.	137.2	139.5	139.7	147.4	121.7	116.5	150.7	156.2	154.7	156.4	124.5	126.0
250.	133.5	136.7	137.5	148.4	123.5	120.7	148.5	156.2	155.0	156.4	130.7	129.2
315.	139.2	141.0	142.2	150.9	129.0	127.0	148.2	157.7	155.0	158.2	136.5	134.2
400.	151.9	151.9	149.9	156.1	141.1	139.4	146.4	155.9	151.9	158.6	134.9	133.1
500.	139.0	141.8	141.8	153.3	127.5	125.8	147.3	155.0	153.8	161.3	134.8	133.3
630.	140.2	143.9	141.4	154.7	127.7	126.9	152.2	156.9	154.9	162.2	133.2	132.4
800.	140.9	143.4	141.9	154.7	124.5	124.5	155.4	159.2	156.9	163.2	129.5	129.7
1000.	137.4	140.2	141.2	155.7	119.4	118.9	150.7	157.2	154.9	163.7	124.9	125.2
1250.	137.3	138.8	141.6	155.9	116.0	116.2	146.6	154.1	153.1	164.7	120.2	121.0
1600.	133.9	140.1	139.4	15 .6	116.6	115.8	145.6	154.6	152.4	164.1	118.8	118.8
2000.	131.4	137.9	137.4	156.9	115.9	115.2	141.9	152.9	150.2	166.2	118.9	120.2
Overall FPL	153.7	154.9	153.9	164.9	142.4	140.5	160.8	167.0	165.1	173.1	142.6	142.8

Table B-1. One-Third Octave Band Spectra from ECCP Phase III CF6-50 Engine Test, (continued).

Frequency (Hz)	c) 30% F_n (Approach) (100% Pilot Fuel)						d) 29.7% F_n (Approach) (50/50 Fuel Split)						
	3.0	3.5 (102°)	3.5 (282°)	4.0	8.0 (A)	8.0 (B)	3.0	3.5 (102°)	3.5 (282°)	4.0	8.0 (A)	8.0 (B)	
50.	139.8	143.3	143.8	148.5	133.3	130.0	139.8	142.3	141.6	129.5	135.6		
63.	138.7	147.2	146.2	154.7	134.0	131.5	137.5	145.5	150.0	129.0	134.6		
80.	142.0	150.0	148.5	155.3	134.3	134.3	138.8	145.3	149.3	128.5	133.9		
100.	145.6	152.1	150.1	156.4	133.9	135.1	140.6	144.1	149.1	128.3	134.2		
125.	147.3	152.3	151.5	157.4	133.2	134.4	143.3	148.5	151.4	129.0	135.6		
160.	150.4	153.9	153.1	156.9	132.1	136.4	147.6	151.6	152.4	132.5	135.8		
200.	148.5	156.5	153.7	158.2	130.0	129.5	145.7	150.7	152.4	135.0	133.6		
250.	148.2	157.2	154.2	158.9	132.0	130.7	146.5	151.5	153.7	126.7	130.4		
315.	149.7	158.7	155.7	160.7	137.5	135.2	150.7	154.2	155.9	127.7	129.8		
400.	148.6	159.4	154.1	161.9	137.6	136.4	152.1	156.1	157.1	127.3	129.7		
500.	148.8	159.0	155.8	163.0	136.3	135.3	148.0	154.3	157.3	125.2	125.5		
630.	152.6	157.9	156.2	163.7	134.7	134.4	153.4	157.2	158.4	124.7	123.9		
800.	155.4	159.2	156.4	165.0	132.2	132.7	156.9	157.7	158.7	124.2	123.7		
1000.	152.9	159.4	156.4	165.4	127.7	128.9	154.4	158.2	158.7	123.5	122.4		
1250.	148.8	158.3	154.8	167.2	123.5	127.0	148.8	156.8	160.2	122.2	121.9		
1600.	147.9	157.9	154.4	166.3	122.1	125.1	151.6	160.1	160.3	122.0	122.5		
2000.	144.2	156.2	152.2	167.9	122.2	125.2	148.9	160.7	161.9	119.8	121.2		
Overall FPL	161.8	169.1	166.2	175.2	145.7	145.5	162.6	167.8	169.2	140.8	144.1		

- OUT -

Table B-1. One-Third Octave Bend Spectra from ECCP Phase III CF6-50 Engine Test, (continued).

Frequency (Hz)	e) 45.4% F_n						f) 64.6% F_n						
	3.0	3.5 (102°)	3.5 (282°)	4.0	8.0 (A)	8.0 (B)	3.0	3.5 (102°)	3.5 (282°)	4.0	8.0 (A)	8.0 (B)	Cell
50.	139.0	139.5	139.0	147.3	139.5	137.5	146.0	142.3	153.3	154.3	138.3	137.3	105.0
63.	137.7	147.5	146.2	155.5	139.2	135.2	142.0	149.2	151.0	160.5	135.0	134.7	108.5
80.	138.5	148.8	146.0	155.8	138.8	135.1	140.8	151.0	150.5	161.1	133.8	134.1	107.3
100.	142.1	147.9	144.9	154.6	138.6	135.6	143.4	153.4	148.1	159.1	133.1	134.1	109.6
125.	141.5	149.5	148.5	157.4	137.9	136.4	143.0	152.5	150.8	162.2	133.4	136.4	107.4
160.	146.9	150.9	147.4	157.1	138.1	137.6	144.1	154.1	153.4	163.4	133.1	134.9	108.1
200.	142.7	151.5	148.2	158.4	137.2	131.2	145.0	154.5	150.5	163.4	131.7	131.2	108.2
250.	144.7	153.2	149.7	158.7	137.0	130.2	146.5	156.0	152.0	163.4	131.0	131.0	113.5
315.	149.2	156.2	152.7	160.7	137.0	132.0	151.7	157.7	156.0	164.7	131.5	131.0	113.5
400.	147.6	157.4	153.1	161.4	137.1	133.1	149.4	159.1	155.6	165.4	131.9	131.4	109.6
500.	151.3	161.8	158.0	163.8	137.0	132.5	151.0	162.0	158.5	165.5	131.3	130.8	109.0
630.	152.4	158.7	156.9	162.2	134.9	130.9	152.7	159.9	157.7	165.2	129.2	129.4	109.9
800.	158.7	160.2	158.4	162.7	134.2	131.0	159.7	161.4	160.2	165.2	128.5	131.0	111.5
1000.	156.4	161.9	158.9	162.2	132.7	128.4	159.4	163.4	161.9	165.2	127.2	128.4	110.7
1250.	151.8	161.3	159.6	163.2	132.7	128.0	154.3	163.8	161.8	165.2	126.7	129.7	111.5
1600.	153.1	163.6	162.6	163.6	131.6	127.6	154.4	164.6	163.9	165.8	126.3	129.8	112.1
2000.	151.2	163.2	162.2	164.4	131.7	127.9	153.4	164.4	164.7	166.9	125.4	130.4	117.2
Overall FPL	163.5	170.9	168.9	173.2	149.2	146.2	165.2	172.3	171.0	176.4	144.6	145.2	123.5

Table B-1. One-Third Octave Band Spectra from ECCP Phase III CF6-50 Engine Test, (concluded)

Frequency (Hz)	g) 82% F_n 3.0	3.5 (102°)	3.5 (282°)	4.0	8.0 (A)	8.0 (B)	Cell	h) 94.6% F_n (Takeoff) 3.0	3.5 (102°)	3.5 (282°)	4.0	8.0 (A)	8.0 (B)	Cell
50.	140.5	145.0	143.0	151.0	138.0	134.8	106.3	141.3		142.5	153.0	136.5	131 8	107.8
63.	147.0	150.0	153.0	158.5	142.2	133.2	109.5	146.2		152.7	160.2	140.2	136.7	111.2
80.	141.5	151.2	151.8	159.3	136	132.3	111.1	143.5		154.0	161.6	140.3	136.3	110.6
100.	144.6	152.5	149.1	159.9	136.	133.9	112.9	145.9		151.9	161.9	137.6	135.6	112.9
125.	145.0	153.1	154.3	160.4	136.4	135.9	110.9	146.3		155.0	161.9	137.9	137.2	111.9
160.	153.4	155.8	156.1	161.4	136.9	134.1	111.9	152.9		157.1	163.6	137.1	139.1	113.9
200.	148.2	155.5	153.7	162.2	135.2	132.2	112.7	150.0		156.2	164.7	134.7	135.0	113.5
250.	148.2	157.8	154.2	163.4	134.2	132.0	115.7	149.5		157.0	165.4	133.7	136.7	117.5
315.	151.2	158.5	157.0	165.2	134.0	132.0	117.5	154.2		158.7	167.9	134.5	137.0	116.7
400.	150.9	159.5	157.1	166.4	133.9	132.4	114.6	152.9		158.4	168.9	134.4	136.9	114.9
500.	151.3	161.2	158.0	165.8	132.8	132.3	115.5	152.8		159.5	168.0	134.3	137.0	114.8
630.	152.9	160.8	158.4	165.2	131.4	131.2	118.2	153.4		159.2	167.4	131.7	135.7	115.7
800.	159.4	160.8	160.9	165.2	132.2	132.7	117.5	159.4		161.9	167.2	131.7	135.7	115.2
1000.	160.7	162.7	162.7	164.4	130.9	131.4	115.9	161.4		162.9	166.9	130.4	134.9	115.4
1250.	156.6	163.6	163.3	166.2	131.2	131.5	116.0	157.3		164.3	167.7	130.2	135.7	115.5
1600.	154.4	163.8	164.6	166.1	131.3	131.3	116.6	155.4		165.1	167.8	130.1	136.8	117.8
2000.	155.2	163.2	165.9	166.4	130.9	130.9	118.9	155.4		166.7	167.9	129.2	135.2	120.2
Overall FPL	166.2	172.0	172.0	176.3	147.9	145.1	127.6	166.9		172.9	178.4	148.0	148.6	127.7

OUT

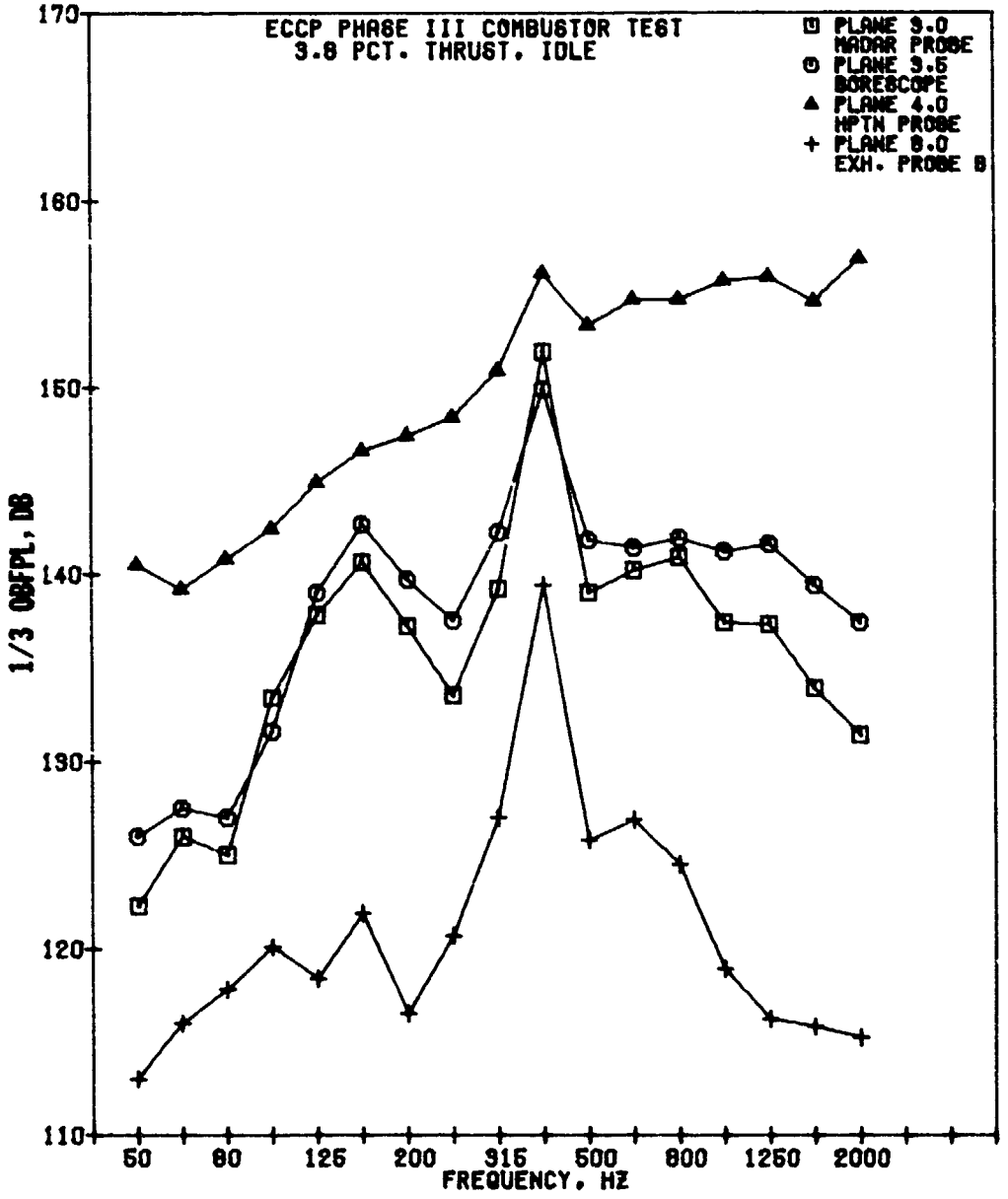

Figure B-1. One-Third Octave Band Spectra for CF6-50 Engine Condition at 3.8 Percent Thrust

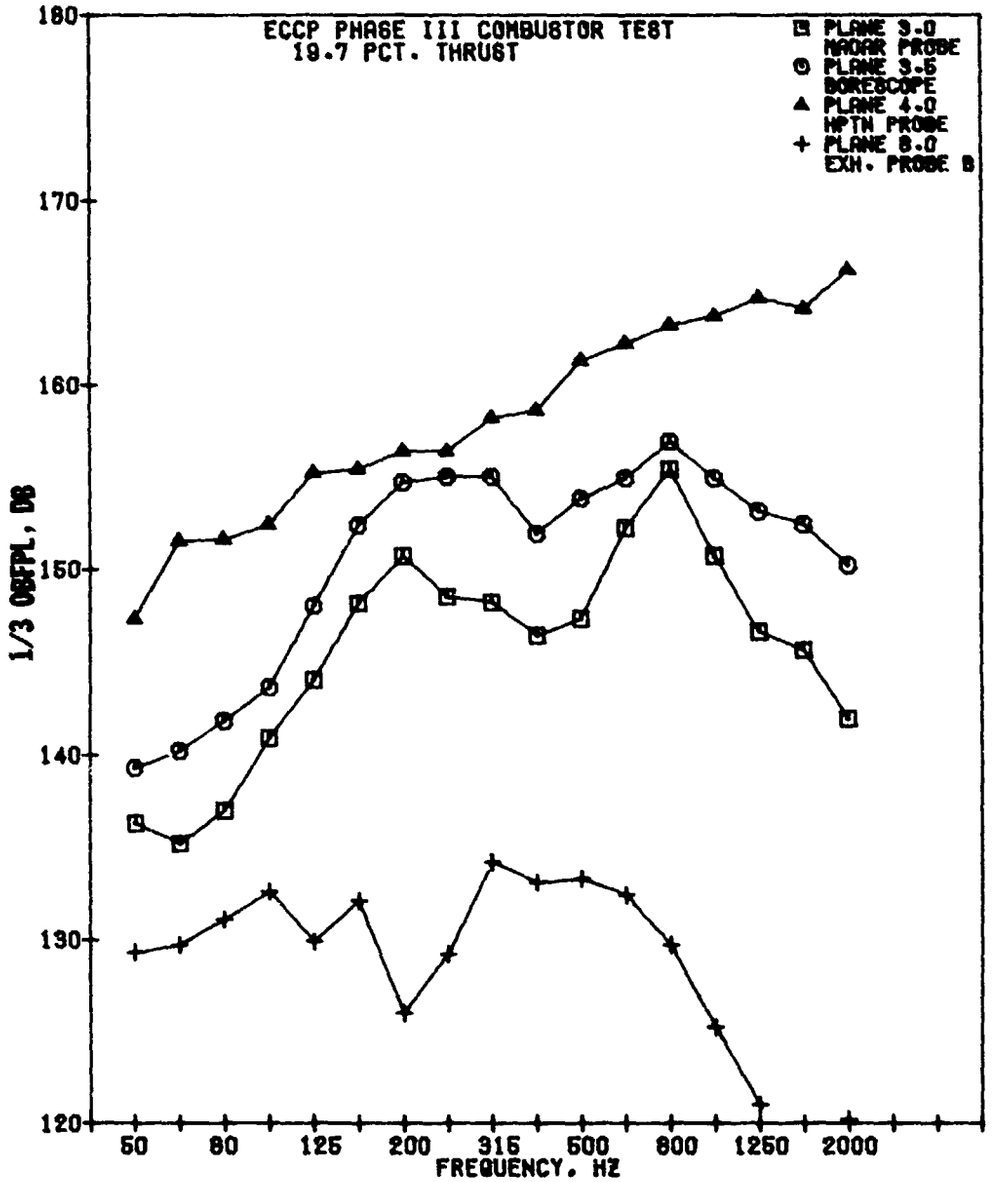

Figure B-2. One-Third Octave Band Spectra for CF6-50 Engine Condition at 19.7 Percent Thrust

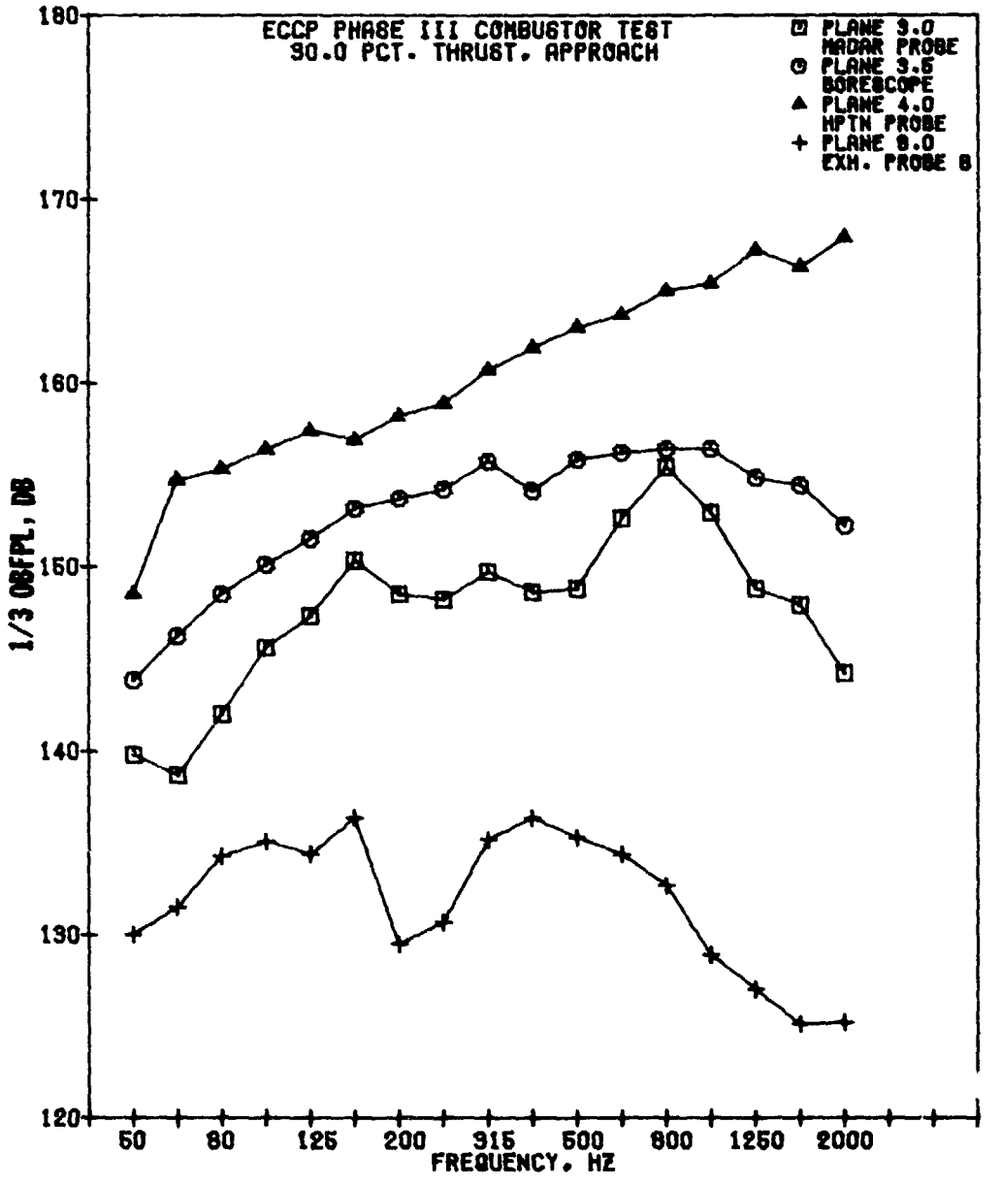

Figure B-3. One-Third Octave Band Spectra for CF6-50 Engine Condition at 30 Percent Thrust

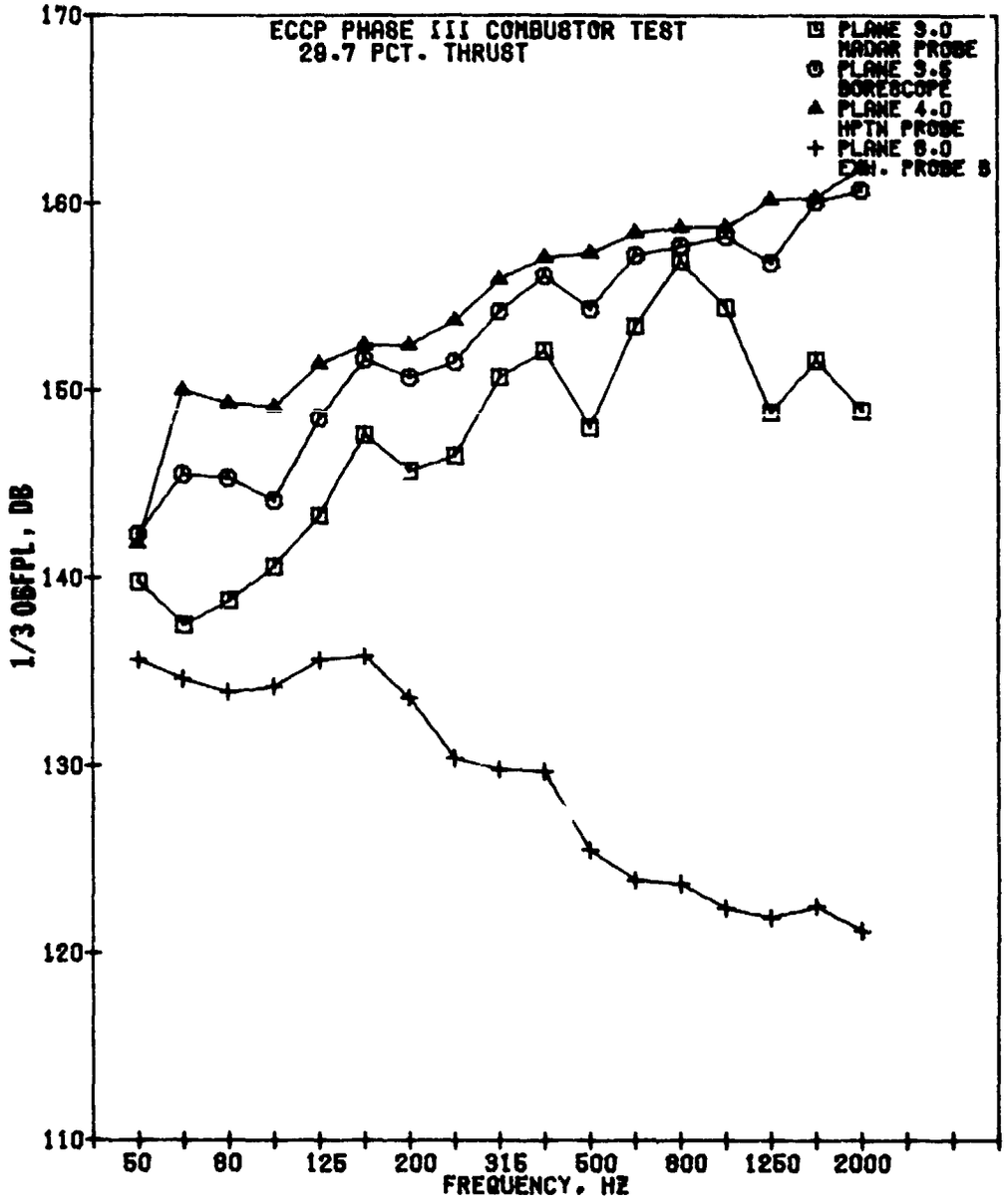

Figure B-4. One-Third Octave Band Spectra for CF6-50 Engine Condition at 29.7 Percent Thrust

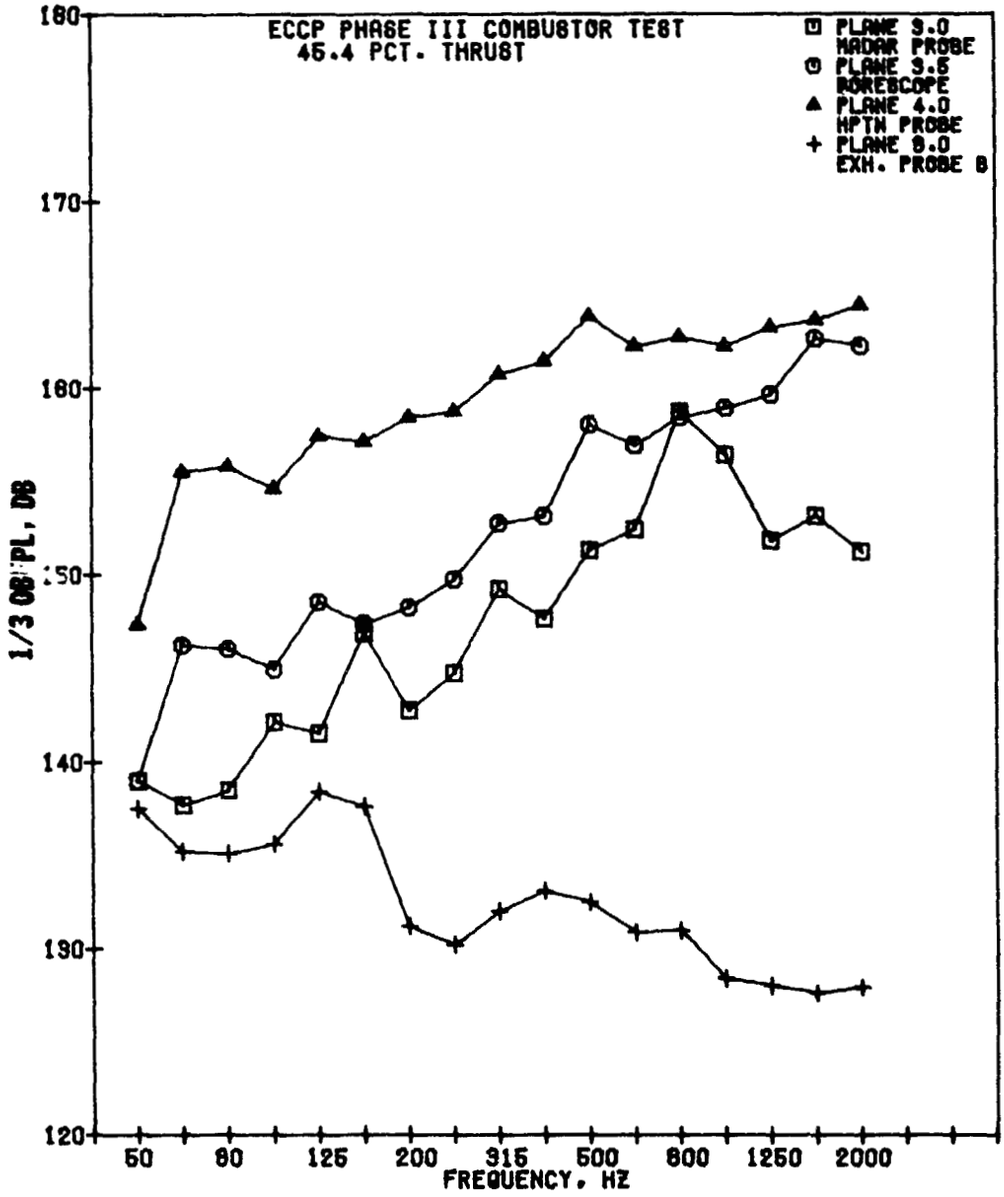

Figure B-5. One-Third Octave Band Spectra for CF6-50 Engine Condition at 45.4 Percent Thrust

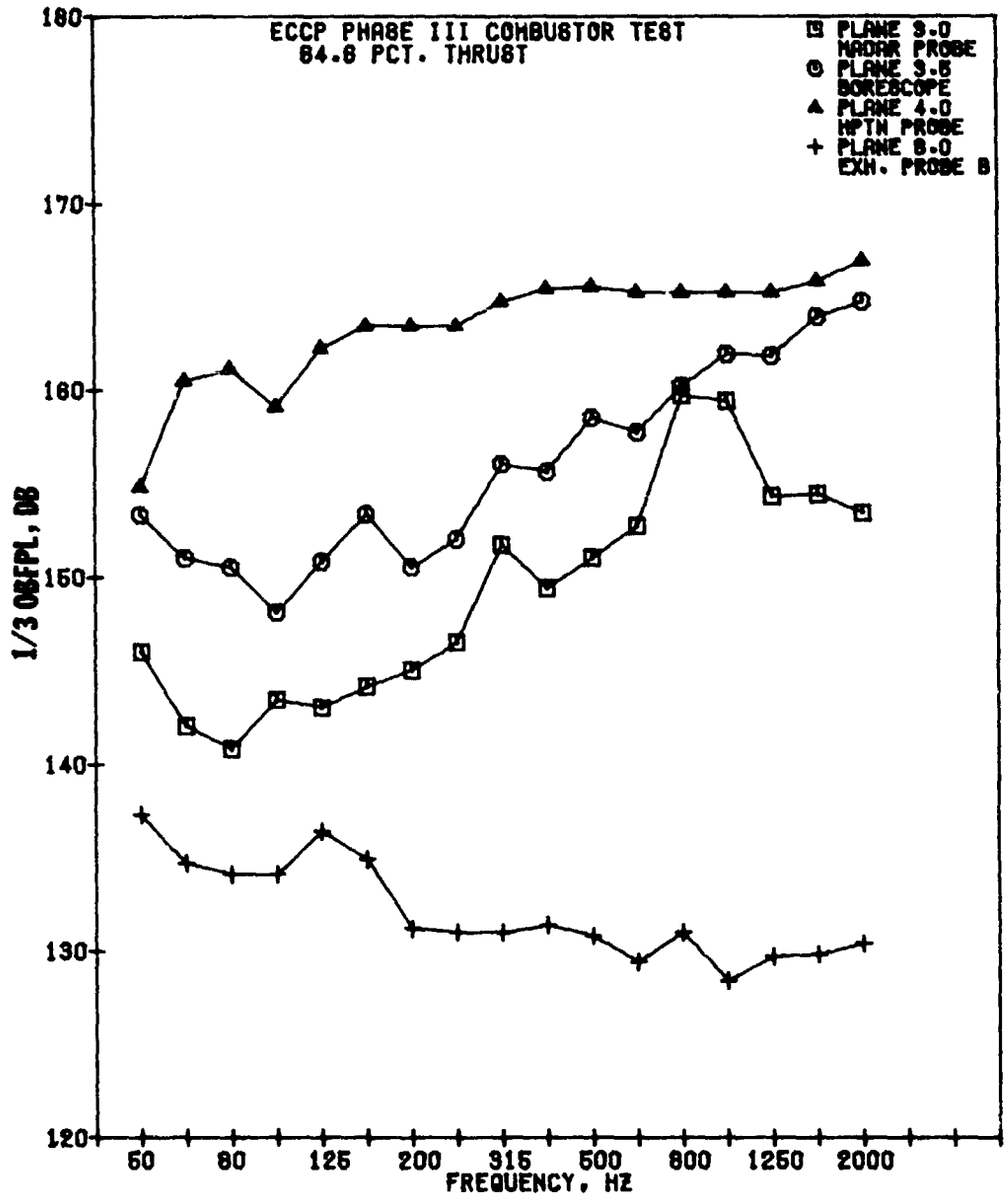

Figure B-6. One-Third Octave Band Spectra for CF6-50 Engine Condition at 64.6 Percent Thrust

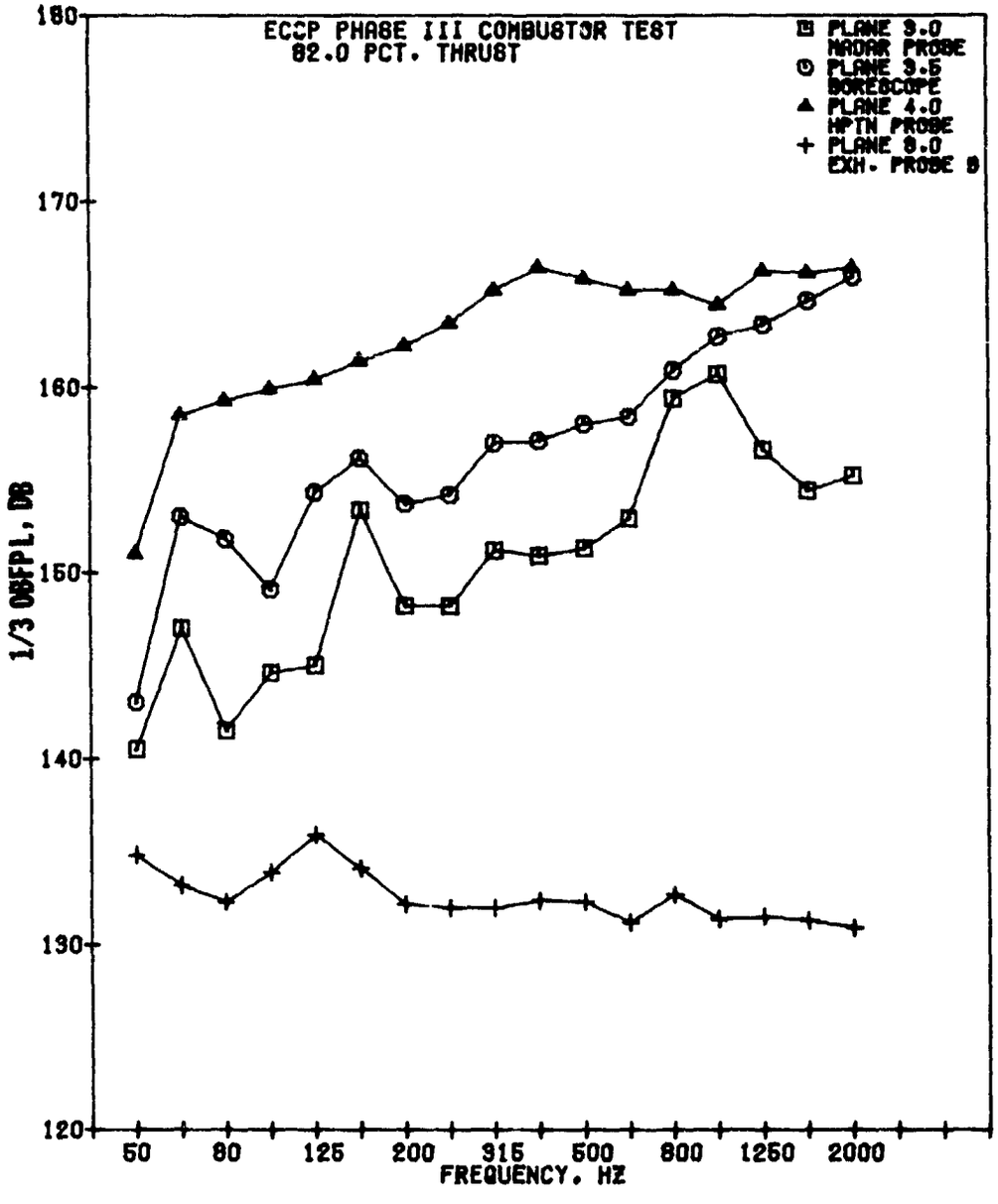

Figure B-7. One-Third Octave Band Spectra for CF6-50 Engine Condition at 82.0 Percent Thrust

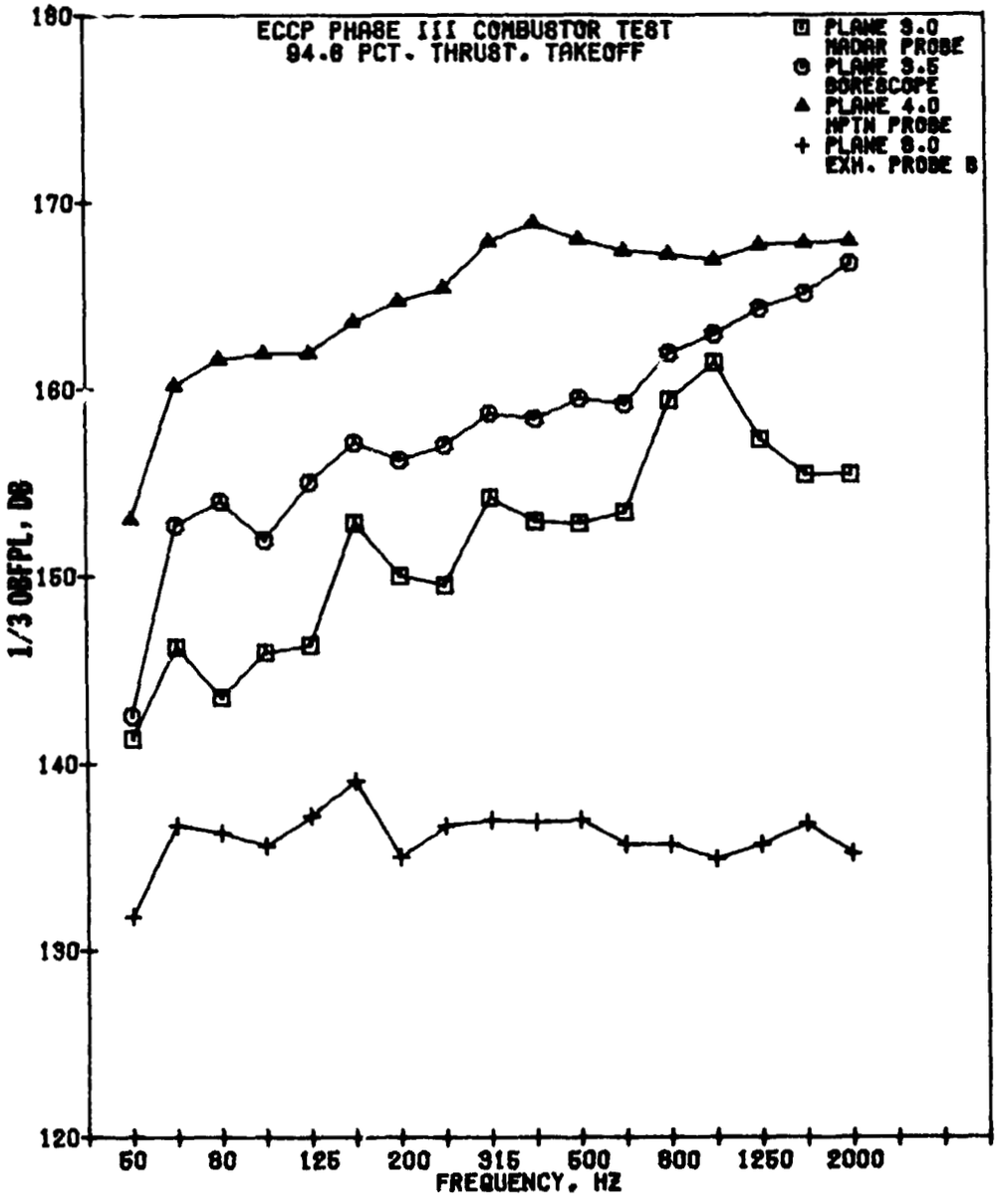

Figure B-8. One-Third Octave Band Spectra for CF6-50 Engine Condition at 94.6 Percent Thrust

APPENDIX C - TURBINE TRANSFER FUNCTION RESULTS

The turbine transfer function results presented in this Appendix are in the form of coherent 1/3 octave band SPL spectra comparisons at each test condition. Turbine attenuations were obtained between the coherent spectra at Plane 4.0 and the coherent spectra at Plane 8.0, both of which are referenced to Plane 3.5. Noted on the spectra are regions where both spectra are in the noise floor 18 dB down from the raw signal. Also noted on the spectra are regions of frequency bands which are 15 to 18 dB down from the raw signal for either Plane 4.0 or Plane 8.0, but not both. The actual attenuations obtained in these regions are either less than or greater than the observed value read from the plots.

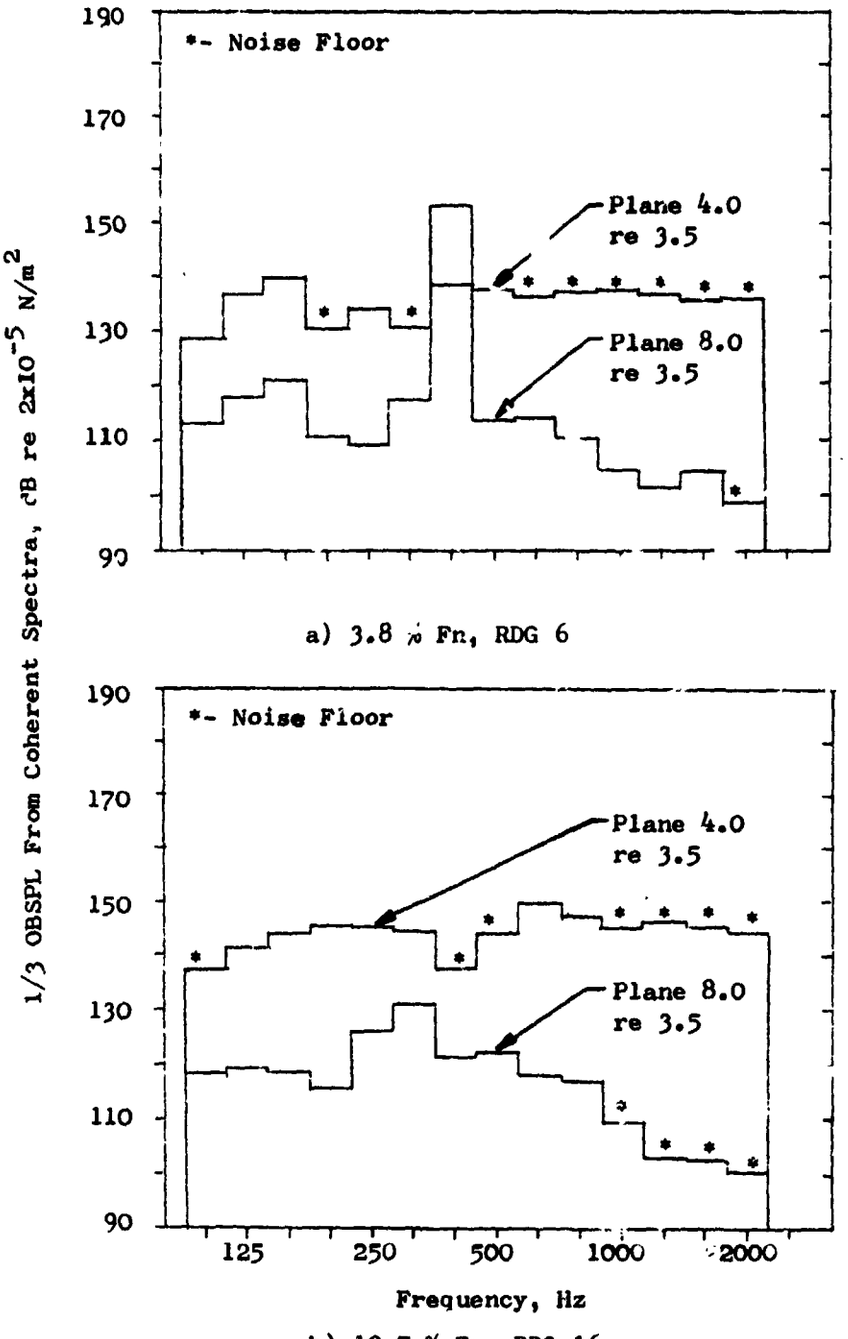

a) 3.8 % Fn, RDG 6

b) 19.7 % Fn. RDG 16

Figure C-1. Coherent Spectra Comparisons For Turbine Attenuation From ECCP Phase III Engine Test

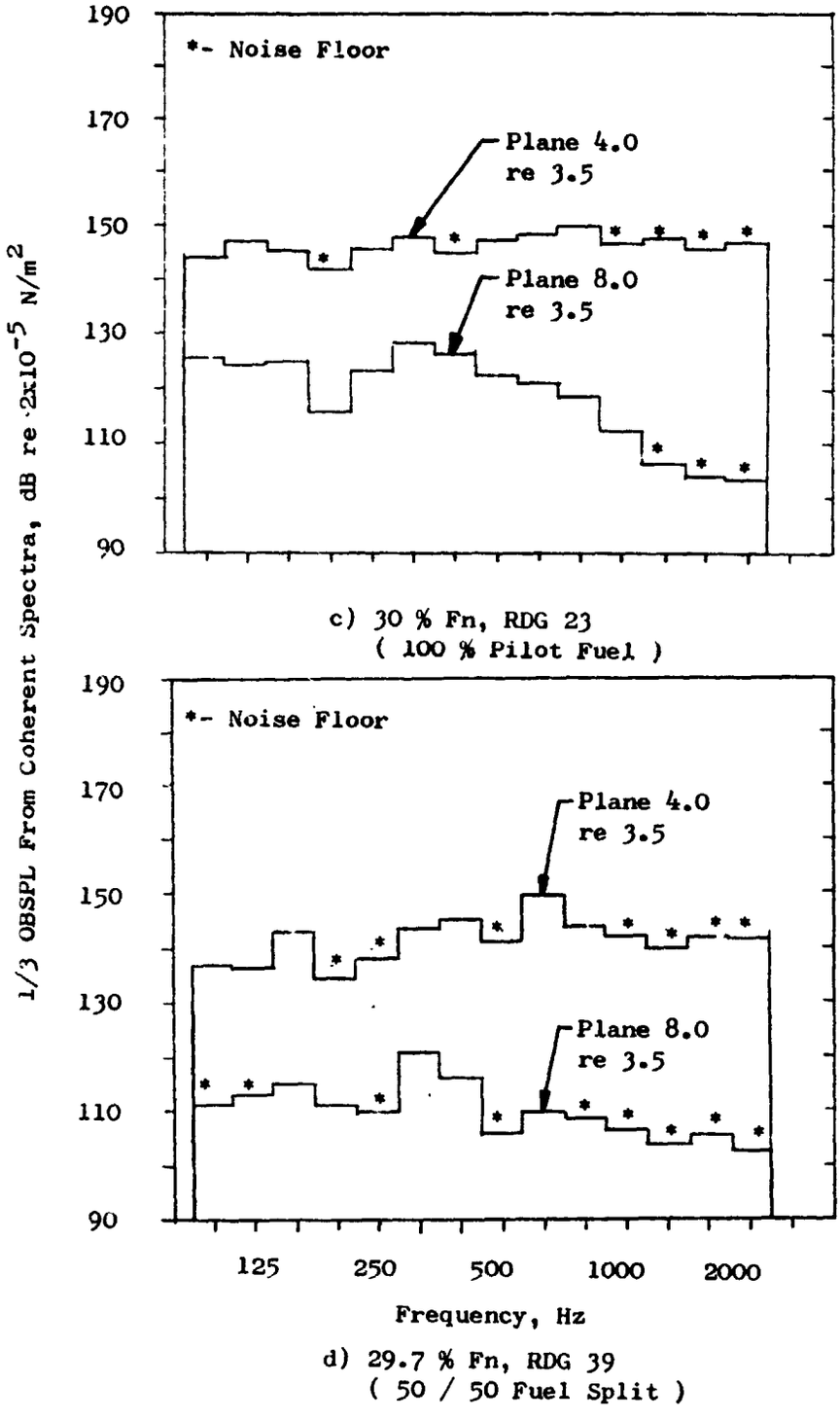

Figure C-1. Coherent Spectra Comparisons For Turbine Attenuation From ECCP Phase III Engine Test (Continued)

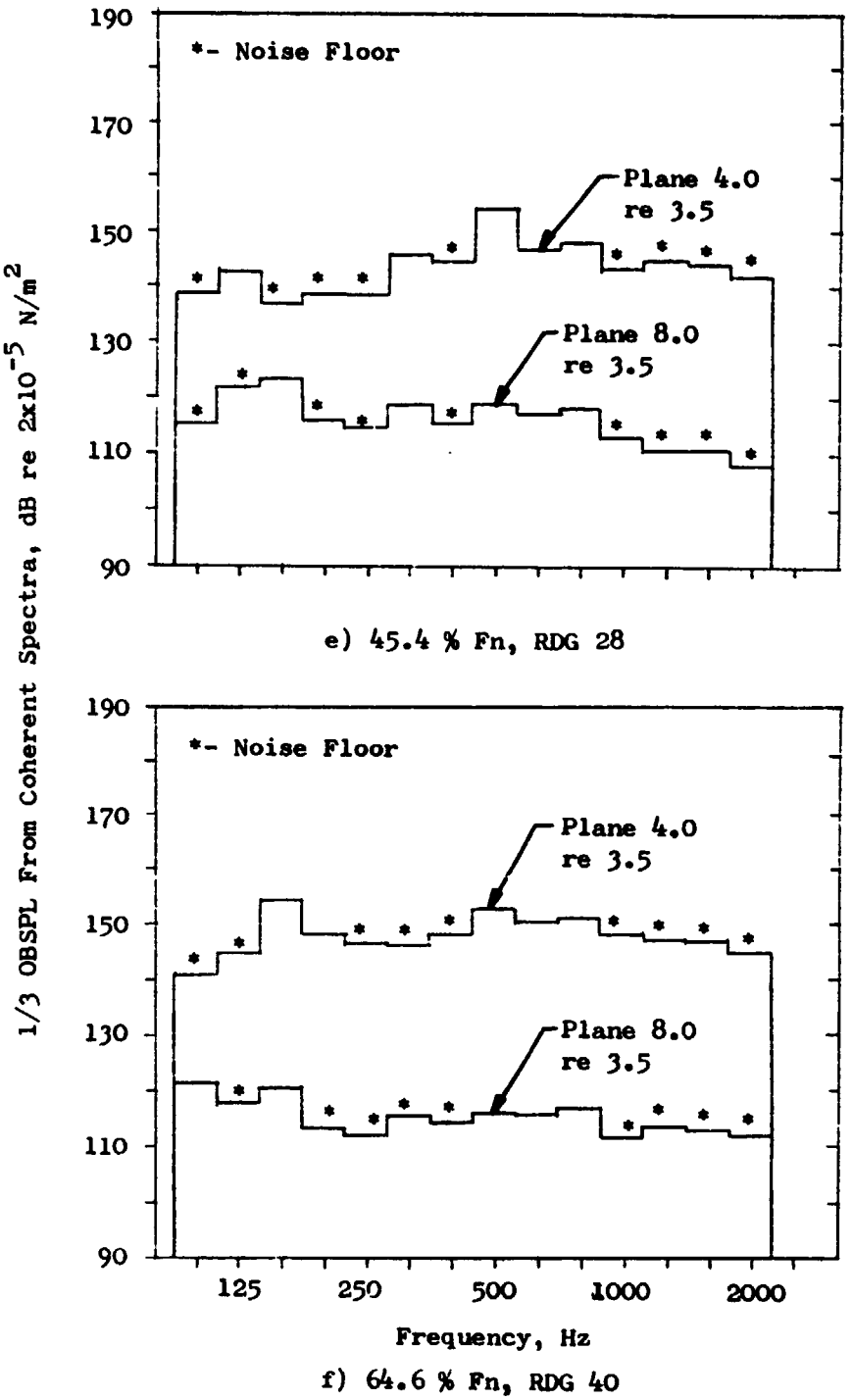

Figure C-1. Coherent Spectra Comparisons For Turbine Attenuation From ECCP Phase III Engine Test (Continued)

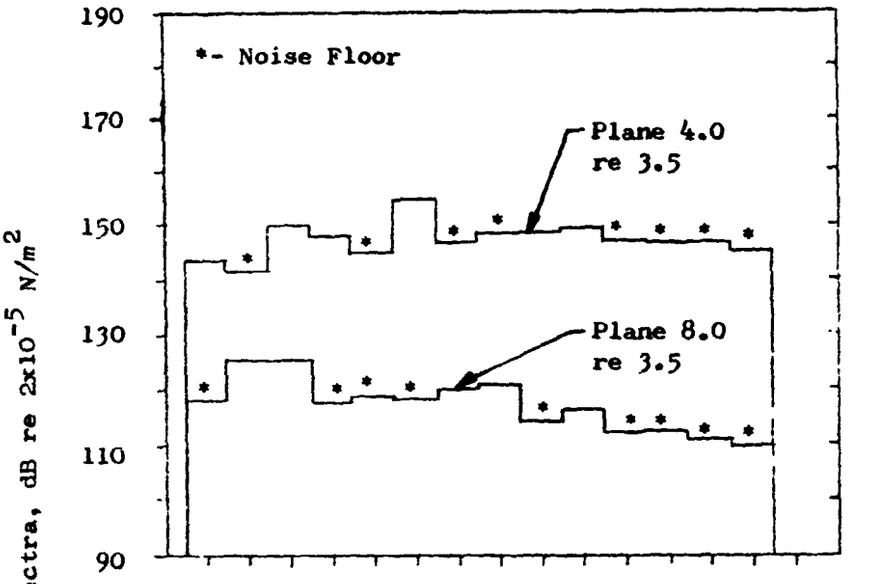

g) 82 % Fn, RDG 18

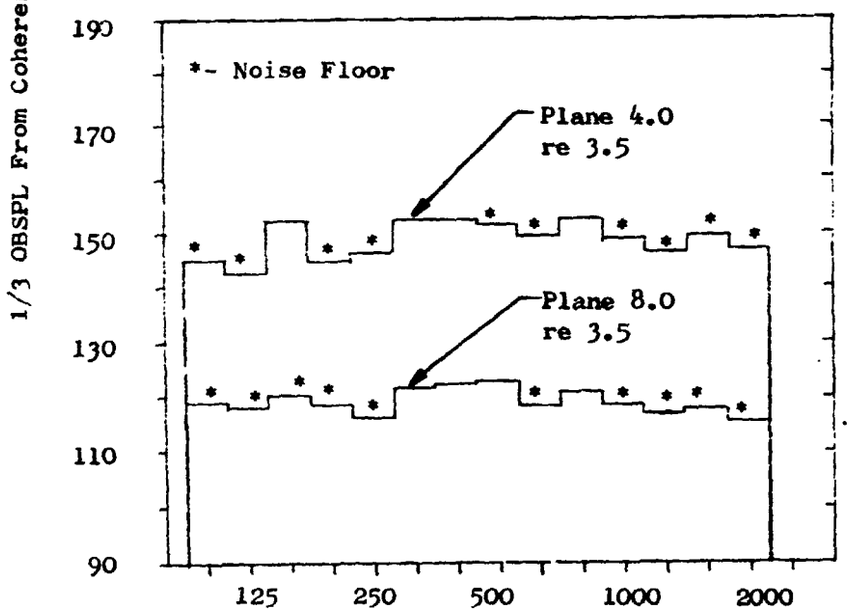

h) 94.6 % Fn, RDG 33

Figure C-1. Coherent Spectra Comparisons For Turbine Attentuation From ECCP Phase III Engine Test (Concluded)

APPENDIX D. EVALUATION OF PROBE RESPONSE AT ELEVATED TEMPERATURES

This Appendix contains the equations, basic assumptions and results of a study conducted on the ECCP Phase III internal Kiite probe measurements to evaluate the effect of elevated temperature on the engine test results.

APPENDIX D - EVALUATION OF PROBE RESPONSE AT ELEVATED TEMPERATURES

The theoretical value of probe attenuation determined from the mathematical equations of Arthur S. Iberall (Reference 12) includes effects of compressible fluid flow, fluid acceleration, and heat conduction. The pressure at any point in the line to the pressure at the probe entrance is related in the form of an amplitude ratio which is a function of frequency.

A simplified computation can be made when assuming no reflection in the system such as in the case of a probe terminated in a constant cross-section "infinite" line (a line in which reflections from its end can be neglected). The basis of this simplified calculation, as given in Olson (Reference 13) is the loss in tubes due to the viscosity of air.

Transmission loss in tubes of circular section can be expressed as

$$A = A_o \, e^{-\alpha x}$$

where A = amplitude (pressure) at a distance x from the amplitude A_o, which exists at the probe entrance. The other terms are given below:

$\alpha = \frac{\gamma'}{Rc} \sqrt{\frac{\omega\mu}{2\rho}}$, transmission coefficient

R = radius of tube

x = length from entrance to point of interest

c = velocity of sound

$\omega = 2 \pi f$

f = frequency in Hz

μ = viscosity coefficient, for air

ρ = density of medium

$\gamma' = 1 + 1.58 \, (\gamma^{1/2} - \gamma^{-1/2})$

γ = ratio of specific heats

The amplitude ratio becomes

$$A/A_o = e^{-\left(\frac{\gamma'}{Rc}\sqrt{\frac{\pi\mu}{\rho}}\right)\sqrt{f}\,x}$$, a function of frequency.

The transmission loss (attenuation) is

$$TL = 20 \log \frac{A}{A_o}$$

This attenuation is due solely to viscous damping within the probe tube and assumes no internal reflections and no non-linear effects associated with sound pressure levels over 120 dB.

The waveguide sensor systems used in the ECCP Phase III program underwent room temperature ambient pressure calibrations. The transmission loss in the sensor tubes located in the Double Annular combustor region as a result of the elevated operating temperatures was estimated assuming that -

1. The temperature in the waveguide tube reaches the sink temperature under the engine cowling of approximately 477 to 505K.
2. This temperature is constant for all operating conditions.
3. The pressure in the tube will be the static pressure in the combustor at the measuring plane.
4. An air medium exists.

For waveguide systems at Planes 3.0 and 3.5

- Conditions

  A. Calibration

  T_o = 293.3 K
  μ_o = 5.685×10^{-7} Pa-sec
  ρ_o = 1.224 kg/m^3
  γ_o = 1.4
  c_o = 341.4 m/s
  R_o = 0.00494 m

  B. Takeoff (Worst Case)

  T_1 = 477.8 K
  μ_1 = 8.036×10^{-7} Pa-sec
  ρ_1 = 19.406 kg/m^3
  γ_1 = 1.39
  c_1 = 438 m/s
  R_1 = 0.00494 m

- Transmission coefficient at f = 2000 Hz

$$\alpha = \frac{\gamma'}{Rc}\sqrt{\frac{\omega\mu}{2\rho}}$$

α_o = 0.2789 1/m for ambient calibration

α_1 = 0.0643 1/m for takeoff condition

- Transmission loss across tube length x = 0.3048 m for f = 2000 Hz

$$TL = 20 \log \frac{A}{A_o}$$

TL_o = - 0.74 dB for ambient calibration

TL_1 = - 0.17 dB for takeoff condition

- Ratio of transmission losses

$$\frac{TL_o}{TL_1} = \frac{-0.74}{-0.17} = 4.35$$

The frequency response loss determined from ambient calibrations is approximately four (4) times greater than the loss determined at the takeoff condition of the CF6-50.

This amounts to a reduction of the response correction from +2 dB at 2000 Hz to +0.5 dB at takeoff operating condtion. This 1.5 dB change is based on the linear assumption for SPL's less than 120 dB. Since the majority of the fluctuating pressure measurements were well above 120 dB (140 to 160 dB) and the ΔdB change was approaching the measurement accuracy, this temperature effect was neglected and the ambient response results were used to correct the data.

APPENDIX E. CROSS-CORRELATION RESULTS

This Appendix contains a tabulated summary of time delays and amplitudes for the major peaks of the cross-correlations between pairs of Kulite sensors for all test conditions on the ECCP Phase III CF6-50 engine test.

Table E-1. Time Delays and Amplitudes of Cross-Correlation Peaks for ECCP Phase III Test Data.

Pct Thrust			3.8	19.7	30.0	29.7	45.4	64.6	82.	94.6
Tape Reading			6	16	23	39	34/28	40/13	43/18	33
Plane 3.0 to 8.0			Point-to-Point Distance, d = 2.764 m, d_z = 2.527 m							
	τ_1	(msec)	+2.5	+5.0	+5.0	+6.0	+4.0	+5.0	---	+2.0
	R_{xy1}		.6	.1	.13	.07	.04	.03	---	.04
	τ_2	(msec)	+5.0	+2.5	+2.5	---	---	---	---	---
	R_{xy2}		.56	.05	.08	---	---	---	---	---
	$\bar{C}$	(m/s)	464.5	498.0	510.2	510.8	529.7	539.5	557.8	563.6
Plane 3.0 to 4.0			Point-to-Point Distance, d = 0.872 m, d_z = 0.634 m							
	τ_1	(msec)	-1.0	-1.5	-1.5	-1.5	-1.5	-1.5	-1.2	-1.5
	R_{xy1}		.18	.13	.8	.14	.1	.08	.1	.06
	τ_2	(msec)	+4.0	+4.0	+6.0	+7.5	+1.0	+1.0	+3.5	+2.5
	R_{xy2}		.21	.03	.02	.05	.06	.04	.03	.03
	$\bar{C}$	(m/s)	515.1	566.0	595.6	595.9	618.1	644.6	668.4	682.1
Plane 3.0 to 3.5			Point-to-Point Distance, d = 0.734 m, d_z = 0.357 m							
	τ_1	(msec)	-2.0	-1.5	-1.5	-1.5	-1.5	-1.5	-1.5	-1.5
	R_{xy1}		.3	.3	.24	.2	1.5	.12	.07	.14
	τ_2	(msec)	+6.0	-3.0	+6.0	+4.5	+4.0	+4.0	---	+4.0
	R_{xy2}		.18	.16	.07	.06	.05	.03	---	.06
	$\bar{C}$	(m/s)	419.1	482.5	504.1	505.1	530.6	545.3	566.3	573.9
Plane 3.5 to 4.0			Point-to-Point Distance, d = 1.271 m, d_z = 0.280 m							
(282°)	τ_1	(msec)	-2.0	-2.0	-1.8	+1.5	-1.5	-1.5	-1.5	-1.5
	R_{xy1}		.15	.08	.07	.10	.04	.04	.03	.03
	τ_2	(msec)	-7.0	+1.5	+1.5	-2.0	+5.0	+6.5	+1.5	+6.5
	R_{xy2}		.16	.08	.02	.07	.04	.03	.03	.03
			Point-to-Point Distance, d = 0.281 m, d_z = 0.280 m							
(102°)	τ_1	(msec)	---	-.30	0	---	---	---	---	---
	R_{xy1}		---	.18	.10	---	---	---	---	---
	$\bar{C}$	(m/s)	515.1	566.0	595.6	595.9	618.1	644.6	668.4	682.1

Table E-1. Time Delays and Amplitudes of Cross-Correlation Peaks for ECCP Phase III Test Data. (Concluded)

Pct Thrust / Tape Reading		3.8 / 6	19.7 / 16	30.0 / 23	29.7 / 39	45.4 / 34/28	64.6 / 40/13	82.0 / 43/18	94.6 / 33
Plane 4.0 to 8.0		Point-to-Point Distance, d = 1.893 m, d_z = 1.893 m							
τ_1	(msec)	+3.0	+3.0	+5.0	+5.5	+5.0	---	---	---
R_{xy1}		.26	.06	.04	.04	0.3	---	---	---
τ_2	(msec)	+6.0	+5.0	+7.0	+8.0	+7.0	---	---	---
R_{xy2}		.2	.05	.03	.04	.03	---	---	---
$\bar{C}$	(m/s)	560.5	581.6	601.7	607.2	638.9	638.9	660.2	671.8
Plane 3.5 (102° to 282°)		Point-to-Point Distance, d = 1.268 m, d_z = 0 m							
τ_1	(msec)	-2.0	+2.0	+2.0	---	+1.5	+1.5	+1.5	---
R_{xy1}		.34	.21	1.4	---	.08	.07	.06	---
τ_2	(msec)	-7.0	-2.0	-2.0	---	-1.5	-2.5	-1.5	---
R_{xy2}		.4	.16	.08	---	.04	.05	.06	---
$\bar{C}$	(m/s)	419.1	482.5	504.1	505.1	530.6	545.3	566.3	573.9
Plane 8.0 (A to B)		Point-to-Point Distance, d = 0.128 m, d_z = 0.128 m							
τ_1	(msec)	0.0	0.0	0.0	0.0	0.0	---	---	---
R_{xy1}		.8	.76	.75	.17	.4	---	---	---
τ_2	(msec)	---	+3.0	+.25	+.3	---	---	---	---
R_{xy2}		---	.2	.1	.06	---	---	---	---
$\bar{C}$	(m/s)	510.2	513.3	516.6	516.6	528.5	533.7	549.6	553.2
Plane 3.5 to 8.0		Point-to-Point Distance, d = 2.030 m, d_z = 2.204 m							
τ_1	(msec)	+3.5	-4.5	+5.5	+6.0	+.7	+.3	---	---
R_{xy1}		.24	1.6	1.1	.04	.04	.03	---	---
τ_2	(msec)	---	+2.0	+3.0	---	---	---	---	---
R_{xy2}		---	.06	.08	---	---	---	---	---
$\bar{C}$	(m/s)	464.6	497.9	510.4	510.8	529.6	539.5	558.0	563.6

APPENDIX F - NOMENCLATURE

Symbol	Description	Units
A	Annulus area, cross-sectional area at combustor measurement planes	m^2
A, A_o	Amplitued (pressure) of wave	
A_{ref}	Combustor reference area	m^2
BPR	Fan-to-core bypass ratio	
C, c	Acoustic velocity	m/s
$\overline{C}$	Average acoustic velocity	m/s
d	Point-to-Point distance between Kulites	m/s
dB	Decibel	
dz	Axial distance between Kulite sensors	m
ΔdB_{PWL}	Turbine attenuation based on PWL	dB
$\hat{e}_p$	Unit vector normal to acoustical wave front	
$\hat{e}_x$	Unit vector, axial component	
f	Frequency	Hz
f/a	Fuel-air ratio	
FAR_{36}	Combustor fuel-air ratio based on W_{36}	
% F_n, PCT FN	Percent net thrust	
FPL	Fluctuating pressure level re 2×10^{-5} N/m^2	dB
FPWL	Power level based on fluctuating pressures re 10^{-13} watts	dB
HPT	High pressure turbine	
HPTN	High pressure turbine nozzle	
HRR	Heat release rate (total fuel flow x heating value of JP5 fuel)	watts
Hz	Hertz: cycles/second	

$\vec{I}$	Intensity flux vector	
ID	Inside diameter	cm
LPT	Low pressure turbine	
M	Mach number	
$\overline{M}$	Average Mach number	
MADAR	Malfunction, detection, analysis and recording subsystem	
N_c	Core speed, corrected	rpm
N_f	Fan speed, corrected	rpm
OAFPL	Overall fluctuating pressure level	dB
OAPWL	Overall sound power level	dB
OASPL	Overall sound pressure level	dB
1/3 OBFPL	One-third octave band fluctuating pressure level	dB
1/3 OBSPL	One-third octave band sound pressure level	dB
OD	Outside diameter	cm
P	Acoustic pressure (rms)	kN/m^2
PCT IN	Percent fuel split to main stage burner	
PCT OUT	Percent fuel split to pilot stage burner	
P_o	Ambient, standard day pressure	atm
P_S	Static pressure	atm
P_T	Total pressure	atm
$\frac{\Delta P34}{P_3}$	PCT combustor pressure drop relative to upstream pressure	%
$\Delta P34$	Combustor total pressure drop	atm
PWL	Sound power level, re 10^{-13} watts	dB
R	Gas constant for air	
R	Radius of tube	m

RDG, Rdg	Reading number	--
R_{xy}	Cross-correlation function	
SLS	Sea level static	
SPL	Sound pressure level, re 2 x 10^{-5} N/m^2	dB
T_o	Ambient, standard day temperature	K
T_{4p}	Total temperature at turbine inlet based on pilot fuel-air ratio	K
T_S	Static temperature	K
T_T	Total temperature	K
ΔT_{34}	Combustor total temperature rise	K
TL	Transmission loss	dB
U	Mean flow velocity	m/s
$\vec{V}$	Absolute flow velocity vector	m/s
V_c	Core jet velocity	m/s
V_e	Effective (mixed jet) velocity	m/s
V_f	Fan jet velocity	m/s
W_3	Compressor discharge airflow	kg/sec
W_{36}	Total combustor discharge airflow	kg/sec
WFT	Total fuel flow	kg/hr
$\frac{W_{36}\sqrt{T_3}}{P_3 A_3}$	Combustor discharge flow corrected to combustor inlet conditions	
X	Axial Cartesian coordinate	
x	Distance along probe tube	m
Y	Tangential Cartesian coordinate	
α	Transmission coefficient	1/m

Δ	Difference, increase or decrease	
γ	Ratio of specific heats	
γ'	$1 + 1.58\ (\gamma^{1/2} - \gamma^{-1/2})$	
τ	Time delay	sec
θ	Angle between acoustic wave front and axial direction	deg
μ	Viscosity coefficiency for air	Pa sec
ρ	Density	kg/m^3
ϕ	Angle between flow and axial direction	deg
ω	Angular frequency, $2\pi f$	

SUBSCRIPTS

a	Air
c	Core
f	Fuel, fan
o	Initial or calibration condition
1	Test [illegible]on
1	Largest peak in cross-correlation
2	Next largest peak in cross-correlation
3.0	Compressor discharge plane
3.5	Combustor inlet plane
4.0	Combustor discharge/turbine inlet plane
8.0	Core nozzle discharge plane

REFERENCES

1. Gleason, C.C., and Bahr, D.W., "Experimental Clean Combustor Program Phase III Final Report," Report No. NASA CR-135384, to be published.

2. Bahr, D.W. and Gleason, C.C., "Experimental Clean Combustor Program - Phase I Final Report," Report No. NASA CR-134737, June 1975.

3. Emmerling, J.J., "Experimental Clean Combustor Program - Noise Measurement Addendum - Phase I Final Report," Report No. NASA CR-134853, July 1975.

4. Gleason, C.C., Rogers, D.W., Bahr, D.W.; "Experimental Clean Combustor Program - Phase II Final Report," Report No. NASA CR-134971, August 1976.

5. Emmerling, J.J. and Bekofske, K.L., "Experimental Clean Combustor Program - Noise Measurement Addendum - Phase II Final Report," Report No. NASA CR-135045, January 1976.

6. Doyle, V.L. and Matta, R.K., "Attenuation of Upstream-Generated Low Frequency Noise by Gas Turbines, "Report No. NASA CR-135219, August 1977.

7. Karchmer, A.M., Roskotko, M., and Montegani, F.J., "Measurement of Farfield Combustion Noise From a Turbofan Engine Using Coherence Functions," AIAA Paper 77-1277, October 1977.

8. Reshotko, M. et al.; "Core Noise Measurements on a YF-102 Turbofan Engine," NASA TMX-73587 (AIAA Paper No. 77-21), January 1977.

9. Matta, R. and Mani, R., "Theory of Low Frequency Noise Transmission Through Turbines," NASA CR 159457 , to be published.

10. Karchmer, A. and Reshotko, M., "Core Noise Source Diagnostics on a Turbofan Engine Using Correlation and Coherence Techniques," NASA TMX-73535, November 1976.

11. Matta, R.K., Sandusky, G.T. and Doyle, V.L., "GE Core Engine Noise Investigation - Low Emission Engines," Report No. FAA-RD-77-4, February 1977.

12. Iberall, Arthur S., "Attenuation of Oscillatory Pressures in Instrument Lines," Journal of Research of the NBS, Vol. 45, p85-108 July 1950.

13. Olson, Harry F., "Acoustical Engineering," 1957 D. Van Nostrand Company, Inc.